HIGH-DIMENSIONAL PROFILING OF IMMUNOTHERAPY-RESPONSIVE IMMUNE CELLS IN CANCER

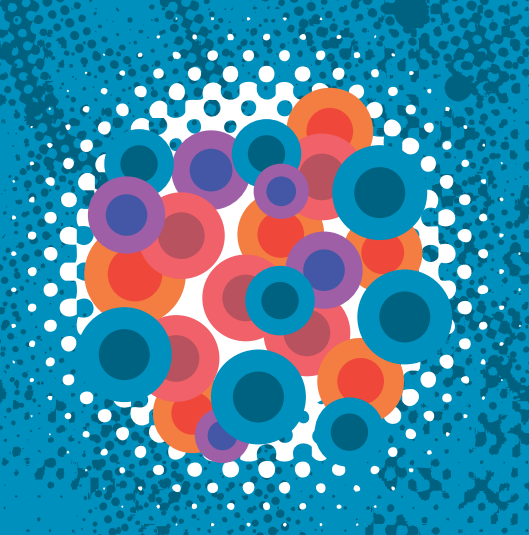

GUILLAUME BEYREND-FRIZON

HIGH DIMENSIONAL PROFILING OF IMMUNOTHERAPY-RESPONSIVE IMMUNE CELLS IN CANCER

Guillaume Beyrend-Frizon

The research performed in this thesis was performed at the Department of Immunology, formely known as the Department of Immunohematology and Blood Transfusion of the Leiden University Medical Center, Leiden, The Netherlands.

Financial support for the publication of this thesis was partially provided by Fluidigm.

ISBN: 978-94-93197-66-4

Cover design: Off Page, Amsterdam
Layout and Printing: Off Page, Amsterdam

HIGH DIMENSIONAL PROFILING OF IMMUNOTHERAPY-RESPONSIVE IMMUNE CELLS IN CANCER

Proefschrift

ter verkrijging van

de graad van doctor aan de Universiteit Leiden,
op gezag van rector magnificus prof.dr.ir. H. Bijl,
volgens besluit van het college voor promoties

te verdedigen
op dinsdag 8 juni 2021
klokke 10 uur

door

Guillaume Beyrend
geboren te Briey, Frankrijk in 1989

Promotor: Prof. dr. F. Ossendorp
Co-promotor: Dr. R. Arens

Leden promotiecommissie:
Prof. dr. J.G. Borst, Leiden University Medical Centre
Prof. dr. J.B.A.G. Haanen, Netherlands Cancer Institute
Prof. dr. J.G.J.V. Aerts, Erasmus Medical Center
Prof. dr. R. van Lier, University Medical Centre of Utrecht

Dédié à mes chers parents

TABLE OF CONTENTS

1

INTRODUCTION

CONTEXT AND HISTORY

With an estimated 37.2 trillion cells (1), the human body is under constant massive cell division, which is prone to errors triggering therefore genetical mutations. Millions of potential cancerous cells are then accidentally created throughout the lifespan of an individual (2) leading to cancer in some cases. Among more than eight thousand different diseases classified by WHO in *International Classification of Diseases and Related Health Problems*, cancer jumped from the eighth to the second place between 1900 and 1940. Currently, cancer is still the second leading cause of mortality in the world (3). It is estimated that one person out of three will suffer from this disease during their lifetime, and about one in six deaths is attributed to cancer. The lethality of this disease is mainly due to the malignant behavior of the cancer cells, exemplified by uncontrolled proliferation and eventually spread throughout the body. Explanatory environmental or genetic factors are complex to ascertain: lung cancer is predominantly caused by smoking but five out of every six smokers will never get lung cancer (4). Therapeutic efforts have been concentrated to target tumor cells and stop their proliferation, thereby using generally non-specific treatments like chemotherapeutic agents or radiotherapy. However, as the primary intention implies, chemotherapy is associated with various side effects linked to the inhibition of any dividing cell, including hair loss, bowel issues or skin problems. To minimize side effects, an alternative way to cure cancer is to target the immune system with the recently developed immune checkpoint blockers by releasing the cytotoxic power of T cells.

The idea that the immune system might play a role against the proliferation of cancer cells is not new. In 1808, an attempt to immunize Louis XVIII against tumor cells with breast cancer tissue extract resulted in a local inflammation and lymph node enlargement (5). This first trial of a prophylactic vaccine was followed at the end of the 19th century by a therapeutic approach, consisting of the activation of the immune system against cancer. William B. Coley injected streptococcal organisms, known as the Coley's Mixed Bacterial Toxins, into a patient with inoperable cancer in 1891 (6). The infection surrounding the tumor triggered the immune system, which responded by attacking the tumor cells and resulting as one of the first immunotherapy examples. Two decades later, in 1909, one year after receiving the Nobel Prize for discovering treatment against syphilis, Paul Ehrlich proposed a first version of the "immune surveillance" hypothesis (7), stating that host defense may prevent neoplastic cells to develop into tumors. This concept of immune surveillance was decades later further developed, by Lewis Thomas, Gross and Macfarlane Burnett stating that the immune system can recognize and destroy transformed cells before they grow into tumors (8, 9).

One of the main actors of the tumor immunity are the T cells, which present the ability to kill tumor cells. Jacques Miller, born in Nice, France, discovered the T and B lymphocytes in 1961 (10). In 1983, the T cell antigen receptor (TCR) was discovered (11, 12), highlighting the specificity of T cells for a determined antigen. T cells recognize antigens

with their TCR, a complex of two protein chains. T cells are selected to not recognize self-antigens (by thymic negative selection), presented by major histocompatibility complex (MHC) molecules but to react strongly to non-self antigens. Both $CD4^+$ (helper T cells) and $CD8^+$ T cells (cytotoxic T cells, CTLs) can recognize tumor cells expressing mutated antigens, called neoantigens, which are not expressed by healthy tissues.

Steven Rosenberg and colleagues paved the path to use tumor infiltrating lymphocytes (TILs) as an adoptive cell transfer therapy to treat cancer in 1986 (13). Briefly, during this procedure, cancer patient's own lymphocytes, mainly CTLs, are expanded *in vitro* and reinfused into the patient. TILs are reinvigorated and can recognize tumor cells expressing neoantigens. However, specific inhibitory receptors can be expressed on the membrane of tumor-specific T cells. Two well-known inhibitory receptors are PD-1 (Program cell Death-1) and CTLA-4 (Cytotoxic T-Lymphocyte-Associated protein 4), which recognize their ligands, PD-L1 and CD80/86 respectively, expressed on either tumor cells or other immune cells. By blocking the interactions of PD-1 (14) or CTLA-4 (15) with their ligands using specific antibodies, cancer treatment was improved in experimental mouse models. Years later, this so-called immune checkpoint blockade (ICB) received FDA approval (CTLA-4 targeting in 2011, and PD-1 targeting in 2014) to be used as a cancer immunotherapeutic approach, and was shown to be especially efficacious against cancers with a high mutation load (16). This new treatment, which was originally based on the discovery of PD-1 and CTLA-4 function in mice, resulted in the award of the Nobel Prize in 2018, which underscores the importance of experimental *in vivo* mouse models to enhance the immunotherapy of cancer in the medical field.

HOW OUR IMMUNE CELLS PLAY A ROLE AGAINST CANCER

The application of new molecular and cellular technologies in the tumor immunology field is a powerful instrument to further understand the interactions between our immune system and cancer. Single-cell analysis that we and others have performed allowed us to have an overall view on the main lineages of the immune system in cancer: dendritic cells (DCs), macrophages, neutrophils, Natural Killer (NK) cells, T and B cells, and as well have an in-depth view regarding the phenotype and function of these cells. All of them are thought to play a unique role against cancer and all these immune cell subsets can be detected by mass cytometry.

Neutrophils, a lineage of the innate immune system, are the first recruited where danger signals are excreted into the tissue. The presence of neutrophils might be linked to pro- or anti-tumorigenic effect and often to increased metastatic potential of tumors (17). The chemokine products released by neutrophils could serve as enablers of tumor cell migration through the extracellular matrix, helping them to migrate to new metastatic sites (18).

After neutrophils have been recruited to the tissue, macrophages, from the innate lineage, reside in tissue after travelling as monocytes in the blood. Macrophages

present such powerful phagocytic activity that they can clear approximately 200 billion erythrocytes each day (almost 3 kg of iron and hemoglobin per year) (19), making them strong candidates to engulf tumor cells and to present neoantigens. Pro-inflammatory macrophages, M1-type, play a relevant role in the elimination of malignant cells. The mechanisms by which macrophages can destroy tumor cells are similar to those that kill infectious agents, essentially through the production of nitric oxide. On the contrary, single-cell technologies frequently show the presence of M2-type macrophages in the tumor microenvironment (TME), promoting tumor growth (20) by different effects, such as stimulating angiogenesis via secretion of VEGF or inducing immunosuppression of anti-tumor effector immune cells. The liberation of IL-10 or TGF-β by macrophages is indeed impairing the activity of the T cells (21).

After the innate cell lineage components triggered an immune response, the adaptive immune system is undergoing drastic changes. T cells represent the principal way of cellular defense against cancer. Cytotoxic T lymphocytes (CTLs) perform surveillance by recognizing and killing tumor cells expressing antigens (such as neoantigens from mutated proteins) on their MHC-I receptors. The importance of CTLs in tumor immunity is such that a classification of tumors based on the number of tumor infiltrating lymphocytes (TILs) have been established and seemed to give reliable prognosis (22, 23). Clinically, TILs are relevant for several reasons. For example, TILs can be used for adoptive cell transfer therapy. In this treatment, lymphocytes are usually directly extracted from tumors, expanded ex vivo with different interleukins including IL-2 and infused back into the patient (24).

Major attention has also been given to the role of helper $CD4^+$ T cells. These cells are implicated in orchestrating the tumor response (25), and co-targeting of $CD4^+$ T cells might be required for efficient antitumor immunity. $CD4^+$ T cells can target tumor cells in multiple manners, either directly by eliminating tumor cells through cytolytic mechanisms or indirectly by modulating the TME and providing help to the $CD8^+$ T cells (26). Another type of $CD4^+$ T cells, the regulatory T cells (T_{regs}), are considered to have an opposite (negative) effect on tumor immunity. These cells, often characterized by the presence of FoxP3 and CD25 (27) can inhibit the cytotoxic power of CTLs thereby enhancing tumor growth.

Antigen presenting cells (APC) such as dendritic cells (DCs) are crucial to prime tumor-specific CTLs and helper $CD4^+$ T cells. During tumor cell death, the tumor cell debris containing tumor-antigens is ingested by DCs, which subsequently present the tumor antigens in both MHC-I and MHC-II molecules. The exogenous antigen uptake and presentation by MHC-I is called cross-presentation and considered as a decisive property of DCs to initiate tumor-specific $CD8^+$ T cell responses. DCs also need to express costimulatory signals to provide additional signals needed for differentiation of naïve T cells (28). However, a major hurdle to mount effective tumor-specific T cell responses is the lack of sufficient DC activation leading to insufficient display of neoantigens to naïve T cells (29), and the lack of upregulating co-stimulatory ligands such as CD80 or

CD86, the ligands of the primary T cell costimulatory receptor CD28, and members of the TNF superfamily ligating the costimulatory TNFR family members (e.g. CD27, OX40 and 4-1BB) expressed by $CD4^+$ and $CD8^+$ T cells.

NK cells are cells belonging to the innate lineage but like T cells, NK cells can also kill tumor cells. They can provide rapid cytolytic responses to infected or cancer cells. If tumor cells have down-modulated their MHC-I on the cell-surface, the NK cells are activated due to their receptors that are stimulated if MHC-I is deficient (30, 31). NK cells, as well as the recently discovered Innate Lymphoid Cells type 1 (ILC1), react especially to (MHC-I deficient) tumors (32), whereas ILC2 might enhance a pro-tumorigenic environment (33). Similarly, γδ T cells can play a role in cancer as their importance in cancer has recently been reported, like in colorectal cancer (34) where their activated phenotype was most exclusively found in mismatch-repaired-deficient cancer tissues. It was previously shown that human peripheral blood γδ T cells express PD-1 and exhibit natural killer-like activity, making these cells potential anti-PD-1-related-therapy targets (35).

Other immune cell subsets like B cells or eosinophils, basophils or myeloid derived suppressor cells are also implicated in the cancer immune response but their role is not further detailed in this thesis.

CANCER THERAPEUTIC STRATEGIES

Cells are often mutating and it is estimated that our body will carry respectively 8 million stem cells containing one mutation on a cancer-associated gene (2). Our immune system limits their development as described by the principles of immunoediting: Elimination, Equilibrium and Escape (36-38). Briefly, the elimination phase is the immunosurveillance where the immune system is killing efficiently tumor cells, followed by the equilibrium phase. During the latter, tumor cells are mutating, and tumor variants acquire resistance to elimination, entering the escape phase. During the escape phase, tumor cells grow and expand, leading to malignancies. The tumor microenvironment has then acquired a suppressive effect on the immune system. The immune system modulates this balance, acting either as a tumor growth promoter or inhibitor (39). Interventional therapies might be needed at this stage to reverse the pro-tumoral microenvironment. Oftentimes this cannot be achieved by only debulking of tumor mass by surgery and/or radio- or chemotherapy. These treatments are meant to target all dividing cells, not specific to tumor cells and are often accompanied by severe side effects. Therefore, more specific treatments, like immunotherapy, were developed to specifically modulate the tumor microenvironment with the advantage to limit the side effects. Immunotherapy treatments help the immune system to destroy cancer cells and stop cancer from spreading. There are several types of immunotherapy, including adoptive T-cell therapy, cancer vaccines, monoclonal antibodies and oncolytic virus therapy.

IMMUNOTHERAPY AND THE IMPORTANCE OF IMMUNE CHECKPOINT BLOCKADE

Activating and inhibitory immune checkpoint molecules have an important regulatory role in the immune system. They are expressed at the cell surface of immune cells and their role is to maintain self-tolerance or to regulate the magnitude of immune responses against microbes. Next to the natural role of these receptors and their ligands in regulating the normal T cells immune response, these molecules are often dysregulated in cancer. The expression is often higher or constitutive in the tumor microenvironment or in the tumor-draining lymphoid organs (40-42) thereby suppressing an anti-cancer immune response. As described above, the two best-defined inhibitory immune checkpoints are CTLA-4 and PD-1, and the targeting of these molecules have been FDA-approved for treatment of many cancers, for some tumor types even as first-line therapy. However, approximately 40% (43, 44) of melanoma patients responds partially or completely to therapy.

PD-1 is mostly expressed on activated cells of the lymphoid lineage, like T lymphocytes or NK cells ***(Figure 1)***. Its ligand, mainly PD-L1, is expressed on cancer cells but also on subsets of the myeloid lineage like macrophages or dendritic cells (45). When PD-1 on a T cell recognizes its ligand PD-L1, the T cell activation signal is inhibited, preventing cytolysis of the tumor (46). Blocking the PD-1/PD-L1 interaction with monoclonal antibodies could thus unleash the cytotoxic power of those T cells towards tumor cells. CTLA-4 is also mainly expressed on activated T cells. Initially, the ligands CD80/86 are expressed on APCs and bind to the T cell costimulatory receptor CD28. Upon activation of the T cell, CTLA-4 is upregulated, and then CD80/86 bind preferentially CTLA-4, thereby inhibiting further T cell activation. CTLA-4 is also a key molecule for T_{regs} to mediate suppression. Monoclonal antibodies blocking CTLA-4 (anti-CTLA4 antibodies) have been designed to specifically block the interaction between CTLA-4 and CD80/86, so that CD28 can still bind to CD80/86, leading to a stronger T cell activation (47). Both PD-1 (14) and CTLA-4 (15) have been historically first studied in animal models. To allow a better clinical success of immune checkpoint therapy, other targetable molecules have been tested such as lymphocyte activation gene-3 (LAG-3). This cell-surface molecule expressed on helper T cells and to a lower extent also on cytotoxic cells presents inhibitory functions, that are distinct from PD-1 and CTLA-4 (48). Since LAG-3 is over-expressed on tumor-infiltrating $CD8^+$ T cells in various tumor types, such as ovarian cancer, hepatocellular carcinoma, renal cell carcinomas and other solid tumors (49, 50),this molecule might be a potential target in cancer immunotherapy

Besides improving immune checkpoint therapy by targeting inhibitory molecules, currently many approaches are tested that are directed toward direct targeting stimulatory receptors. In this respect, the co-stimulatory TNF receptor (TNFR) superfamily members, and especially CD27, OX40 and 4-1BB, are promising new immunotherapeutic targets (51, 52). CD27 is constitutively expressed on the majority of CD4 and CD8 T cells, whereas OX40 and 4-1BB are upregulated on these cells upon activation. Whereas OX40

is most profoundly expressed by activated CD4+ T cells, 4-1BB is higher expressed on CD8+ T cells. The expression of the ligands, however, are all strictly regulated in their expression by APCs, and only transient expression has been observed after APC activation. All these costimulatory TNFR-like molecules play important roles in the proliferation, survival and differentiation of effector and memory T cells as exemplified by specific blockade or activation. Especially, the studies in which monoclonal antibodies to CD27, OX40 and 4-1BB with agonistic properties were used gained attention in the tumor immunotherapy field.

In most experimental tumor models, agonistic ligation of these TNFR-like molecules resulted T-cell activation but eradication of established tumors depended highly on the timing of administration and on combination with other therapies (53). Currently, the effectivity of targeting the costimulatory TNFR superfamily members is being evaluated in the clinic (54-56).

SINGLE-CELL TECHNOLOGIES: A HIGHLIGHT ON MASS CYTOMETRY AND SC-RNA-SEQUENCING

Major breakthroughs related to the function and heterogeneity of the immune system have been made possible through the apparition of novel single cell technologies.

On the proteomic level, flow cytometry has been existing for more than half a century (57), to sort cell populations based on their phenotypes (58). Briefly, cells are stained with

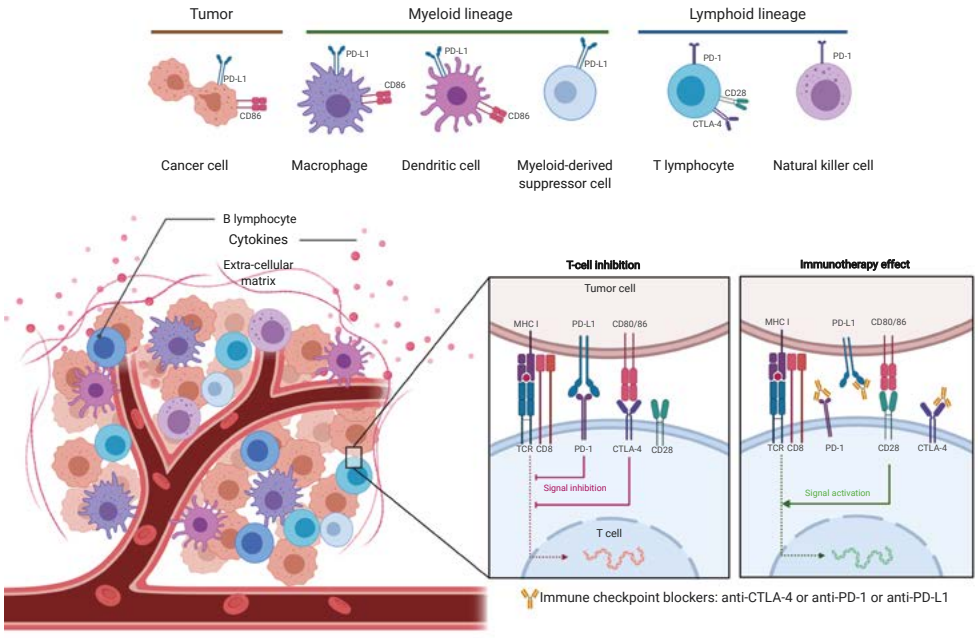

Figure 1. Presentation of immunotherapy effect in the tumor microenvironment.

fluorescent antibodies recognizing and binding specific extra or intra-cellular markers. Cells are then analyzed with a flow cytometer, passing through multiple lasers able to detect the fluorescent antibodies attached to each cell. Every single cell expressed different markers according to their phenotypes, meaning that the combination of the markers present at the cell surface defines a specific phenotype. The number of parameters or markers used can reach approximately 14 markers with conventional instruments, but the recent development of technologies based on full spectra increases this number up to 30, without decreasing the analysis flowrate. In contrast to most immune cells, tumor cells generally show a high auto-fluorescence background, which is difficult to discriminate with marker-related-fluorescence.

A new technology, named mass cytometry, is based on metal isotopes and not on fluorescence. This technique has revolutionized the way to analyze the immune system without compensation required or fluorescence background (59). The number of metals possibly extracted with a sufficient purity is currently set at 55, but the number of channels available to receive a specific signal is theoretically over a 100. The use of many more markers allows deeper surface phenotyping and also functional screening with intracellular signaling of the immune system (60). Although mass cytometry presents an unprecedented high resolution, there are still some challenges to overcome. The limit of detection of the instrument is not sufficient enough for the detection of subtle expression markers. The cell acquisition is more than 30 times slower (300 events/ sec in average) compared to flow cytometry analyzers (10 000 events/ sec). Cells can be sorted at the end of flow cytometry analysis for functional analysis, but this is impossible in mass cytometry, where cells are burnt.

On the genomic side, single-cell technology has improved the analysis of biological systems, via tumor genome sequencing (Navin et al., 2011; Vitak et al., 2017), tumor clonality dynamic (61), chromatin accessibility (62) and even spatial positioning (63). Whereas bulk RNA-sequencing measures the average expression analysis level for each gene in a large population of cells, single-cell-RNA sequencing (sc-RNA-seq) measures the expression analysis of each gene of every single cell of a sample, revealing heterogeneity of cell populations. Sc-RNA-seq research was first used in a four-cell-stage blastomere (64). At a larger scale, when used on e.g. the TME, it allows for example a deep genotyping of every single cell present in the TME, allowing to genetically characterize different subsets (65). The resolution of subset definition can be high enough to only focus on one lineage of the immune subset, previously sorted. For example, analysis of NK cells based on sc-RNA-seq have been performed (66) as well as on T cells (67).

ANALYSIS PIPELINE

Advanced flow and mass cytometers can generate highly complex data with up to 30 and 50 parameters, respectively. Conventional methods to analyze such data are implying biased, subjective and time-consuming gating strategies (68). They are usually based on

the interpretation of numerous two-dimensional plots by selecting different positive or negative populations with the help of markers historically defined by immunologists. This so-called gating strategy, if applicable in a known and limited panel, is unfeasible to analyze large data sets with many markers such as those we developed in our study; a 38-mouse-marker panel and a 46-human-marker panel. To analyze the data, we used automatic clustering techniques like Cytosplore (69), which are based on t-SNE (t-distributed Stochastic Neighbor Embedding) (70) and HSNE algorithm (Hierarchical Stochastic Neighbor Embedding) or FlowSOM (71). These clustering algorithms take all the markers into account and reduce the high-dimensional data into a two-dimensional plot. Such plots reflect the multidimensional relationship of the data and limit the intervention of the users by avoiding the definition of manual gates, known to be a significant source of variability (72). If these algorithms help the immunologists to define cell subsets in an unbiased manner and decrease variability, they do not automatically highlight treatment-related clusters and often do not offer a complete visualization of the data. An analyzing tool combining an efficient clustering method together with a visualization process was needed to automatically highlight immunological patterns between groups, leading to the creation of *Cytofast*, reported in this thesis.

OUTLINE

In this thesis, the latest single-cell technologies were used to advance insight in the complex immune responses to cancer raised by the variability of ICB immunotherapy.

The goal of this work is to improve current immunotherapy settings, by tailoring treatment and understanding the underlying factors preventing ICB to effectively lead to tumor regression. For this aim mass cytometry and software to properly analyze the complex data was used. A novel software method to analyze the data in an efficient manner by creating a tailored bioinformatic pipeline, named *Cytofast* was developed (**Chapter 2**). As a proof of concept, *Cytofast* analysis was run. Their results were confirmed and also new findings were discovered, reporting the usefulness of the new algorithm. The *Cytofast* method was further improved and explained in a visualized protocol (**Chapter 3**), where it was shown how PD-L1 treatment shaped the NK cell-tumor response at an early stage. Once the methodology was completed, the complexity of ICB immunotherapy was investigated (**Chapter 4**) and focused on the impact of PD-1/PD-L1 blockade. Extensive mass cytometry experiments were performed and processed by *Cytofast* to better understand the effect of PD-1 blockade on the immune response in the TME in order to improve this ICB. Next, the systemic immunity upon effective immune checkpoint therapy (PD-1 blockade combined with targeting direct T-cell costimulation) was studied in experimental models using the combination of genomic tools like sc-RNA-seq and proteomic technologies (**Chapter 5**). In **Chapter 6** the impact of immunotherapy on the blood immune cells as an important immunological compartment, as perceived in this thesis, was reviewed. Finally, the main findings of this thesis are discussed in **Chapter 7**.

REFERENCES

1. Bianconi E, Piovesan A, Facchin F, Beraudi A, Casadei R, Frabetti F, et al. An estimation of the number of cells in the human body. Annals of Human Biology. 2013;40(6):463-71.
2. Jackson AL, Loeb LA. The mutation rate and cancer. Genetics. 1998;148(4):1483-90.
3. Ferlay J, Soerjomataram I, Dikshit R, Eser S, Mathers C, Rebelo M, et al. Cancer incidence and mortality worldwide: Sources, methods and major patterns in GLOBOCAN 2012. International Journal of Cancer. 2015;136(5):E359-E86.
4. Brennan P, Crispo A, Zaridze D, Szeszenia-Dabrowska N, Rudnai P, Lissowska J, et al. High Cumulative Risk of Lung Cancer Death among Smokers and Nonsmokers in Central and Eastern Europe. American Journal of Epidemiology. 2006;164(12):1233-41.
5. Rosenberg SA. A new era of cancer immunotherapy: converting theory to performance. CA Cancer J Clin. 1999;49(2):70-3, 65.
6. Coley WB. The treatment of malignant tumors by repeated inoculations of erysipelas. With a report of ten original cases. 1893. Clin Orthop Relat Res. 1893(262):3-11.
7. Ehrlich P. Ueber den jetzigen Stand der Karzinomforschung1908.
8. Burnet FM. The concept of immunological surveillance. Prog Exp Tumor Res. 1970;13:1-27.
9. Burnet M. Cancer—A Biological Approach. III Viruses Associated with Neoplastic Conditions IV Practical Applications. 1957;1(5023):841-7.
10. Miller JFAP. Immunological function of the thymus. The Lancet. 1961;278(7205):748-9.
11. Acuto O, Meuer SC, Hodgdon JC, Schlossman SF, Reinherz EL. Peptide variability exists within alpha and beta subunits of the T cell receptor for antigen. J Exp Med. 1983;158(4):1368-73.
12. Reinherz EL, Meuer SC, Schlossman SF. The delineation of antigen receptors on human T lymphocytes. Immunol Today. 1983;4(1):5-8.
13. Rosenberg SA, Spiess P, Lafreniere R. A new approach to the adoptive immunotherapy of cancer with tumor-infiltrating lymphocytes. Science. 1986;233(4770):1318-21.
14. Ishida Y, Agata Y, Shibahara K, Honjo T. Induced expression of PD-1, a novel member of the immunoglobulin gene superfamily, upon programmed cell death. EMBO J. 1992;11(11):3887-95.
15. Leach DR, Krummel MF, Allison JP. Enhancement of Antitumor Immunity by CTLA-4 Blockade. Science. 1996;271(5256):1734-6.
16. Wu X, Gu Z, Chen Y, Chen B, Chen W, Weng L, et al. Application of PD-1 Blockade in Cancer Immunotherapy. Comput Struct Biotechnol J. 2019;17:661-74.
17. De Larco JE, Wuertz BR, Furcht LT. The potential role of neutrophils in promoting the metastatic phenotype of tumors releasing interleukin-8. Clin Cancer Res. 2004;10(15):4895-900.
18. Huh SJ, Liang S, Sharma A, Dong C, Robertson GP. Transiently entrapped circulating tumor cells interact with neutrophils to facilitate lung metastasis development. Cancer Res. 2010;70(14):6071-82.
19. Mosser DM, Edwards JP. Exploring the full spectrum of macrophage activation. Nature reviews Immunology. 2008;8(12):958-69.
20. Mantovani A, Sozzani S, Locati M, Allavena P, Sica A. Macrophage polarization: tumor-associated macrophages as a paradigm for polarized M2 mononuclear phagocytes. Trends in Immunology. 2002;23(11):549-55.
21. Taylor A, Verhagen J, Blaser K, Akdis M, Akdis CA. Mechanisms of immune suppression by interleukin-10 and transforming growth

factor-beta: the role of T regulatory cells. Immunology. 2006;117(4):433-42.

22. Galon J, Angell Helen K, Bedognetti D, Marincola Francesco M. The Continuum of Cancer Immunosurveillance: Prognostic, Predictive, and Mechanistic Signatures. Immunity. 2013;39(1):11-26.

23. Galon J, Costes A, Sanchez-Cabo F, Kirilovsky A, Mlecnik B, Lagorce-Pages C, et al. Type, density, and location of immune cells within human colorectal tumors predict clinical outcome. Science. 2006;313(5795):1960-4.

24. Rosenberg SA, Restifo NP. Adoptive cell transfer as personalized immunotherapy for human cancer. Science. 2015;348(6230):62-8.

25. Spitzer MH, Carmi Y, Reticker-Flynn NE, Kwek SS, Madhireddy D, Martins MM, et al. Systemic Immunity Is Required for Effective Cancer Immunotherapy. Cell. 2017;168(3):487-502 e15.

26. Borst J, Ahrends T, Bąbała N, Melief CJM, Kastenmüller W. CD4+ T cell help in cancer immunology and immunotherapy. Nature Reviews Immunology. 2018.

27. Corthay A. How do regulatory T cells work? Scandinavian journal of immunology. 2009;70(4):326-36.

28. Gardner A, Ruffell B. Dendritic Cells and Cancer Immunity. Trends Immunol. 2016;37(12):855-65.

29. Gardner A, Ruffell B. Dendritic Cells and Cancer Immunity. Trends in Immunology. 2016;37(12):855-65.

30. Marcus A, Gowen BG, Thompson TW, Iannello A, Ardolino M, Deng W, et al. Recognition of tumors by the innate immune system and natural killer cells. Adv Immunol. 2014;122:91-128.

31. Freeman AJ, Vervoort SJ, Ramsbottom KM, Kelly MJ, Michie J, Pijpers L, et al. Natural Killer Cells Suppress T Cell-Associated Tumor Immune Evasion. Cell Reports. 2019;28(11):2784-94.e5.

32. Vivier E, Artis D, Colonna M, Diefenbach A, Di Santo JP, Eberl G, et al. Innate Lymphoid Cells: 10 Years On. Cell. 2018;174(5):1054-66.

33. Tumino N, Vacca P, Quatrini L, Munari E, Moretta F, Pelosi A, et al. Helper Innate Lymphoid Cells in Human Tumors: A Double-Edged Sword? Frontiers in Immunology. 2020;10(3140).

34. de Vries NL, van Unen V, Ijsselsteijn ME, Abdelaal T, van der Breggen R, Farina Sarasqueta A, et al. High-dimensional cytometric analysis of colorectal cancer reveals novel mediators of antitumour immunity. Gut. 2020;69(4):691-703.

35. Iwasaki M, Tanaka Y, Kobayashi H, Murata-Hirai K, Miyabe H, Sugie T, et al. Expression and function of PD-1 in human gammadelta T cells that recognize phosphoantigens. Eur J Immunol. 2011;41(2):345-55.

36. Dunn GP, Bruce AT, Ikeda H, Old LJ, Schreiber RD. Cancer immunoediting: from immunosurveillance to tumor escape. Nat Immunol. 2002;3(11):991-8.

37. Dunn GP, Old LJ, Schreiber RD. The Immunobiology of Cancer Immunosurveillance and Immunoediting. Immunity. 2004;21(2):137-48.

38. Dunn GP, Old LJ, Schreiber RD. The Three Es of Cancer Immunoediting. Annual Review of Immunology. 2004;22(1):329-60.

39. Schreiber RD, Old LJ, Smyth MJ. Cancer Immunoediting: Integrating Immunity's Roles in Cancer Suppression and Promotion. Science. 2011;331(6024):1565-70.

40. Wagner J, Rapsomaniki MA, Chevrier S, Anzeneder T, Langwieder C, Dykgers A, et al. A Single-Cell Atlas of the Tumor and Immune Ecosystem of Human Breast Cancer. Cell. 2019.

41. Gonzalez VD, Samusik N, Chen TJ, Savig ES, Aghaeepour N, Quigley DA, et al. Commonly Occurring Cell Subsets in High-Grade Serous Ovarian Tumors Identified by Single-Cell Mass Cytometry. Cell Rep. 2018;22(7):1875-88.

42. Chevrier S, Levine JH, Zanotelli VRT, Silina K, Schulz D, Bacac M, et al. An Immune Atlas of Clear Cell Renal Cell Carcinoma. Cell. 2017;169(4):736-49 e18.

43. Topalian SL, Hodi FS, Brahmer JR, Gettinger SN, Smith DC, McDermott DF, et al. Safety, activity, and immune correlates of anti-PD-1 antibody in cancer. The New England journal of medicine. 2012;366(26):2443-54.

44. Wolchok JD, Kluger H, Callahan MK, Postow MA, Rizvi NA, Lesokhin AM, et al. Nivolumab plus ipilimumab in advanced melanoma. The New England journal of medicine. 2013;369(2):122-33.

45. Sharpe AH, Pauken KE. The diverse functions of the PD1 inhibitory pathway. Nat Rev Immunol. 2018;18(3):153-67.

46. Okazaki T, Honjo T. PD-1 and PD-1 ligands: from discovery to clinical application. International Immunology. 2007;19(7):813-24.

47. Sansom DM. CD28, CTLA-4 and their ligands: who does what and to whom? Immunology. 2000;101(2):169-77.

48. Goldberg MV, Drake CG. LAG-3 in Cancer Immunotherapy. Curr Top Microbiol Immunol. 2011;344:269-78.

49. Hemon P, Jean-Louis F, Ramgolam K, Brignone C, Viguier M, Bachelez H, et al. MHC class II engagement by its ligand LAG-3 (CD223) contributes to melanoma resistance to apoptosis. J Immunol. 2011;186(9):5173-83.

50. Li FJ, Zhang Y, Jin GX, Yao L, Wu DQ. Expression of LAG-3 is coincident with the impaired effector function of HBV-specific CD8(+) T cell in HCC patients. Immunol Lett. 2013;150(1-2):116-22.

51. Borst J, Hendriks J, Xiao Y. CD27 and CD70 in T cell and B cell activation. Curr Opin Immunol. 2005;17(3):275-81.

52. Arens R, Tesselaar K, Baars PA, van Schijndel GM, Hendriks J, Pals ST, et al. Constitutive CD27/CD70 interaction induces expansion of effector-type T cells and results in IFNgamma-mediated B cell depletion. Immunity. 2001;15(5):801-12.

53. Bayat Mokhtari R, Homayouni TS, Baluch N, Morgatskaya E, Kumar S, Das B, et al. Combination therapy in combating cancer. Oncotarget. 2017;8(23):38022-43.

54. Massarelli E, Lam VK, Parra ER, Rodriguez-Canales J, Behrens C, Diao L, et al. High OX-40 expression in the tumor immune infiltrate is a favorable prognostic factor of overall survival in non-small cell lung cancer. Journal for ImmunoTherapy of Cancer. 2019;7(1):351.

55. Miller RE, Jones J, Le T, Whitmore J, Boiani N, Gliniak B, et al. 4-1BB-specific monoclonal antibody promotes the generation of tumor-specific immune responses by direct activation of CD8 T cells in a CD40-dependent manner. J Immunol. 2002;169(4):1792-800.

56. Marigo I, Zilio S, Desantis G, Mlecnik B, Agnellini AH, Ugel S, et al. T Cell Cancer Therapy Requires CD40-CD40L Activation of Tumor Necrosis Factor and Inducible Nitric-Oxide-Synthase-Producing Dendritic Cells. Cancer Cell. 2016;30(3):377-90.

57. Fulwyler MJ. Electronic separation of biological cells by volume. Science. 1965;150(3698):910-1.

58. Herzenberg LA, Sweet RG, Herzenberg LA. Fluorescence-activated cell sorting. Sci Am. 1976;234(3):108-17.

59. Bandura DR, Baranov VI, Ornatsky OI, Antonov A, Kinach R, Lou X, et al. Mass Cytometry: Technique for Real Time Single Cell Multitarget Immunoassay Based on Inductively Coupled Plasma Time-of-Flight Mass Spectrometry. Analytical Chemistry. 2009;81(16):6813-22.

60. Levine JH, Simonds EF, Bendall SC, Davis KL, Amir el AD, Tadmor MD, et al. Data-Driven Phenotypic Dissection of AML Reveals Progenitor-like Cells that Correlate with Prognosis. Cell. 2015;162(1):184-97.

61. Yost KE, Satpathy AT, Wells DK, Qi Y, Wang C, Kageyama R, et al. Clonal replacement of tumor-specific T cells following PD-1 blockade. Nature Medicine. 2019;25(8):1251-9.

62. Clark SJ, Argelaguet R, Kapourani C-A, Stubbs TM, Lee HJ, Alda-Catalinas C, et al. scNMT-seq enables joint profiling of chromatin accessibility DNA methylation and transcription in single cells. Nature Communications. 2018;9(1):781.

63. Moffitt JR, Bambah-Mukku D, Eichhorn SW, Vaughn E, Shekhar K, Perez JD, et al. Molecular, spatial, and functional single-cell profiling of the hypothalamic preoptic region. Science. 2018;362(6416).

64. Tang F, Barbacioru C, Wang Y, Nordman E, Lee C, Xu N, et al. mRNA-Seq whole-transcriptome analysis of a single cell. Nature Methods. 2009;6(5):377-82.

65. Azizi E, Carr AJ, Plitas G, Cornish AE, Konopacki C, Prabhakaran S, et al. Single-Cell Map of Diverse Immune Phenotypes in the Breast Tumor Microenvironment. Cell. 2018;174(5):1293-308.e36.

66. Crinier A, Milpied P, Escalière B, Piperoglou C, Galluso J, Balsamo A, et al. High-Dimensional Single-Cell Analysis Identifies Organ-Specific Signatures and Conserved NK Cell Subsets in Humans and Mice. Immunity. 2018.

67. Szabo PA, Levitin HM, Miron M, Snyder ME, Senda T, Yuan J, et al. Single-cell transcriptomics of human T cells reveals tissue and activation signatures in health and disease. Nature Communications. 2019;10(1):4706.

68. Mair F, Hartmann FJ, Mrdjen D, Tosevski V, Krieg C, Becher B. The end of gating? An introduction to automated analysis of high dimensional cytometry data. Eur J Immunol. 2016;46(1):34-43.

69. Hollt T, Pezzotti N, van Unen V, Koning F, Eisemann E, Lelieveldt B, et al. Cytosplore: Interactive Immune Cell Phenotyping for Large Single-Cell Datasets. Comput Graph Forum. 2016;35(3):171-80.

70. van der Maaten L, Hinton, G. Visualizing Data using t-SNE. Journal of Machine Learning Research. 2008.

71. Van Gassen S, Callebaut B, Van Helden MJ, Lambrecht BN, Demeester P, Dhaene T, et al. FlowSOM: Using self-organizing maps for visualization and interpretation of cytometry data. Cytometry A. 2015;87(7):636-45.

72. Maecker HT, Rinfret A, D'Souza P, Darden J, Roig E, Landry C, et al. Standardization of cytokine flow cytometry assays. BMC Immunology. 2005;6(1):13.

CYTOFAST: A WORKFLOW FOR VISUAL AND QUANTITATIVE ANALYSIS OF FLOW AND MASS CYTOMETRY DATA TO DISCOVER IMMUNE SIGNATURES AND CORRELATIONS

2

ABSTRACT

Multi-parametric flow and mass cytometry allows exceptional high-resolution exploration of the cellular compo- sition of the immune system. A large panel of computational tools have been developed to analyze the high- dimensional landscape of the data generated. Analysis frameworks such as FlowSOM or Cytosplore incorporate clustering and dimensionality reduction techniques and include algorithms allowing visualization of multi- parametric cytometric analysis. To additionally provide means to quantify specific cell clusters and correlations between samples, we developed an R-package, called *cytofast*, for further downstream analysis. Specifically, *cytofast* enables the visualization and quantification of cell clusters for an efficient discovery of cell populations associated with diseases or physiology. We used *cytofast* on mass and flow cytometry datasets based on the modulation of the immune system upon immunotherapy. With *cytofast,* we rapidly generated visual representations of group-related immune cell clusters and showed correlations with the immune system composition. We dis- covered macrophage subsets that significantly decrease upon cancer immunotherapy and distinct prime-boost effects of prophylactic vaccines on the myeloid compartment. *Cytofast* is a time-efficient tool for comprehensive cytometric analysis to reveal immune signatures and correlations. *Cytofast* is available at Bioconductor.

Comput Struct Biotechnol J. 2018 Oct 24;16:435-442

Guillaume Beyrend [a,*], Koen Stam [b], Thomas Höllt [c], Ferry Ossendorp [a], Ramon Arens [a]

[a] Department of Immunohematology and Blood Transfusion, Leiden University Medical Center, Albinusdreef 2, Leiden 2333 ZA, The Netherlands
[b] Department of Parasitology, Leiden University Medical Center, Leiden, The Netherlands
[c] Department of Computer Graphics and Visualization Group, Faculty of Electrical Engineering, Mathematics and Computer Science, Delft University of Technology, Delft, the Netherlands

INTRODUCTION

Mass cytometry (cytometry by time-of-flight; CyTOF) can detect as many as 40 markers present on millions of single cells. The number of studies based on mass cytometry has considerably increased over the last few years, broadening simultaneously the choice of clustering tech- niques, such as SPADE (1), FlowMaps (2), FlowSOM (3), Phenograph (4), VorteX (5) and Scaffold maps (6), but also dimensionality reduction- based techniques including PCA (7), t-SNE (8) and Diffusion Map (9). A recent new computational tool, HSNE (10), embedded in Cytosplore (11), proposed a combination of the two aforementioned techniques, building a hierarchical representation of the complete data that pre- serves the non-linear high-dimensional relationships between cells and avoids any down-sampling (12). The aforementioned computation- al tools lack, however, the means for downstream analysis, where no automatic process has been proposed to link clusters abundance with e.g. clinical outcome and to visually interpret the data in the context of the experimental setup. Citrus (13) is currently a broadly used analy- sis tool for statistical comparison but presents several limitations. The number of samples to be included in such analysis should be more than eight and the number of cells are randomly downsampled before analysis. Moreover, Citrus is using agglomerative clustering, which brings complexity in data visualization.

Here, we developed a workflow, called *cytofast*, for a fast and quan- titative analysis of flow and mass cytometry data. *Cytofast* allows the vi- sualization of cluster phenotypes, their abundance per sample and per group and additionally enables statistical comparisons taking in account different clinical outcome variables.

We verified our workflow on a non-paired mass cytometry dataset originating from a published study focused on differences between ef- fective and ineffective treatment. We also demonstrated the use of *cytofast* on a paired dataset of a prime-boost vaccination study. In addi- tion, we verified *cytofast* on a flow cytometry dataset. Together these analyses showed that our workflow is valid, replicating similar findings previously described and in addition provided a deeper exploration of the data by newly identifying cell clusters that correlate to treatment.

RESULTS AND DISCUSSION

Cytofast: workflow presentation

We designed an R package, named *cytofast*, and introduced a workflow to quantify and identify significant group-related subsets. *Cytofast* can be used after cluster analysis (for example with Cytosplore or FlowSOM) has been performed. Here, we fo- cused on the clustering analysis with Cytosplore using mass and flow cytometry datasets.

The workflow of *cytofast* can be divided in four parts (Fig. 1). First, a heatmap with a dendrogram is generated showing the median ArcSinh- transformed marker expression values (blue-to-red scale) for all the identified clusters (cluster phenotype overview). Second, a quantitative heatmap is generated showing the cell frequency calculated for

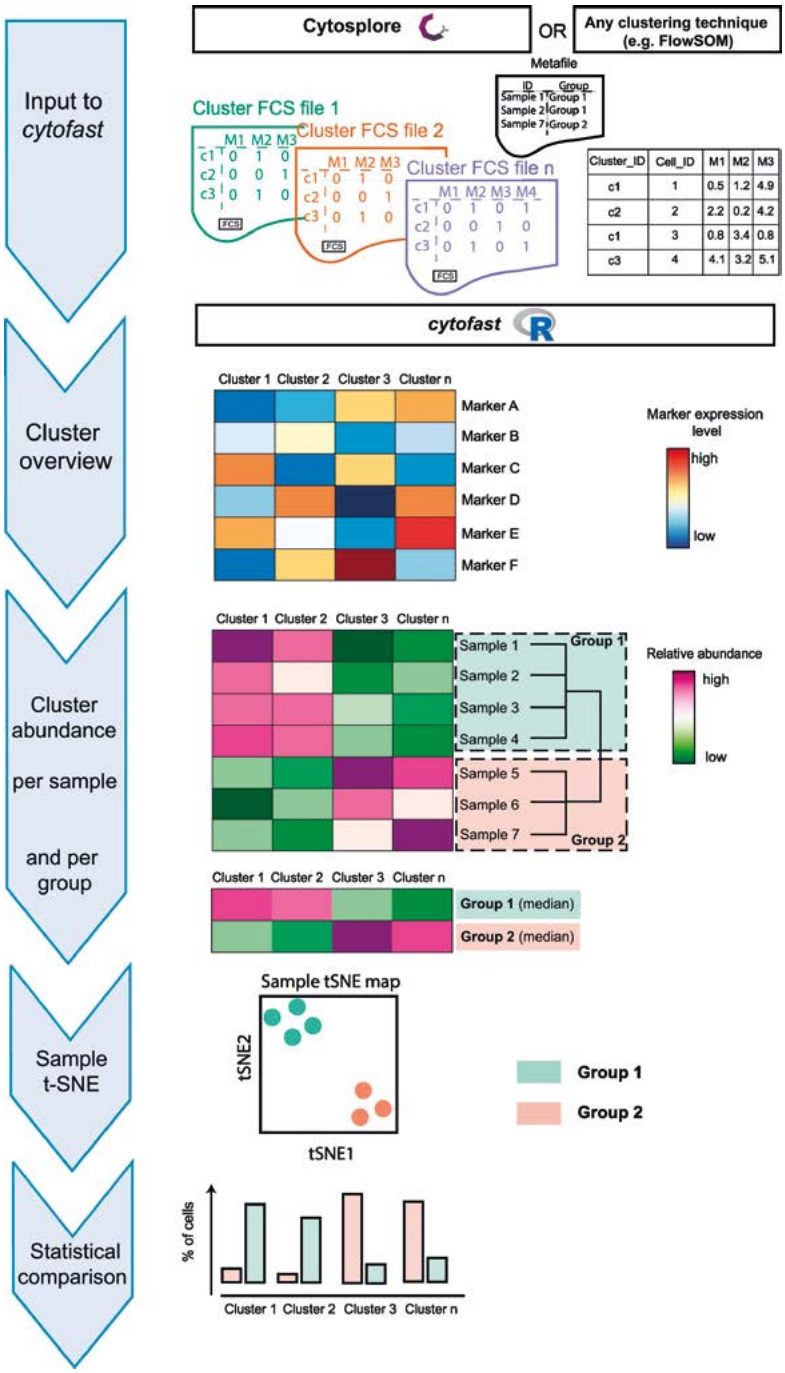

Figure 1. Schematic overview of the *cytofast* workflow. Flow and mass cytometry data processed by Cytosplore or other clustering techniques (e.g. FlowSOM) can be used as input for quantification and exploration of cell subset clusters. Cluster visualization, cluster abundance per sample and quantitative comparisons are automated and displayed in a user-friendly manner.

each cluster stratified per individual sample. Thus, one row is representing one biological sample and the identified subsets are displayed per column (cluster abundance per sample). A dendro- gram, represented on the side of the panel, indicates the clustering of the samples sharing phenotypic similarities. Hierarchical clustering was performed on subset frequencies using the Euclidean distance and complete linkage clustering. The summary of the quantitative heatmap can be displayed underneath taking in account the median abundance of each cluster per group. Next, a dimensionality reduction analysis based on cluster fre- quency is performed. As a result, a t-SNE map is drawn, where one dot is representing one sample colored by group assignment, proposing an alternative way to represent similarities between samples. Finally, the abundance of each cluster per group is repre- sented in a quantitative bar graph. Statistical comparison is per- formed to highlight significant changes in cluster abundance between groups.

Cytofast applied to a non-paired mass cytometry datasets: comparison between effective and ineffective cancer immunotherapy

We tested our workflow on an unpaired mass cytometry data set from *Spitzer et al.* (14). The authors characterized two effective therapies in mice by a combination of tumor-binding antibodies and adjuvants (B6-alloIgG + anti-CD40 + IFN-γ, CD-1-alloIgG + anti-CD40 + IFN- γ; together called Eff) and compared these to two ineffective therapies (15) (anti-PD-1, no treatment; together called Ineff).

The experimental mouse model used was the spontaneous MMTV-PyMT (murine mam- mary tumor virus-polyoma middle T) model of breast cancer, which is refractory to other immunotherapies such as checkpoint blockade (i.e. anti-PD-1). At an early (Day 3) and later (Day 8) stage, mice were sacrificed and immune cells analyzed (n = 3–4 per treatment, per timepoint). We focused on comparing the effective and ineffective immune responses in the spleen at the two different timepoints. The data from the two effective and the two ineffective treatments were combined, resulting in one large effective treated group and one large ineffective treated group. Next, the data from the early and later timepoints of the effective and ineffective treated groups were pooled, resulting in four different groups. This approach allows then the simultaneous analysis of both treatment and time.

Upon processing the data (containing 3.8 million cells) with Cytosplore, thirty-one clusters could be identified (Fig. 2A), and included distinct subsets of cytotoxic T cells (clusters 12, 16), helper T cells (e.g. clusters 17, 28), B cells (e.g. clusters 29, 22, 30), myeloid cells (e.g. cluster 21 identifying granulocytes) and erythroid lineages (clusters 4 and 27). The generated abundance heatmap for each individual sample quantitatively compared the abundance of each cluster be- tween ineffective and effective groups or between an early (Day 3) and late (Day 8) response, (Fig. 2B). The two treatment groups (inef- fective and effective) on the dendrogram of the heatmap could be distinguished.

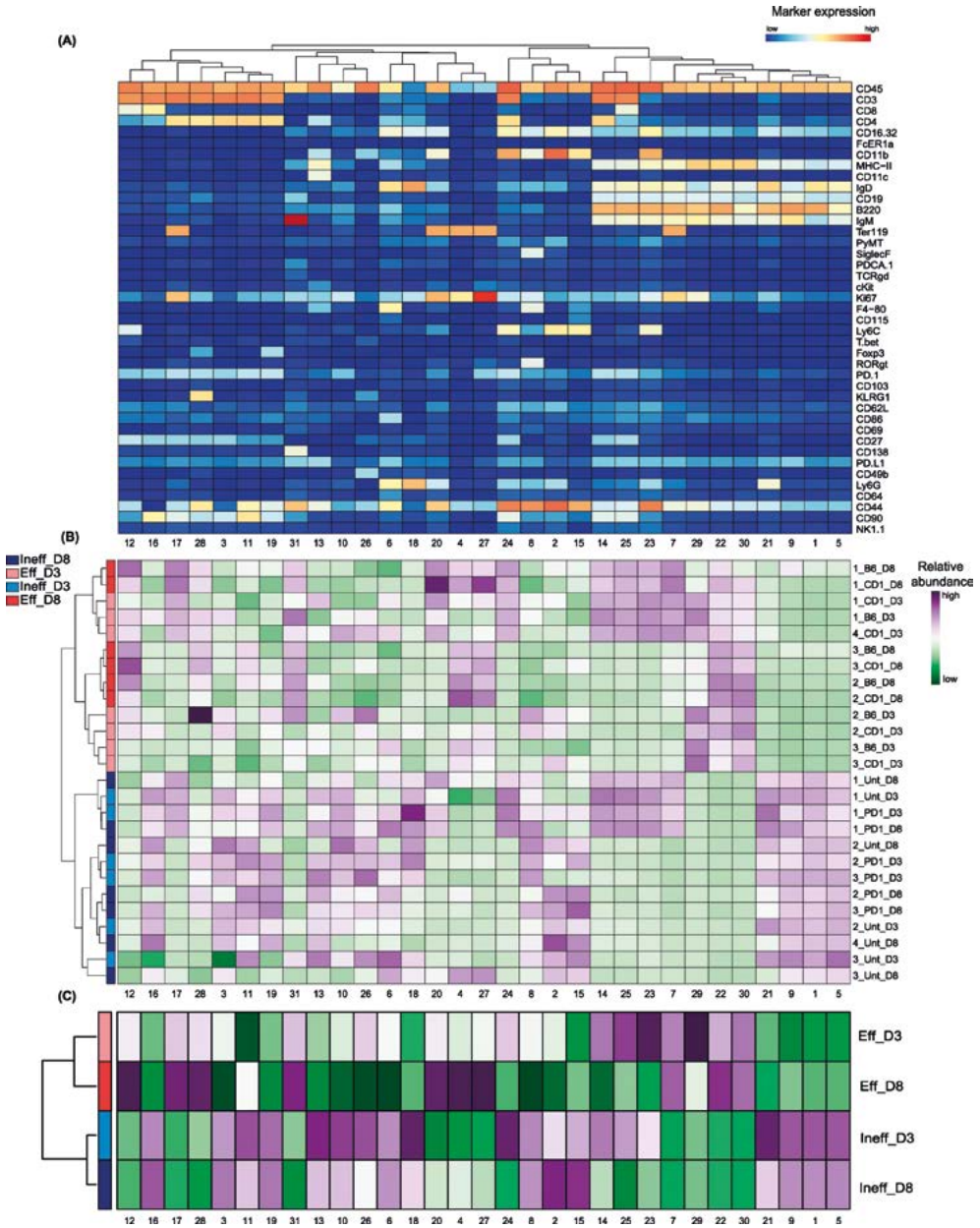

Figure 2. Identification and abundance of CD45⁺ cell clusters by *cytofast*. (A) Mass cytometry data of CD45⁺ immune cells in the spleen of mice that received effective and ineffective treatment at two different timepoints (Day 3 and Day 8). Heatmap of all 31 CD45⁺ cell clusters identified independent of treatment based on Cytosplore clustering. Level of ArcSinh5- transformed expression marker is displayed by a blue-to-red scale. Dendrogram on the top represents the hierarchical similarity between the identified clusters and is based on Euclidean distance and complete linkage clustering. (B) Heatmap of relative abundance (expressed as variance or dispersion from the mean) for each cluster identified above in each individual mouse. One row is representing one mouse sample,

subsets are displayed per column. A green or a purple square is representative of a lower or a higher number of cells, respec- tively, compared to the average. The dendrogram displayed on the left is based on hierarchical clustering using Euclidean distance and complete linkage clustering. (C) Summary of the data represented on the panel above by using the median for each group.

The summary heatmap, which displays the data based on the median of each group, is displayed to recapitulate the observed changes (Fig. 2C).

Based on the abundance of each cluster per sample, we established a sample-t-SNE map (Fig. 3A). We could reveal that the ineffective treated mice clustered together and that also the effective treated mice clustered, irrespective of the time-point of analysis. The absence of substantial differences on the immune system at an early stage (Day 3) or later stage (Day 8) indicates that the treatment effect is rapid and remains prevailing in time. We next analyzed the abundance of each cluster per group and per timepoint (Fig. 3B). We established that B cells ex- pressing MHC class II (MHC-II) (clusters 29, 22 and 30) were more abundant upon effective treatment. Moreover, we newly identified two myeloid clusters (clusters 6 and 8), which were significantly reduced upon effective therapy, specifically at a later stage. These two subsets presented the highest expression in F4/80 among all the identified clusters (cluster 6: F4/80+/Ly6G+/CD44+/IgD+, cluster 8: F4/80+/ CD11b+/Siglec-F+).

In conclusion, our workflow enables the overview of a large data set containing four different groups and improves the profiling of immune subsets that relate to therapy.

Cytofast applied to paired mass cytometry datasets: effect of prime-boost vaccination

To analyze paired samples by *cytofast*, we selected a partial dataset from *Palgen et al.* (16). The mass cytometry data consists of blood im- mune cells analysed one day after first and second immunization of cy- nomolgus macaques with modified vaccinia virus Ankara (MVA).

The clustering analysis from Cytosplore identified twenty-three clusters, whose phenotype were presented by the heatmap (Fig. 4A). The abundance of each cluster stratified per sample showed a clear dis- tinction between the immune response after prime and boost (Fig. 4B). The difference between the two groups are clearly represented by the sample t-SNE map (Fig. 5A). The two populations after prime and boost are distinct, and do not cluster per individual, revealing that the variation triggered on the immune system of each individual is stronger than their intrinsic immune signature. The average abundance of each cluster per group can be displayed in bar graphs, and such quantification of the data allows thus direct comparisons between groups. We choose to characterize here the difference between the two groups by paired analysis for each identified cluster (Fig. 5B). After prime, certain cell subsets (characterized by $CCR7^+$, $IL\text{-}8^+$ and $IL\text{-}10^+$) were absent but these were specifically detected after boost (clusters 1, 7, 12, 14, 15, 16). Conversely, other clusters, displaying low cytokine levels like

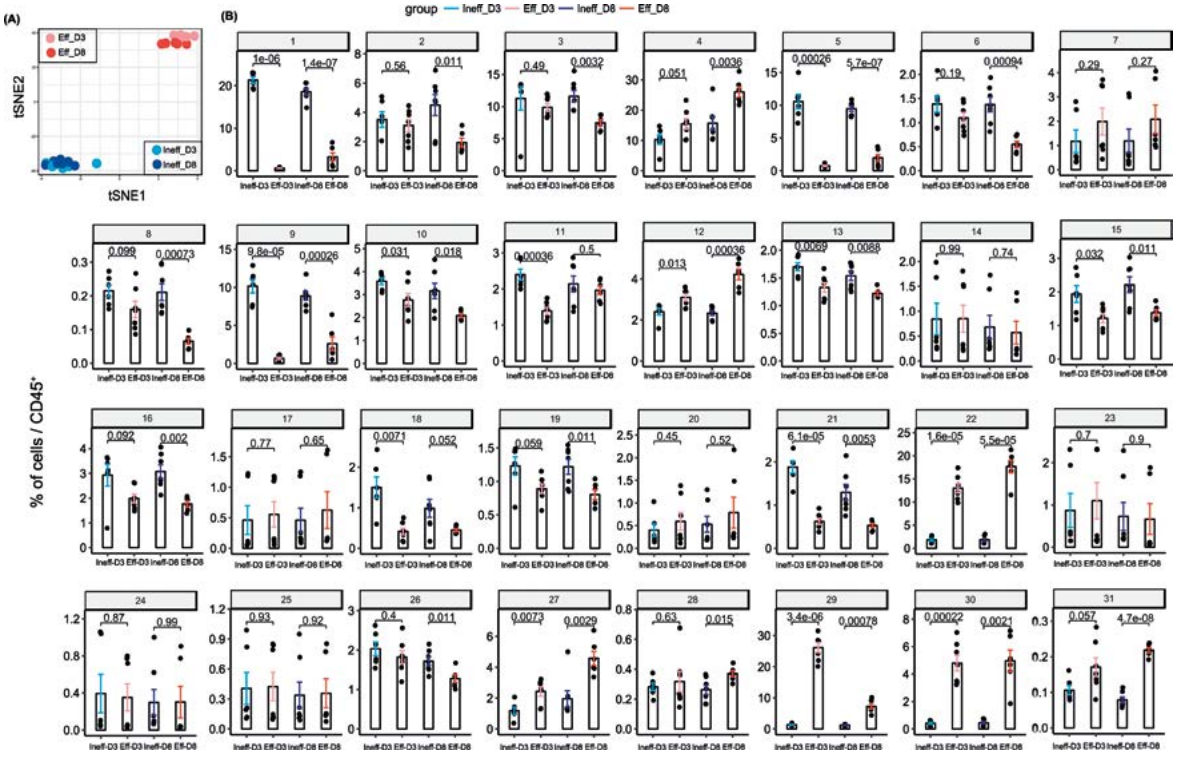

Figure 3. Quantitative comparison of cell clusters from unpaired samples by *cytofast*. (A) Sample t-SNE of the data of Fig. 2 where one dot is representing one sample, based on the cluster frequencies. The two groups, ineffective and effective, can be clearly distinguished, showing that the immune system is differently shaped by treatment efficiency. (B) Bar graphs representing the average of each sample per group overlaid with the dot plots representing the percentage of the cluster for each sample. P-values are provided to indicate significant differences between the ineffective and the effective group for both timepoints. Statistical analysis was performed on individual clusters (annotated from 1 to 31) using a t-test.

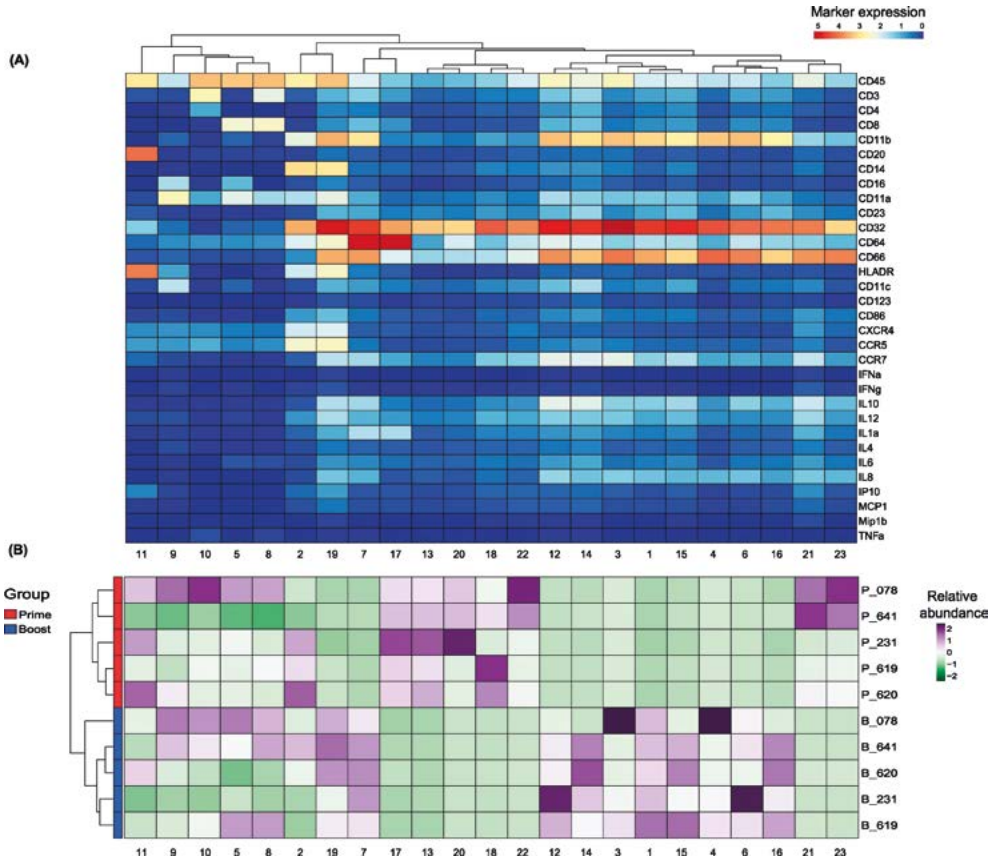

Figure 4. Identification and abundance of CD45⁺ cell clusters in the blood of cynomolgus macaques after prime and boost immunization with modified vaccinia virus Ankara. (A) Heatmap of all 23 CD45⁺ cell clusters identified independent of treatment based on Cytosplore clustering. Level of ArcSinh5-transformed expression marker is displayed by a blue-to-red scale. Den- drogram on the top represents the hierarchical similarity between the identified clusters. Dendrogram displayed above is based on hierarchical clustering using Euclidean distance and complete linkage clustering. (B) Heatmap of relative abundance (expressed as variance or dispersion from the mean) for each cluster identified above in each individual macaque. One row is representing one macaque blood sample, subsets are displayed per column. A green or a purple square is representative of respectively a lower or a higher number of cells compared to the average. Dendrogram displayed on the left is based on hierarchical clustering using Euclidean distance and complete linkage clustering.

IL- 10, IL-8 or the CCR7 receptor were only identified after prime but absent after boost (clusters 17, 18, 20, 21, 22, 23).

Cytofast applied to flow cytometry data

With proper adjustment of the clustering in Cytosplore, *cytofast* can also be applied to flow cytometry datasets. We tested here a flow cytometry dataset comparing phenotypes

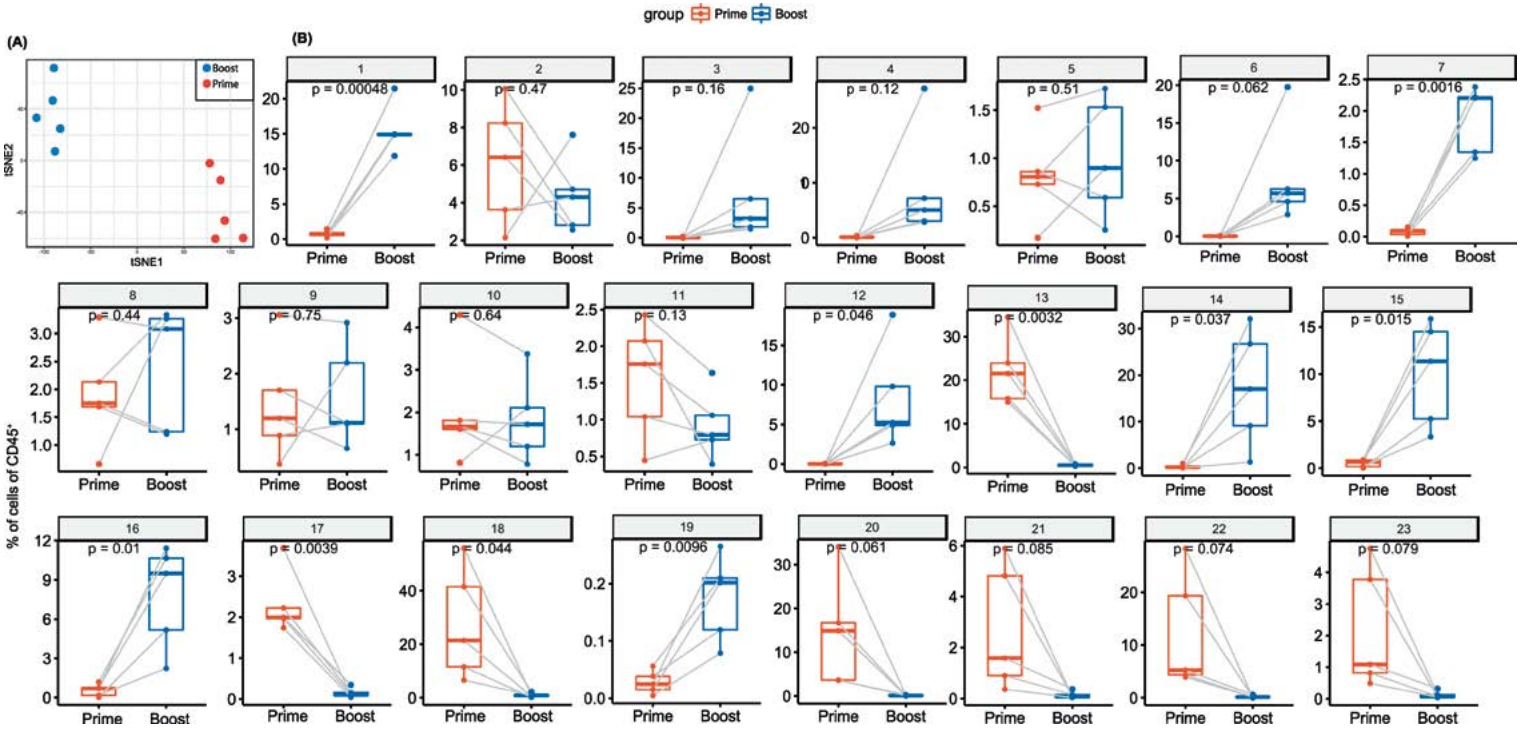

Figure 5. Quantitative comparison of cell clusters from paired samples by *cytofast*. (A) Sample t-SNE where one dot is representing one sample, based on the sample frequencies. The two groups can be clearly distinguished, showing that the immune system is differently shaped upon the two immunizations. (B) Box plots representing the average and standard deviation of each sample per group. Samples are paired. P-values are provided to indicate the significance between different groups. Statistical analysis was performed for each individual cluster (annotated from 1 to 23) using a t-test.

of blood cells between patients suffering from acute myeloid leukemia (AML) and non-affected patients (17) (downloaded from FlowRepository (18)). After processing six ran- dom samples from each group (non-affected patients called *Normal*, and affected patients called *AML*), we applied *cytofast* and obtained a similar visualization output to mass cytometry data (Fig. S1). Thus, *cytofast* is also operational for visualization of complex flow cytometry data sets and can rapidly identify immune subset changes between groups.

CONCLUSION

Here we report the helpfulness of an R-based workflow, named *cytofast*, which is designed for visual and quantitative analysis of flow and mass cytometry data to discover immune signatures and correla tions. We used a non-paired dataset generated by Spitzer and colleagues in which the effects of immunotherapy were examined, and newly identified with *cytofast* two macrophage clusters ($F4/80^+$/$Ly6G^+$/ $CD44^+$/ IgD^+ and $F4/80^+$/ $MHC\text{-}II^+$/ $Siglec\text{-}F^+$) that were significantly reduced upon effective therapy, specifically at a later stage. In a prophy- lactic vaccine study by Palgen and colleagues, paired samples were analysed and showed clear booster effects of the vaccine on myeloid cell subsets. The usefulness of *cytofast* to distinguish different immune signatures between groups was also observed with flow cytometry datasets of immune cells in the blood of leukemia patients and non- affected individuals.

Some of the displayed clusters appear highly similar in the heatmaps. It is optional for the user to merge similar clusters. Such clus-ter merging might remove subtleties, yet this might also make the results more robust against individual sample variation or batch effects.

For all tested datasets, *cytofast* yielded rapid results. With standard modern computer hardware and specifications (32GB RAM memory), the output was produced in less than thirty seconds (excluding clustering analysis with e.g. Cytosplore), making this tool highly suitable for a rapid and visual data screening.

MATERIAL AND METHODS

Use of clustering method

The two cohort mass cytometry datasets were downloaded from *Cytobank.*

Use of cytosplore

The files were uploaded to Cytosplore, already pre-gated by the original authors. Files were sample-tagged by adding the CSPRL_ST channel, their marker expression arcsinh5 transformed and subjected to dimensionality reduction. The iterations chosen of the HSNE analysis were 1,000. We clustered the data with a kernel size sigma of 30 on the over-view level and exported the resulting clusters without manually modifying it. Lastly, in R we used *cytofast* for further analysis of those files.

Use of other clustering method

The use of *cytofast* is not restricted to a pre-processing of the data with Cytosplore. Most of the clustering providing a cluster assignment to each cell can be used (e.g. FlowSOM as detailed in the *vignette*).

Use of cytofast

Our workflow is linked to the use of an upstream clustering tools such as Cytosplore or FlowSOM. We load the clusters produced by applying the HSNE dimensionality reductions and mean shift clustering in Cytosplore and saved as FCS files. After loading the FCS files of all clusters, *cytofast* analysis is based on the sample characteristics written to a single file, gathering relevant information like sample name, clinical outcome and sample tag (also named CSPRL_ST in Cytosplore). The clinical input can be any qualitative clinical data like gender, or group affiliation, or quantitative like tumor size or age.

The *vignette*, where all the steps are explained to facilitate the repro- ducibility of the figures and the package itself will be deposited on Bioconductor. A downsampled number of cells from the *Spitzer* study is included in the vignette. Differences might be seen between the downsampled dataset provided in the vignette and the analysis from this paper due to the downsampling.

Flow cytometry data

We confirmed that our R script was also valid to represent flow cytometry datasets. We downloaded data files from FlowRepository (https://flowrepository.org/id/FR-FCM-ZZYA) and selected six patients per group (Files 0006.FCS, 0014.FCS, 0022.FCS, 0030,FCS, 0046.FCS, 0062.FCS from the *Normal* group; Files 0038.FCS, 0070.FCS, 0206.FCS, 0262. FCS, 0294.FCS, 0390.FCS from the *AML* group). Data was clustered with Cytosplore, clusters sharing high similarities were manually merged and the resulted output were processed with *cytofast*.

AUTHOR CONTRIBUTIONS

GB wrote the manuscript and the workflow. KS wrote and embedded the workflow into the R package *cytofast*. TH reviewed the manuscript and gave conceptual input. FO gave conceptual input. RA wrote the manuscript and supervised the project.

CONFLICT OF INTEREST

The authors declare no financial or commercial conflict of interest.

ACKNOWLEDGMENTS

We acknowledge funding from the European Commission of a H2020 MSCA award under proposal number 675743 (ISPIC).

APPENDIX A. SUPPLEMENTARY DATA

Supplementary data to this article can be found online at https://doi. org/10.1016/j.csbj.2018.10.004.

REFERENCES

1. Anchang B, et al. Visualization and cellular hierarchy inference of single-cell data using SPADE. Nat Protoc 2016;11(7):1264–79.
2. Zunder ER, et al. A continuous molecular roadmap to iPSC reprogramming through progression analysis of single-cell mass cytometry. Cell Stem Cell 2015;16(3): 323–37.
3. Van Gassen S, et al. FlowSOM: Using self-organizing maps for visualization and in- terpretation of cytometry data. Cytometry A 2015;87(7):636–45.
4. Levine JH, et al. Data-driven phenotypic dissection of AML reveals progenitor-like cells that correlate with prognosis. Cell 2015;162(1):184–97.
5. Samusik N, et al. Automated mapping of phenotype space with single-cell data. Nat Methods 2016;13(6):493–6.
6. Spitzer MH, et al. IMMUNOLOGY. An interactive reference framework for modeling a dynamic immune system. Science 2015;349(6244):1259425.
7. Hotelling H. Analysis of a complex of statistical variables into principal components. J Edu Psychol 1933;24(6):417–41.
8. Maaten LJP, Hinton GE. Visualizing high-dimensional data using t-SNE. J Mach Learn Res 2008;9:2579–605.
9. Haghverdi L, Buettner F, Theis FJ. Diffusion maps for high-dimensional single-cell analysis of differentiation data. Bioinformatics 2015;31(18):2989–98.
10. Pezzotti N, et al. Hierarchical Stochastic Neighbor Embedding. Comp Graph Forum 2016;35(3):21–30.
11. Hollt T, et al. Cytosplore: Interactive immune cell phenotyping for large single-cell datasets. Comp Graph Forum 2016;35(3):171–80.
12. van Unen V, et al. Visual analysis of mass cytometry data by hierarchical stochastic neighbour embedding reveals rare cell types. Nat Commun 2017;8(1):1740.
13. Bruggner RV, et al. Automated identification of stratifying signatures in cellular sub- populations. Proc Natl Acad Sci U S A 2014;111(26):E2770–7.
14. Spitzer MH, et al. Systemic immunity is required for effective cancer immunotherapy. Cell 2017;168(3):487–502.
15. Bos PD, et al. Transient regulatory T cell ablation deters oncogene-driven breast can- cer and enhances radiotherapy. J Exp Med 2013;210(11):2435–66.
16. Palgen JL, et al. Prime and boost vaccination elicit a distinct innate myeloid cell immune response. Sci Rep 2018;8(1):3087.
17. Aghaeepour N, et al. Critical assessment of automated flow cytometry data analysis techniques. Nature Methods 2013;10:228.
18. Spidlen J, et al. FlowRepository: a resource of annotated flow cytometry datasets associated with peer-reviewed publications. Cytometry A 2012;81(9):727–31.

3

VISUALIZATION AND QUANTIFICATION OF HIGH-DIMENSIONAL CYTOMETRY DATA USING CYTOFAST AND THE UPSTREAM CLUSTERING METHODS FLOWSOM AND CYTOSPLORE

ABSTRACT

The complexity of data generated by mass cytometry has necessitated new tools to rapidly visualize analytic outcomes. Clustering methods like *Cytosplore* or *FlowSOM* are used for the visualization and identification of cell clusters. For downstream analysis, a newly developed R package, *Cytofast*, can generate a rapid visualization of results from clustering methods. *Cytofast* takes into account the phenotypic characterization of cell clusters, calculates the cell cluster abundance, then quantitatively compares groups. This protocol explains the applications of *Cytofast* to the use of mass cytometry data based on modulation of the immune system in the tumor microenvironment (i.e., the natural killer [NK] cell response) upon tumor challenge followed by immunotherapy (PD-L1 blockade). Demonstration of the usefulness of *Cytofast* with *FlowSOM* and *Cytosplore* is shown. *Cytofast* rapidly generates visual representations of group-related immune cell clusters and correlations with immune system composition. Differences are observed in the clustering analysis, but separation between groups are visible with both clustering methods. *Cytofast* visually shows the patterns induced by PD-L1 treatment that include a higher abundance of activated NK cell subsets, expressing a higher intensity of activation markers (i.e., CD54 or CD11c).

Video Link

The video component of this article can be found at https://www.jove.com/video/60525/
URL: https://www.jove.com/video/60525 DOI: doi:10.3791/60525

Keywords: Immunology and Infection, Issue 154, flow and mass cytometry analysis, R package, high-dimensional analysis, single-cell analysis, visualization tool, data mining

Citation: Beyrend, G., Stam, K., Ossendorp, F., Arens, R. Visualization and Quantification of High-Dimensional Cytometry Data using Cytofast and the Upstream Clustering Methods FlowSOM and Cytosplore. *J. Vis. Exp.* (154), e60525, doi:10.3791/60525 (2019).

J Vis Exp. 2019 Dec 12;(154)

Guillaume Beyrend[1], Koen Stam[2], Ferry Ossendorp[1], Ramon Arens[1]

[1] Department of Immunohematology and Blood Transfusion, Leiden University Medical Center
[2] Department of Parasitology, Leiden University Medical Center

INTRODUCTION

Mass cytometry (cytometry by time-of-flight, or CyTOF) allows detection of a wide range of intracellular or extracellular biomarkers in millions of single cells. The high-dimensional nature of mass cytometry data necessitates certain analysis tools, such as cell clustering techniques like *SPADE*(1), *FlowMaps* (2), *FlowSOM* (3), *Phenograph* (4), *VorteX*(5), and *scaffold maps*6. In addition, various dimensionality reduction-based techniques have been developed (i.e., principal component analysis [PCA] (7), t-distributed stochastic neighbor embedding [t-SNE] (8), hierarchical stochastic neighbor embedding [HSNE] (9), uniform manifold approximation and projection [UMAP] (10), and diffusion maps (11)) to improve the speed, interpretation and visualization of high-dimensional datasets.

Downstream analysis of high-dimensional flow and mass cytometric data often lacks automatic processes to perform statistical tests on cluster frequency and links with clinical outcomes. Previously, we developed an R-based workflow known as *Cytofast*[12], which allows for visual and quantitative downstream analyses of clustering techniques by *Cytosplore* or *FlowSOM*.

The protocol described here clarifies the use of *Cytofast* in R and shows how to generate quantitative and qualitative heatmaps and graphs. Furthermore, it facilitates the determination of connections between observed immune phenotypes and clinical outcomes. This report also describes the analysis of a specific mass cytometry dataset using two different clustering procedures: *FlowSOM* and *Cytosplore*. By using *Cytofast* with both clustering methods, it is correspondingly shown that the activation phenotype of NK cells is influenced by PD-L1 immune checkpoint blockade.

PROTOCOL

All animal experiments were approved by the Animal Experiments Committee of LUMC and were executed according to the animal experimentation guidelines of the LUMC in compliance with the guidelines of Dutch and European committees.

NOTE: For experimental set-up, C57BL/6 mice were subcutaneously inoculated on the right flank with the murine colon tumor MC38 at a concentration of 0.3 x 10^6 cells/200 µL of phosphate-buffered saline (PBS). After 10 days, when tumors were palpable, the mice were treated with PD-L1 blocking antibodies (clone MIH-5, 200 µg/mouse, intra-peritoneal injection) or were mock-treated. The tumors were resected 3 days later after PD-L1 injection, processed ex vivo, and analyzed by CyTOF mass cytometry using 38 markers (13).

Equipment and Software for Data Analysis

NOTE: Use a computer (Windows 7 or newer) and processor I5 at 2.4 GHz or equivalent, installed memory RAM 6 GB, and 10 GB of free hard drive space. The R package *Cytofast* uses existing functions: mainly *flowCore*, *pheatmap*, and *ggplot*. The command lines

to be executed in R are included in the protocol. The resource for R instructions can be found at https://education.rstudio.com/.

1. To install the *Cytofast* package, start R (version "3.6") and install *Bioconductor* version 3.9 by entering the following code: if (!requireNamespace("BiocManager", quietly = TRUE))
   install.packages("BiocManager")BiocManager::install("cytofast")
2. Ensure that the package is loaded in the desired environment by running the following: library(cytofast)

Creating Clusters

NOTE: To showcase the two clustering methods *Cytosplore* and *FlowSOM* with *Cytofast*, the NK cells ($CD161^+$) in the tumor micro-environment 3 days after PD-L1 treatment are analyzed.

1. Clustering performed by *Cytosplore*
   1. After downloading and installing *Cytosplore*, hosted at <www.*Cytosplore*.org>, upload the .fcs files (**Supplementary Files 1.1–1.8** [Cytosplore input files]) by clicking **File | Open FCS File(s)** in *Cytosplore*. Add a unique sample tag as channel by clicking **Add unique sample tag as channel** when prompted and select a cofactor for hyperbolic arcsinh transformation (default is 5).
   2. Select **Run H-SNE**, run a HSNE level of 3, and wait for the map to be generated.
      NOTE: This step may require some time, depending on the number of cells analyzed and level of HSNE chosen.
   3. On the first HSNE level, check the cells that are positive for CD161. Select the $CD161^+$ cells and right-click **Zoom into selection**. At the second level, repeat the procedure to reach the third level with only $CD161^+$ events.
   4. Once the last tSNE map is generated, save the clusters defined by *Cytosplore* by right-clicking on the tSNE map and choose **Save Clusters**. Choose the directory of the output files as prompted by *Cytosplore* and note this location, because this directory will then be used to load the .fcs files into R.
      NOTE: The number of subsets can be manually changed by changing the sigma value. The sigma value is set by default at 30; however, the actual number of subsets depends on the input. Here, *Cytosplore* detected 10 different subsets, with each file representing one subset.
   5. Use a simple name (characters only) when renaming the output files, which will make identification and further handling easier. Save the output files by selecting **Save**.
      NOTE: After saving, a folder is being created by *Cytosplore* with the .fcs files, with each file corresponding to the identified clusters in *Cytosplore*. The next step will be loading the files into R with the help of *Cytofast*. Here, the generated

output files are provided in **Supplementary Files 2.1–2.10** (Cytosplore output files).

6. Load the output files generated by *Cytosplore* into R with the designated function: readCytosploreFCS. dirFCS <- "C:\\Users\\username\\Desktop\\tostudy"
   cfData <- readCytosploreFCS(dir = dirFCS, colNames = "description")
7. Clean the data by removing some parameters such as "Time" and "Background". Check the position of the column related to its unnecessary parameters and remove it from the matrix.
   colnames(cfData@expr)
   cfData@expr <- cfData@expr[,-c(3,4,6,8:10,46:49,51:54)]
   NOTE: The unnecessary columns can be seen by reading the column names of the generated matrix. By running colnames(cfData@expr) once more, ensure that only the desired parameters are obtained.
8. Re-order the markers so that lineage markers are displayed first, followed by functional markers. cfData@expr <- cfData@expr[,c(1,2,3,35,36,31,9,10,18,8
   ,37,20,
   29,40,5,30,33,11,34,14,19,
   32,28,6,7,4,12,13,17,16,15,
   21,22,24,25,26,27,38,39)]
   NOTE: Step 2.1.8 is optional.
9. Link the meta datafile to the generated data from *Cytosplore* by uploading the spreadsheet metafile containing clinical information (**Supplementary File 3**).
   library(readxl)
   meta <- read_excel("C:\\Users\\username\\Desktop\\sample_id.xlsx") cfData@samples <- data.frame(meta)
   NOTE: The clustering being performed by *Cytosplore* is now finished. An alternative clustering option to *Cytosplore* is *FlowSOM* and is described in section 2.2. Once one of the two clustering steps is performed, proceed with the visualization step (section 3).

2. Clustering performed by *FlowSOM*
   1. First install *FlowSOM* in R by running the following command: if (!requireNamespace("BiocManager", quietly = TRUE)) install.packages("BiocManager") BiocManager::install("FlowSOM")
      library(FlowSOM)
   2. Install the flowCore package using a similar method and load it in the environment by running the following: if (!requireNamespace("BiocManager", quietly = TRUE))
      install.packages("BiocManager")
      BiocManager::install("flowCore")library(FlowSOM)

3. Load the raw data provided in **Supplementary Files 4.1–4.8** (FCS FlowSOM input), which were previously gated on CD161+ events, in R with the read.flowSet function.
   fcs_raw <- read.flowSet(path="C:\\Users\\username\\Desktop\\tocluster", pattern = ".fcs", transformation = FALSE, truncate_max_range = FALSE, seed=123)
4. Select the relevant biological markers (remove "Background" or "Time") by selecting the proper columns and transform the data in an arcsinh5 manner as shown in the code below (here, remove columns 1, 2, 4, 5, 6, 17, 21, 24, 25, 34, 35, 37, 38, 51, which do not correspond to any biological marker). Apply a cofactor of 5 as previously applied with *Cytosplore*, by choosing **cofactor=5** in the function below.
   fcs_raw <- fsApply(fcs_raw, function(x, cofactor=5){ colnames(x) <- fcs_raw[[1]]@parameters@data$desc expr <- exprs(x)
   expr <- asinh(expr[,-c(1,2,4,5,6,17,21,24,25,34,35,37,38,51)]/ cofactor) exprs(x) <- expr
   return(x)})
5. Cluster the data using the *FlowSOM* function. To compare *FlowSOM* and *Cytosplore*, choose to cluster the data in ten subsets as the output previously yielded by *Cytosplore*.
   fsom <- FlowSOM(fcs_raw, transformFunction = FALSE, scale = FALSE, scaled.center = FALSE, scaled.scale = FALSE, silent = FALSE, colsToUse = c(1:37), nClus = 10, maxMeta = 10, importance = NULL, seed = 123)
   NOTE: This can be changed manually by the user.
6. Assign each cell to its identified subset and sample ID. subset_id <- as.factor(fsom$FlowSOM$map$mapping[,1]) levels(subset_id) <- fsom$metaclustering
   head(subset_id)
7. Load the metadata file in R (available in **Supplementary File 5**) containing the group assignment and link it to the .fcs files. sampleid <- read_excel("C:\\Users\\username\\Desktop\\sample_id.xlsx")
   sampleid <- na.omit(sampleid)
   sampleid$sampleID <- as.factor(sampleid$sampleID) sampleid$group <- as.factor(sampleid$group) sampleid$CSPLR_ST <- as.factor(sampleid$CSPLR_ST) sampleid <- as.data.frame(sampleid)
   names(sampleid)[3] <- "sampleID"
   sampleID <- lapply(fsom$FlowSOM$metaData, function(x){rep(x[1], each = length(x[1]:x[2]))}) attr(sampleID, 'names') <- NULL
   sampleID <- as.factor(unlist(sampleID)) sampleid <- data.frame(sampleid)
   levels(sampleID) <- paste("ID", 1:dim(sampleid)[1], sep="_")

df <- data.frame(subset_id, sampleID, fsom$FlowSOM$data[, c(1:37)]) rename <- data.frame(colpar=fcs_raw[[1]]@parameters@data$desc) colnames(df) <- c("clusterID", "sampleID", rename$colpar[c(1:37)])
df$ clusterID <- as.factor(df$ clusterID) df$sampleID <- as.factor(df$sampleID)

8. Create a cfList based on the dataframe obtained from *FlowSOM* by running the following script: cfData <- cfList(samples = sampleid,
expr = df)
Re-order the markers to appear similarly to the output from the *Cytosplore* analysis. cfData@expr <- cfData@expr[,c(1,2,34,36,37,10,23,24,31,22,
38,15,8,3,27,9,11,28,35,26,
14,33,17,20,21,18,25,29,13,
30,12,16,32,4,5,6,7,19,39)]
NOTE: The clustering by *FlowSOM* is now finished. Next, perform visualization of the clustering output.

Visualization: Post-processing Clustering Analysis

NOTE: This step is a method that is common to both clustering methods. Therefore, it can be performed after clustering either with *FlowSOM* or *Cytosplore*.

1. Before creating the heatmaps, generate the count table per sample by using the function cellCounts as shown in the code below. Since some clusters contain fewer cells than others, scale the data per cluster by specifying "scale = TRUE" inside the function cellCounts, so that the dispersion among samples can be easily seen.
cfData <- cellCounts(cfData, frequency = TRUE, scale = TRUE)
NOTE: The data can now be visualized.
2. Visualize with heatmap.
NOTE: One of the main functions of this package is cytoHeatmaps, which is used to visualize the phenotype of the created clusters as well as their heterogeneity with respect to the samples.
cytoHeatmaps (cfData, group="group", legend=TRUE)
3. Visualization with boxplots
NOTE: Data can be represented in a quantitative way by calling the function cytoBoxplots. The output of this function represents the proportion of each sample for every cluster.
    1. Generate the cell count as done in step 3.1, but do not scale the data to obtain the frequency of each cluster. cfData <- cellCounts(cfData, frequency = TRUE, scale = FALSE)
    cytoBoxplots(cfData, group = "group")
4. Visualization with median intensity signal histogram

NOTE: The data can also be visualized by representing the median intensity signal histogram.

1. Visualize the expression intensity of three markers: CD45, CD11c, and CD54.
2. Check the names of the desired markers by calling the following line. Note the marker names and include it in the msiPlot function. names(cfData@expr)

NOTE: Here, focus on CD45, CD11c, and CD54. Check the exact spelling of the markers and adjust if needed: msiPlot(cfData, markers = c("89Y_CD45", "167Er_CD11c","164Dy_CD54"), byGroup='group')

REPRESENTATIVE RESULTS

The workflow *Cytofast* (**Figure 1**) is meant to provide a quantitative and qualitative overview of the data originally clustered by analysis software(i.e., *FlowSOM* or *Cytosplore*). *Cytofast* runs several possible outputs, including the heatmap of all clusters identified in the analysis and based on marker expression (**Figure 2** and **Figure 3**). The dendrogram on the top represents the hierarchical similarity between the identified clusters. The upper panel displays another heatmap showing the relative quantity of corresponding subsets in each sample. The dendrogram on the right shows the similarity between samples and is based on hierarchical clustering performed on the Euclidean distances between samples. The combined heatmaps are shown for *FlowSOM* followed by *Cytofast* in **Figure 2** and for *Cytosplore* followed by *Cytofast* in **Figure 3**. *Cytofast* can also be used to present the data quantitatively and display the results in boxplots (by using cytoBoxplots function), as shown in **Figure 4** and **Figure 5**.

Similar clusters were found between the two different methods (e.g., cluster 8 from *Cytosplore* corresponds to cluster 10 from *FlowSOM*), and co-expression of some inhibitory markers like PD-1 and LAG-3 were still visible in both methods). Both clustering methods allowed discrimination between PD-L1 *vs*. PBS treated mice. In contrast, some differences between both methods can be highlighted. *FlowSOM* identifies 2 clusters (MHC-II^{+}), whereas *Cytosplore* shows only one cluster (MHC-II^{+dim}). This is due to the initial gating strategy in which NK cells were manually gated on CD161^{+} cells, then further processed by *FlowSOM*. However, *Cytosplore* automatically gated cells from the CD45^{+} population on the first HSNE level, which were then clustered in a higher hierarchical level. Thus, *Cytosplore* defined the NK cell subsets more precisely than how manual gating focused on CD161. Nevertheless, hierarchical clustering of the samples was preserved, as shown in the dendrogram on the right, indicating that segregation between the two groups (PD-L1 and PBS) was not dependent on the chosen clustering method.

Figure 1. Workflow of *Cytofast* package. The data were generated by mass cytometry from a tumor 3 days after treatment with immunotherapy or left untreated. Two different clustering techniques were compared: *Cytosplore* and *FlowSOM*. *Cytofast* was used to visualize differences between the two techniques.

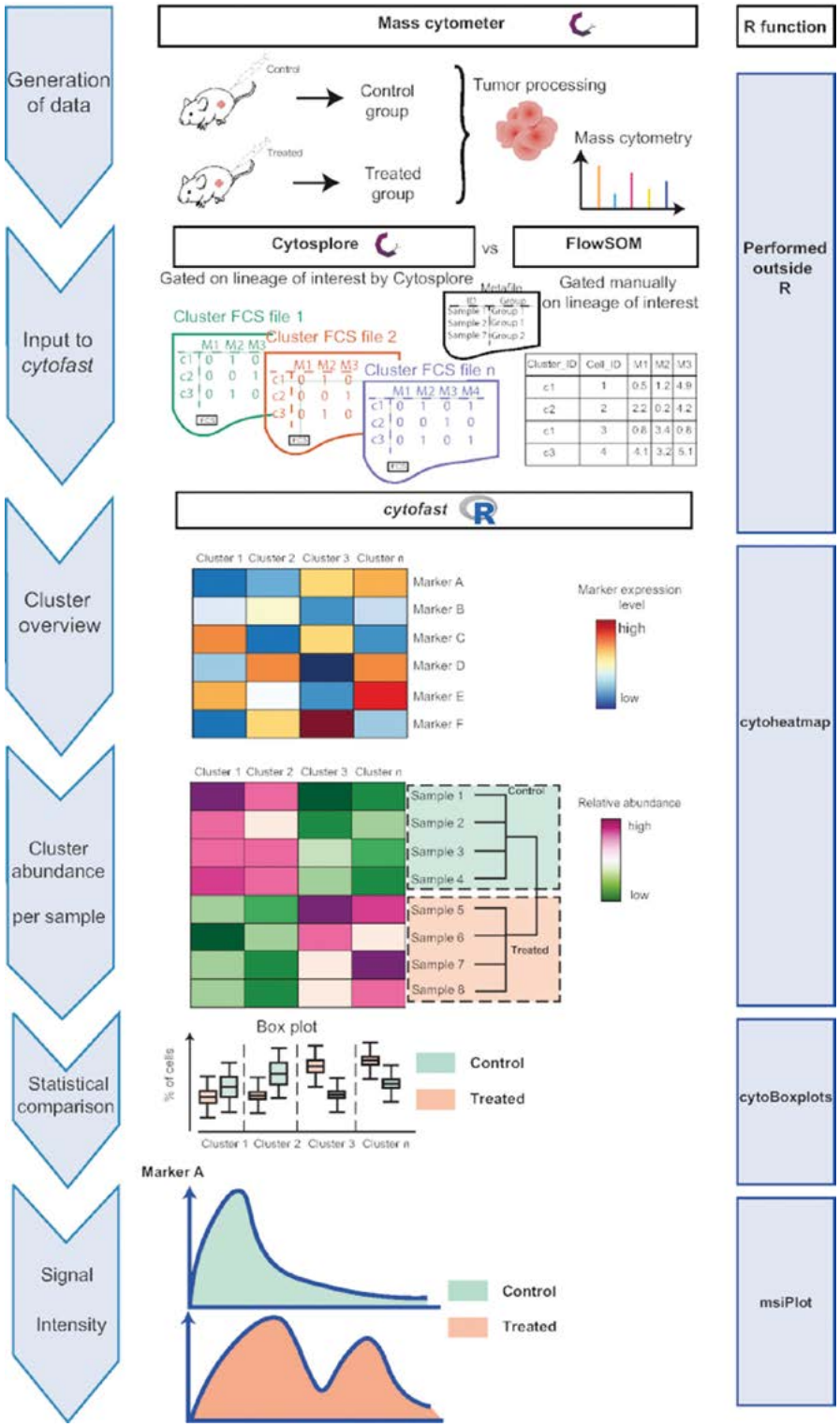
Generation of data
Input to cytofast
Cluster overview
Cluster abundance per sample
Statistical comparison
Signal Intensity
Mass cytometer
R function
Control
Control group
Treated
Treated group
Tumor processing
Mass cytometry
Performed outside R
Cytosplore
vs
FlowSOM
Gated on lineage of interest by Cytosplore
Gated manually on lineage of interest
Cluster FCS file 1
Cluster FCS file 2
Cluster FCS file n
cytofast
Cluster_ID
Cell_ID
M1
M2
M3
Cluster 1 Cluster 2 Cluster 3 Cluster n
Marker A
Marker B
Marker C
Marker D
Marker E
Marker F
Marker expression level
high
low
cytoheatmap
Sample 1
Sample 2
Sample 3
Sample 4
Sample 5
Sample 6
Sample 7
Sample 8
Control
Treated
Relative abundance
Box plot
% of cells
Control
Treated
cytoBoxplots
Marker A
msiPlot

The number of clusters can be manually defined using both methods. *Cytofast* enables the user to assess the heterogeneity of their data and can provide insight into how to choose the number of clusters into which the data should be divided. Other features are included in the *Cytofast* package, such as the msiPlot function (step 3.4.2), showing the median signal Intensity (MSI) plot of every marker per group (**Figure 6** and

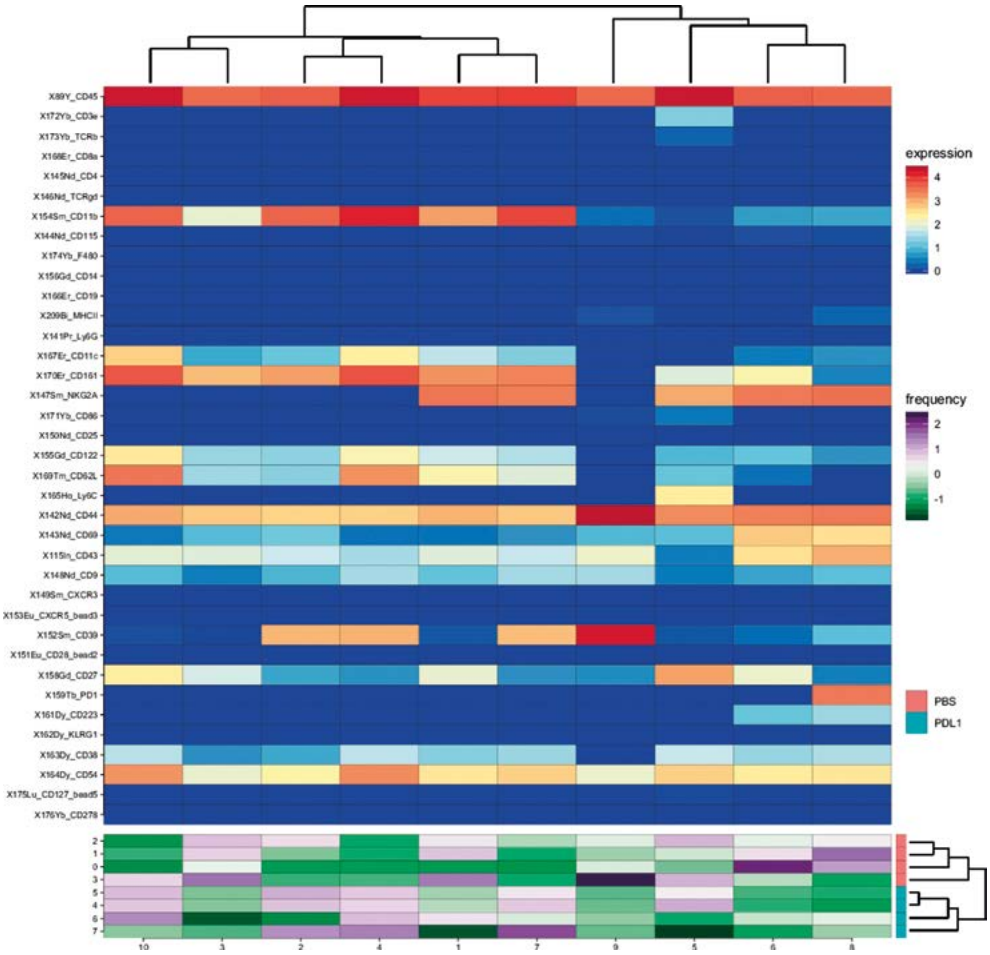

Figure 2. Cluster overview and cluster abundance per group as analyzed by *Cytofast* following *Cytosplore*. Heatmap of all NK cell clusters (CD161 cells defined automatically by *Cytosplore*), which were identified 3 days after immunotherapy (PD-L1). Data shown is based on *Cytosplore* clustering and pooled from the untreated and PD-L1 treated groups. Levels of ArcSinh5-transformed expression marker are displayed on a rainbow scale. On the lower panel, the relative abundance of each sample is represented by the green-to-purple scale. The dendrogram on the right represents the similarity between samples based on subset frequencies. The frequency scale represents the dispersion of the mean. A low or a high frequency is represented by a green or purple color, respectively.

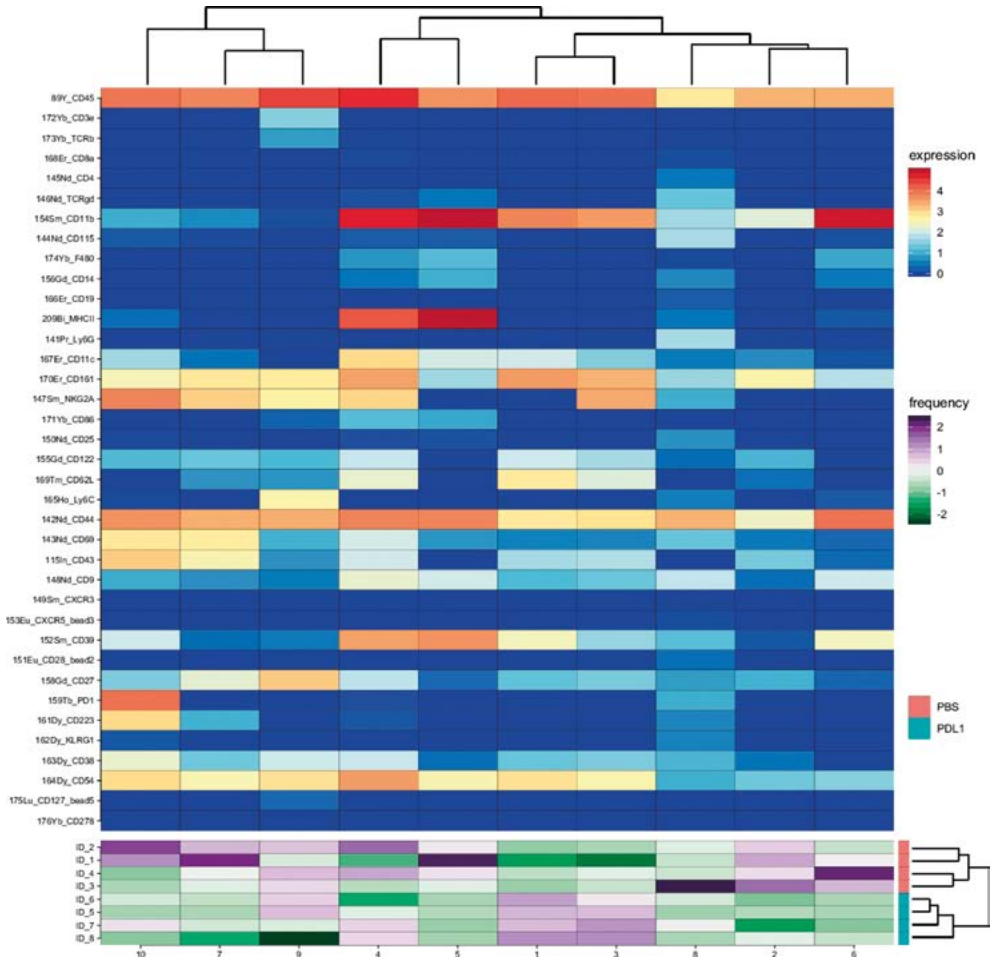

Figure 3. Cluster overview and cluster abundance per group as analyzed by *Cytofast* following *FlowSOM*. Heatmap of all NK cell clusters (pre-gated on CD161 events), which were identified 3 days after immunotherapy (PD-L1). Data shown is based on *FlowSOM* clustering and pooled from the untreated and PD-L1 treated groups. Levels of ArcSinh5-transformed expression marker are displayed on a rainbow scale. On the lower panel, the relative abundance of each sample is represented by the green-to-purple scale. The dendrogram on the right represents the similarity between samples based on subset frequencies. The frequency scale represents the dispersion of the mean. A low or a high frequencyis represented by a green or purple color, respectively.

Figure 7). This function allows detection of global changes, such as increases in the expression of CD54 or CD11c in NK cells of the PD-L1- treated group. Optional features can be incorporated in the *Cytofast* package, such as displaying data in bar graphs and other methods of data representation. The latter requires the addition of ggplot tools, which can be generated by R.

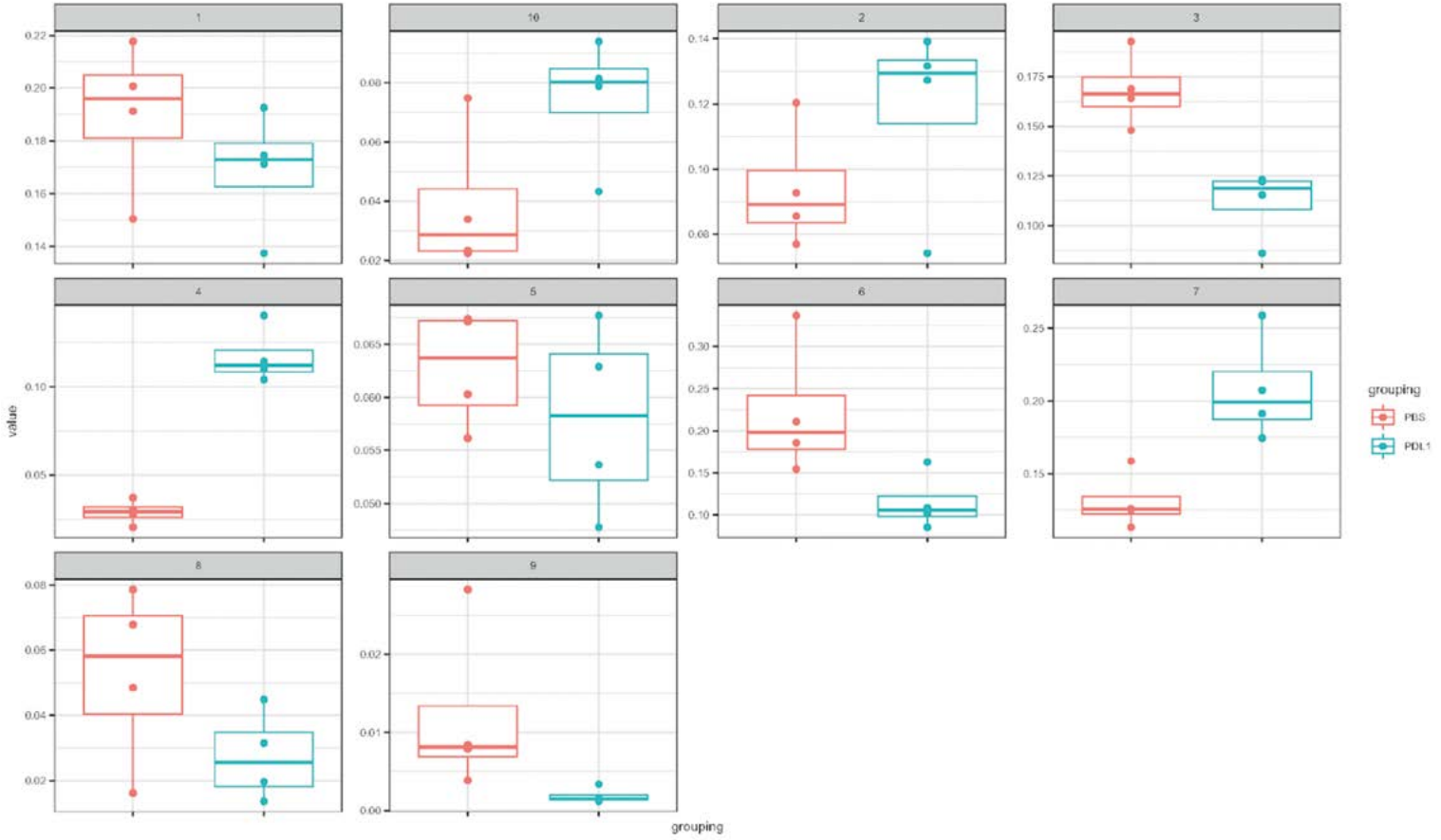

Figure 4. *Cytofast* representation with boxplots of the clusters defined by *Cytosplore*. The frequency of each cluster is represented ina boxplot, separated into the two groups (PBS and PD-L1). One individual dot corresponds to one mouse.

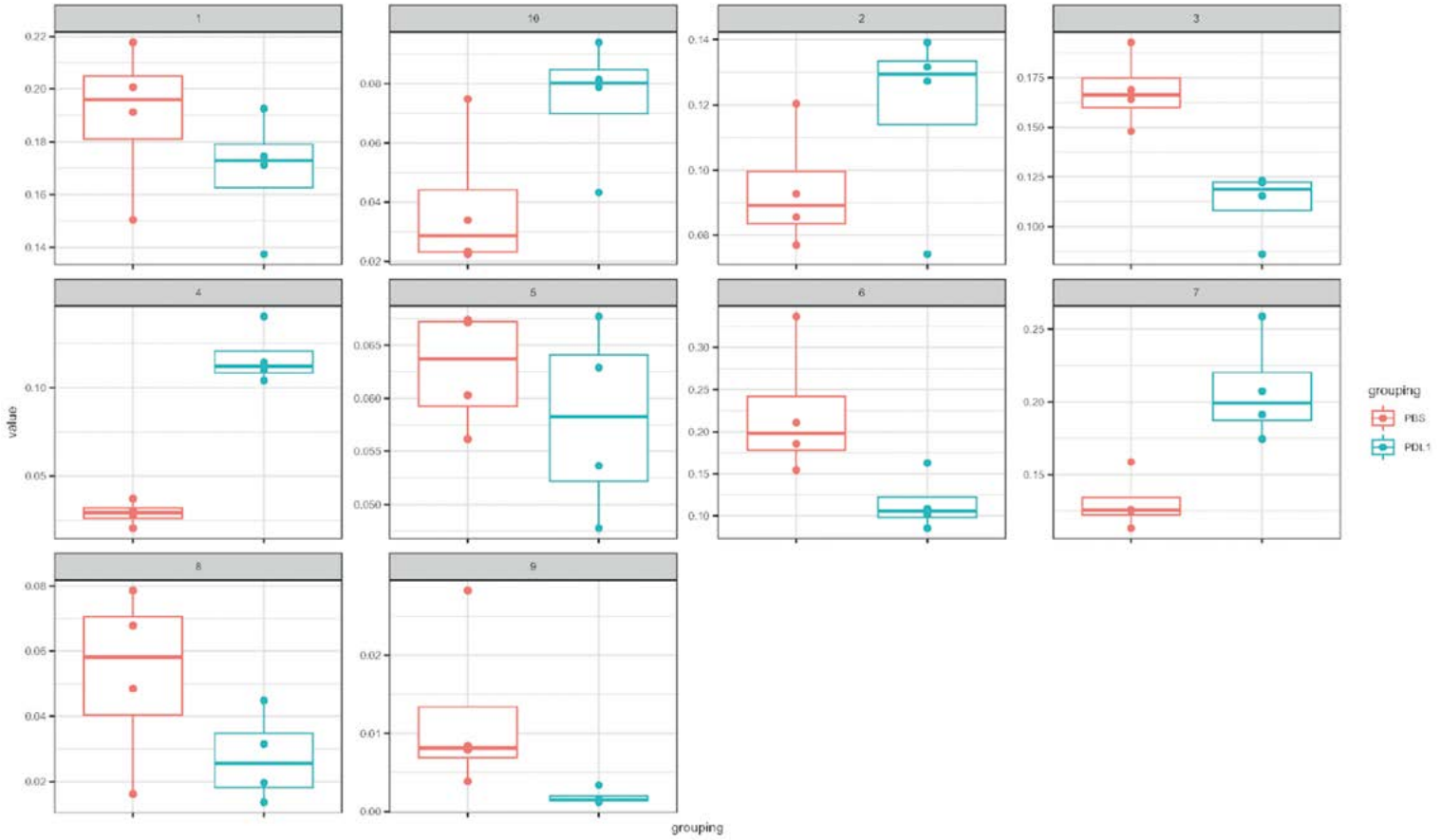

Figure 5. *Cytofast* representation with boxplots of the clusters defined by *FlowSOM.* The frequency of each cluster is represented ina boxplot, separated into the two groups (PBS and PD-L1). One individual dot corresponds to one mouse.

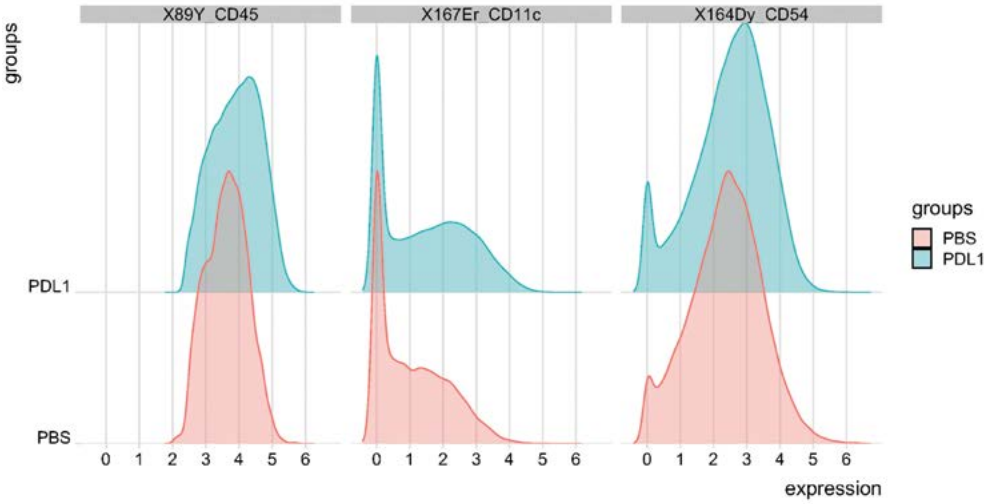

Figure 6. Distribution of signal intensity plots from NK cells automatically gated by *Cytosplore*. Distribution of signal intensities are shownin a histogram for three specific markers: CD45, CD11c, and CD54.

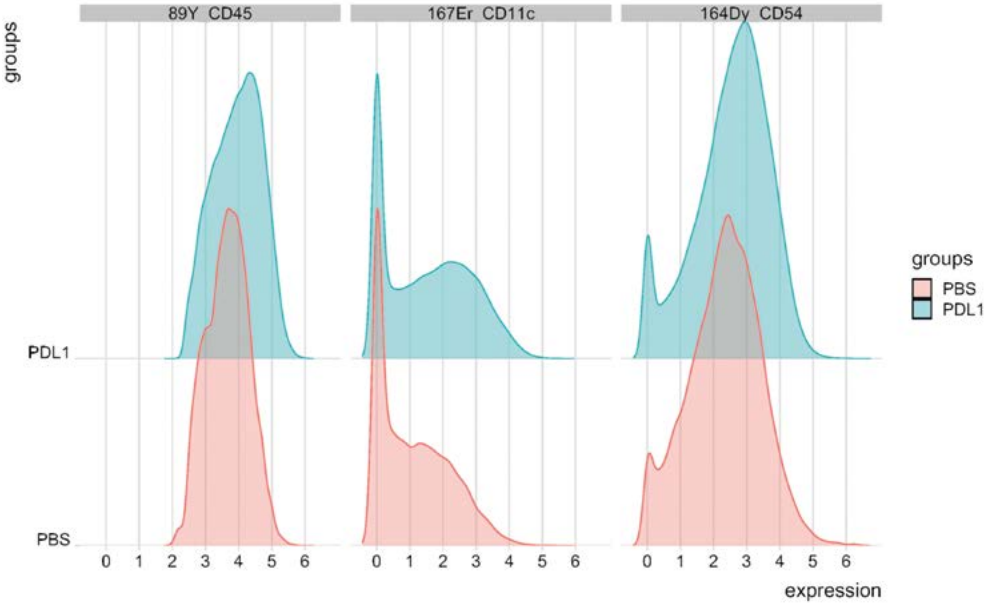

Figure 7. Distribution of signal intensity plots from NK cells automatically gated by *FlowSOM*. Distribution of signal intensities are shownin a histogram for three specific markers: CD45, CD11c, and CD54, segregated by groups PBS and PD-L1.

Cytofast is a rapid computational tool that provides a quick and global exploration of cytometric data by highlighting and quantifying treatment- specific cellular subsets. The protocol described aims to further process clustering analyses with *Cytosplore* or *FlowSOM*. Other clustering analysis tools are suitable for *Cytofast*, but this requires the use of *Cytofast* to assign each cell to a subset. *Cytofast*, however, is not a clustering method, and therefore requires clustering procedures before use.

The analysis performed here showed that certain CD161$^+$ NK cell subsets in the tumor microenvironment were sensitive to a PD-L1 blockade. This was evidenced by changes in their phenotype and abundance, which were observed using both *Cytosplore* and *FlowSOM* as clustering methods. Both methods distinguished the main NK cell cluster (CD11b$^+$ NKG2A$^+$) with slightly different frequencies (15%–20% for *Cytosplore*, 30%–40% for *FlowSOM*). The differences in abundance and this approximation did not affect the global pattern, because both dendrograms displayed in the right panels of **Figure 2** and **Figure 3** showed similar results. By using *Cytofast*, it is thus possible (independent from the clustering method chosen) to segregate PD-L1-treated and untreated mice based on analyses of NK cell cluster phenotype and abundance.

Depending on the recorded parameters, modifications to the protocol are needed. Specifically, certain parameters such as time and background must be removed while performing the clustering analysis. In addition, it is important that each cell is assigned to a subset. The cfData function will simply add the raw cell counts per cluster per sample into the cfList. From this step, the cytoheatmap can be built as explained in section 3.

Cytofast has been successfully used as a visualization and quantification tool to compare different clustering methods (13). This R package is also compatible with advanced features, such as the *globaltest* (14), which can test associations between groups of clusters using clinical variables. In the future, the *globaltest* tool and other algorithms can be integrated with *Cytofast* for more in-depth visualization and quantification.

DISCLOSURES

The authors have nothing to disclose.

ACKNOWLEDGMENTS

We acknowledge funding from the European Commission of a H2020 MSCA award under proposal number 675743 (ISPIC). We thank Tetje van der Sluis and Iris Pardieck for testing the protocol.

REFERENCES

1. Anchang, B. et al. Visualization and cellular hierarchy inference of single-cell data using SPADE. *Nature Protocols.* **11** (7), 1264-1279 (2016).
2. Zunder, E. R., Lujan, E., Goltsev, Y., Wernig, M., Nolan, G. P. A continuous molecular roadmap to iPSC reprogramming through progression analysis of single-cell mass cytometry. *Cell Stem Cell.* **16** (3), 323-337 (2015).
3. Van Gassen, S. et al. *FlowSOM*: Using self-organizing maps for visualization and interpretation of cytometry data. *Cytometry A.* **87** (7), 636-645 (2015).
4. Levine, J. H. et al. Data-Driven Phenotypic Dissection of AML Reveals Progenitor-like Cells that Correlate with Prognosis. *Cell.* **162** (1), 184-197 (2015).
5. Samusik, N., Good, Z., Spitzer, M. H., Davis, K. L., Nolan, G. P. Automated mapping of phenotype space with single-cell data. *Nature Methods.* **13** (6), 493-496 (2016).
6. Spitzer, M. H. et al. IMMUNOLOGY. An interactive reference framework for modeling a dynamic immune system. *Science.* **349** (6244), 1259425, (2015).
7. Hotelling, H. Analysis of a complex of statistical variables into principal components. *Journal of Educational Psychology.* **24** (6), 417-441 (1933).
8. van der Maaten, L., Hinton, G. Visualizing Data using t-SNE. *Journal of Machine Learning Research.* (2008).
9. Pezzotti, N., Hollt, T., Lelieveldt, B., Eisemann, E., Vilanova, A. Hierarchical Stochastic Neighbor Embedding. *Computer Graphics Forum.* **35** (3), 21-30 (2016).
10. Becht, E. et al. Dimensionality reduction for visualizing single-cell data using UMAP. *Nature Biotechnology.* **37**, 38 (2018).
11. Haghverdi, L., Buettner, F., Theis, F. J. Diffusion maps for high-dimensional single-cell analysis of differentiation data. *Bioinformatics.* **31** (18), 2989-2998 (2015).
12. Beyrend, G., Stam, K., Höllt, T., Ossendorp, F., Arens, R. *Cytofast*: A workflow for visual and quantitative analysis of flow and mass cytometry data to discover immune signatures and correlations. *Computational and Structural Biotechnology Journal.* **16** 435-442 (2018).
13. Beyrend, G. et al. PD-L1 blockade engages tumor-infiltrating lymphocytes to co-express targetable activating and inhibitory receptors. *Journal for ImmunoTherapy of Cancer.* **7** (1), 217 (2019).
14. Goeman, J. J., van de Geer, S. A., de Kort, F., van Houwelingen, H. C. A global test for groups of genes: testing association with a clinical outcome. *Bioinformatics.* **20** (1), 93-99 (2004).

PD-L1 BLOCKADE ENGAGES TUMOR-INFILTRATING LYMPHOCYTES TO CO-EXPRESS TARGETABLE ACTIVATING AND INHIBITORY RECEPTORS

4

ABSTRACT

Background

The clinical benefit of immunotherapeutic approaches against cancer has been well established although complete responses are only observed in a minority of patients. Combination immunotherapy offers an attractive avenue to develop more effective cancer therapies by improving the efficacy and duration of the tumor- specific T-cell response. Here, we aimed at deciphering the mechanisms governing the response to PD-1/PD-L1 checkpoint blockade to support the rational design of combination immunotherapy.

Methods

Mice bearing subcutaneous MC-38 tumors were treated with blocking PD-L1 antibodies. To establish high-dimensional immune signatures of immunotherapy-specific responses, the tumor microenvironment was analyzed by CyTOF mass cytometry using 38 cellular markers. Findings were further examined and validated by flow cytometry and by functional *in vivo* experiments. Immune profiling was extended to the tumor microenvironment of colorectal cancer patients.

Results

PD-L1 blockade induced selectively the expansion of tumor-infiltrating CD4+ and CD8+ T-cell subsets, co- expressing both activating (ICOS) and inhibitory (LAG-3, PD-1) molecules. By therapeutically co-targeting these molecules on the TAI cell subsets *in vivo* by agonistic and antagonist antibodies, we were able to enhance PD-L1 blockade therapy as evidenced by an increased number of TAI cells within the tumor micro-environment and improved tumor protection. Moreover, TAI cells were also found in the tumor-microenvironment of colorectal cancer patients.

J Immunother Cancer. 2019 Aug 14;7(1):217

Guillaume Beyrend[1], Esmé van der Gracht[1], Ayse Yilmaz[1], Suzanne van Duikeren[1], Marcel Camps[1], Thomas Höllt[2,3], Anna Vilanova[4], Vincent van Unen[1], Frits Koning[1], Noel F. C. C. de Miranda[5], Ramon Arens[1*†] and Ferry Ossendorp[1*†]

[1] Department of Immunohematology and Blood Transfusion, Leiden University Medical Center, Albinusdreef 2, 2333, ZA, Leiden, The Netherlands.
[2] Leiden Computational Biology Center, Leiden University Medical Center, Leiden, The Netherlands.
[3] Department of Computer Graphics and Visualization Group, Delft, the Netherlands.
[4] Computer Graphics and Visualization Group, faculty of Electrical Engineering, Mathematics and Computer Science, Delft University of Technology, Delft, the Netherlands.
[5] Department of Pathology, Leiden University Medical Center, Leiden, The Netherlands.

Conclusions

This study shows the presence of T cell subsets in the tumor micro-environment expressing both activating and inhibitory receptors. These TAI cells can be targeted by combined immunotherapy leading to improved survival.

Keywords: Mass cytometry, Combinatorial immunotherapy, T cells

INTRODUCTION

Immunotherapy has become an important treatment op- tion for cancer patients. Especially, clinical trials with anti- bodies that block the interaction between the inhibitory receptor PD-1, expressed on previously activated T cells, with its broadly expressed ligand PD-L1, resulted in unprecedented clinical response rates for patients with ad- vanced cancer (1–3). Despite these encouraging results, still only a fraction of patients show durable responses, whereas the majority of treated patients show no benefi- cial clinical response (1, 4). Therefore, there is a need for more effective treatment regimens, like combinatorial im- munotherapies, which offer an attractive avenue to im- prove the efficacy and the duration of the tumor specific T-cell response.

Both $CD8^+$ and $CD4^+$ T cells can mount responses against many human cancer types, especially those with higher mutational burden (5). Studies have shown that T cells are however partially inhibited by PD-1/PD-L1 inter- actions (6) and releasing this constraint by blocking the PD-1 pathway can to some extent reinvigorate T cells lead- ing to clinical benefit in a number of cancer patients (7). However, tumor-specific T cells are also restrained by sev- eral other inhibitory mechanisms (8, 9), which put forward the premise that PD-1/PD-L1-based monotherapies could be enhanced so that the majority of patients will have dur- able clinical benefit. Indeed, recent studies reported co- treatment regimens to PD-1 blockade (10–13). In depth mechanistic studies of PD-1/PD-L1 blockade *in vivo* may lead to rational design of improved co-treatment protocols.

Identification of biomarkers related to immunothera- peutic response and resistance could support the ra- tional design of complementary therapies in which the additional targeting of those biomarkers would lead to more effective cancer therapies. Identification of the relevant responding cell types to therapy reveals insight into the underlying immunological mechanisms of on- going clinical response, as well as into the development of adaptive resistance during such a therapy. Here we used high-dimensional, single-cell mass cytometry and a customized bioinformatics pipeline *Cytofast* (14) to gen- erate an in-depth analysis of the tumor-infiltrating im- mune cells upon PD-L1-based treatment. Our aim was to identify responsiveness-associated targets to improve immunotherapy. We discovered unique $CD4^+$ and $CD8^+$ T cell subsets that increased after anti-PD-L1 immuno- therapy and were characterized by expression of both activating and inhibitory receptors, hence we defined these cells as T_{AI} cells. By therapeutic targeting of the activating and inhibitory receptors on the T_{AI} cells *in vivo*, significant improvement of immunotherapy was shown, correlating with an increase of the $CD8^+$ T_{AI} cells in the tumor micro- environment (TME). T_{AI} cells were also present within tumor-infiltrated immune cells from mismatch repair-deficient (MMRd) colorectal can- cer patients. Together, our data show the importance of the T_{AI} cells and their possible targetability to induce tumor regression in colorectal cancer.

METHODS

Mice

C57BL/6 J mice were purchased from The Jackson Laboratory. All animal experiments were approved by the Animal Experiments Committee of LUMC and were executed according to the animal experimentation guidelines of the LUMC in compliance with the guide- lines of Dutch and European committees.

Staining and acquisition for CyTOF mass cytometry

Metal conjugated antibodies were purchased from Flui- digm or conjugated to unlabeled antibodies in-house. All non-platinum conjugations were performed using X8 polymer as per manufacturer's protocol (Fluidigm) and were performed at 100 µg scale. Conjugation with 208 Bismuth was performed using a protocol adapted from M. Spitzer (15). All in-house conjugated antibodies were diluted to 0.5 mg/ml in antibody stabilizer supplemented with 0.05% sodium azide (Candor Biosciences). Appro- priate antibody dilution was determined by serial dilu- tion staining to minimize background and optimize detection of positively expressing populations.

CyTOF data were acquired and analyzed on-the-fly, using dual-count mode and noise-reduction on. All other settings were either default settings or optimized with tun- ing solution, as instructed by Fluidigm Sciences. After data acquisition, the mass bead signal was used to normalize the short-term signal fluctuations with the reference EQ passport P13H2302 during the course of each experiment and the bead events were removed (16).

CyTOF mass cytometry data analysis

To isolate immune cells from the tumor, solid tumors were excised after a flushing step to remove the blood from TME. Exclusion criteria were ulceration of tumors, incomplete or unsuccessful flushing (determined by an unexpected high numbers of B cells in the TME). Sin- gle-cell suspensions were then prepared by mechanical and enzymatic (collagenase D and DNase, Sigma-Al- drich) dissociation, followed by density gradient centrifu- gation on an 100% / 70% / 40% / 30% Percoll (GE Healthcare) gradient.

After staining cells according to van Unen et al. (17), we analyzed live immune cells from the TME. We set our gating strategy to live single cells, positive for CD45, and excluded reference beads. For further analysis, live $CD45^{+}$ gated files were sample-tagged, their marker ex- pression arcsinh5 transformed and subjected to dimen- sionality reduction analyzes in Cytosplore (18). All markers were taken in account to process the clustering analysis except PD-L1, which is a marker used only as a quality control to check the efficacy of PD-L1 blocking antibodies. The PD-L1 blocking antibody we used (clone MIH5, rat-anti-mouse, IgG2a subtype) binds to FcγRIIb and FcγRIII but not to FcγRI and FcγRIV, and is not able to mediate specific killing or depletion (19). By staining with the same antibody clone, PD-L1 downmodulation was determined to show the effectiveness of the pro- vided therapeutic antibodies to block PD-L1 binding.

Pooled samples from control and PD-L1 treated groups were analyzed by hierarchical stochastic neighbourhood em- bedding (HSNE) (20) based on approximated t-distributed stochastic neighbourhood embedding (A-tSNE) (21). The default perplexity and iterations of the HSNE analysis were 30 and 1.000, respectively. If some clusters showed a similar phenotype, they were manually merged in Cytosplore. For further data exploration, $CD4^+$ T cell, $CD8^+$ T cell, $CD19^+$ B cell, $CD11b^+$ myeloid cell lineages were analyzed separately. Downstream analysis was performed by *Cytofast* (14) and *Cytofworkflow* (22).

Diffusion map

Diffusion map was generated with R using the *cytofkit* package (23) by displaying only $CD3^+$ metaclusters iden- tified by PhenoGraph (24) as a confirmation method of the HSNE clustering.

Reference standard comparison

Reference standard samples were compared with each other by calculating the similarity between their respect- ive t-SNE maps. We used the Jensen-Shannon (JS) diver- gence to quantify the similarity between t-SNE maps. After converting t-SNE maps into two-dimensional probability density functions, the similarity between two maps is quantified as the JS divergence between their corresponding probability density functions. We used the base 2 logarithm in the JS divergence computation, which results in a continuous range of JS divergence values between 0 (for identical distributions) and 1 (for fully disjoint distributions), the algorithm being provided by E.D. Amir (25). The average overlap frequency (AOF) is determined as described by E.D. Amir (26)

Flow cytometry

Mouse

Single-cell suspensions were prepared from TME (27) obtained from untreated or PD-L1 treated mice by an incubation of 15 min with collagenase and DNase IV (Roche) and by mincing the tumor tissue through a 70- µm cell strainer (BD Bioscience). Live cells were washed with RPMI-1640 supplemented with 8% FBS and P/S and once with FACS buffer. Subsequently, samples were incubated with Fc block mouse (2%) and mouse serum (5%) for 10 min, then stained with antibodies (Add- itional file 1: Table S1A) for 30 min at 4 °C in the dark and finally rinsed two times with PBS containing 0.5% BSA solution. Samples were acquired using the LSR For- tessa (BD Biosciences) and results analyzed with FlowJo and Cytosplore software.

Granzyme B staining of tumor-infiltrated T cells

MC-38 tumors were injected subcutaneously in C57BL/ 6 J mice, consecutively treated with 200 µg PD-L1 at three different timepoints (10, 13 and 16 days after tumor inoculation). At day 8 post treatment, tumors were excised and single-cell suspensions were generated as described above. Cells were next stimulated overnight *in vitro* with MC-38 tumor cells

with a concentration of Brefeldine A of 4 µg/mL. Cells were then cell surface stained with antibodies to CD45, CD3, CD8, CD4, PD-1 and CD39 followed by intracellular Granzyme B staining after fixation. The phenotype was assessed by flow cy- tometry using the LSR Fortessa and results were ana- lyzed with FlowJo.

Human studies

Cryopreserved colorectal tumor digests (excision and single cell suspension preparation by mechanical dissoci- ation followed by slow freezing in 10% DMSO) were thawed and mashed through 70 µm filters into RPMI- 1640 supplemented with 8% FBS and P/S. Live cells were washed once with RPMI-1640 with 8% FBS and P/S and once with FACS buffer. Two staining reactions of 1×10^6 cells per tumor sample were analyzed. All samples were then incubated with 2% of each bovine, murine, rat, hamster, and rabbit serum PBS with human TruS- tain FcX (Biolegend, 422,302) at 4 °C for 10 min. Sam- ples were processed for surface staining (Additional file 1: Table S1B) and analyzed using a similar protocol as described for processing, staining and analyzing murine tumor samples. All specimens were anonymized and handled according to the ethical guidelines described in the Code for Proper Secondary Use of Human Tissue in the Netherlands of the Dutch Federation of Medical Sci- entific Societies.

In vivo murine tumor experiments

MC-38 colon adenocarcinoma cells were injected at a dose of 0.3×10^6 cells subcutaneously (s.c.) in the right flank. Antibodies blocking LAG-3 and PD-L1 were injected intraperitoneally and agonistic anti-ICOS anti- bodies were given subcutaneously, next to the tumor. Tumor diameter was measured every 2 to 3 days with a calliper and reported as volume using the formula (w × h× l) x (π/6).

Statistical analyses

Statistical analyses were performed using R software or Prism (GraphPad). Unpaired two-tailed t-tests were used for subset abundance comparisons.

RESULTS

Efficacy of PD-L1 blockade parallels with an increase in tumor infiltrating CD8+ T cells over time

To examine the effect of PD-L1 blocking therapy, we used the colorectal adenocarcinoma mouse model MC-38. Mice were inoculated with MC-38 tumor cells, and when tumors were established after 10 days (tumor vol- ume of 30–40 mm^3), mice were treated with PD-L1 blockade therapy or left untreated (control group) (Fig. 1A). To identify biomarkers that respond to im- munotherapy with PD-L1 blockade, we set up a CyTOF mass cytometry panel for in-depth phenotypic characterization of tumor-infiltrated lymphocytes (TILs) in preclinical tumor models, which allows kinetic dissec- tion of anti-tumor immune

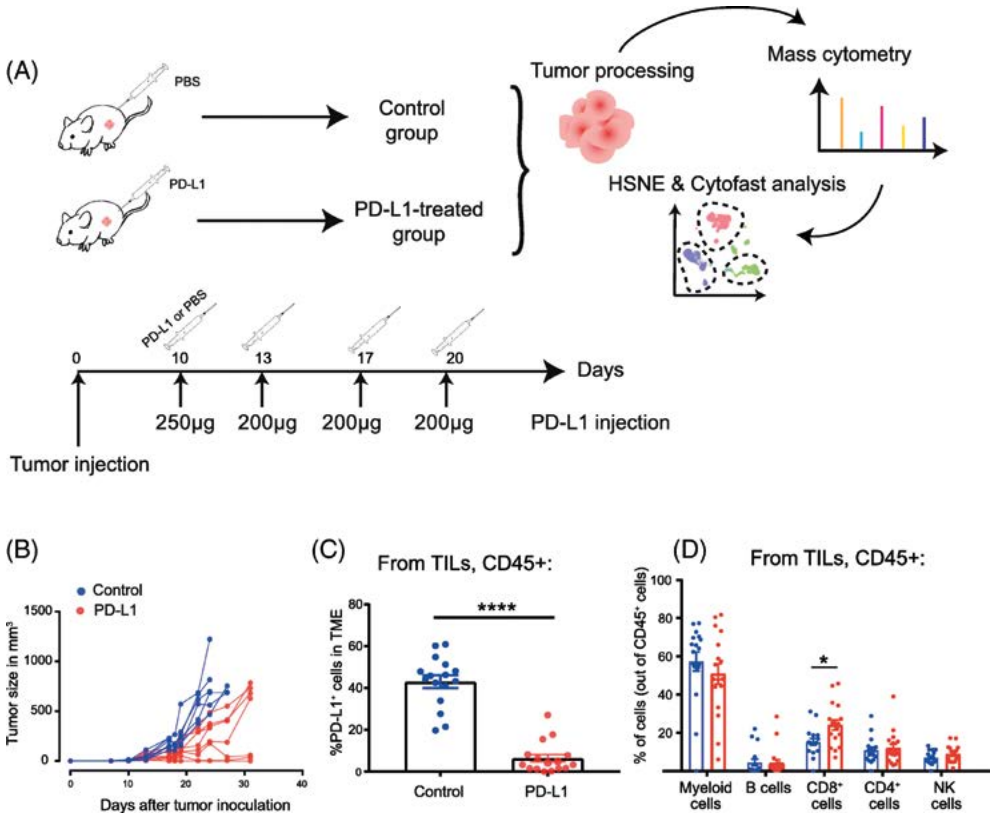

Figure 1. PD-L1-blocking treatment induces delay of MC-38 tumor growth. (a) Schematic of CyTOF mass cytometry experiment investigating the effect of PD-L1 antibody treatment on the TME. Mice were challenged with MC-38 tumor cells and subsequently tumor-bearing mice were treated either with PBS (n = 16 mice) or PD-L1 blocking antibodies (n = 16 mice). Tumors were isolated and analyzed by mass cytometry (CyTOF). Cluster identification was performed with HSNE and downstream analysis was done with Cytofast. (b) Tumor growth curves of individual mice in the control group (mock injected with PBS, blue lines) and PD-L1-treated group (red lines). (c) Frequency of $CD45^+$ $PD\text{-}L1^+$ cells in the TME 8 days after therapy starts displayed on a per-mouse basis with mean ± SEM. (d) Overview of the immune cell composition in the TME shown in percentage of cells on a per-mouse basis with mean ± SEM (n = 16 mice per group)

responses. The panel con- sisted of 38 cell surface markers and was designed to identify the major lymphoid and myeloid subsets and to ascertain the differentiation and activation status of these subsets (Additional file 1: Figure S1). We isolated immune cells from the tumor 8 days after start of im- munotherapy and stained the single cell suspensions followed by mass cytometry acquisition of 3.5 million cells in total. In parallel, tumor growth was measured to assess the therapeutic benefit of the PD-L1 blockade treatment. Treated animals displayed a significant delay in tumor progression or even had complete tumor eradi- cation (Fig. 1B). To determine the effectiveness of the provided therapeutic

antibodies to block PD-L1 binding, the cell surface expression of PD-L1 in the TME was assessed by staining with the same antibody clone (i.e. MIH5). Indeed, the PD-L1 expression on CD45$^+$ tumor-in- filtrated immune cells from the treated group was significantly decreased compared to control animals (Fig. 1C).

To monitor the robustness of the measurement, we in- cluded reference standard acquisitions and used the Jensen- Shannon (JS) divergence calculation to determine similarity between samples. The results yielded consistency between the measurements with low JS distance, meaning high simi- larities between samples (Additional file 1: Figure S2A). We also tested the quality of our staining by using the Average Overlap Frequency (AOF), a metric to evaluate and quantify the robustness of staining and clustering quality in high-di- mensional data (26). Importantly, all the markers involved in the cluster identification of CD3$^+$ cells (e.g. CD4, CD8, PD- 1, ICOS, etc.) showed an AOF < 0.3, which indicates a valid staining of the samples and a clear separation between nega- tive and positive signals (Additional file 1: Figure S2B). To- gether, these data showed a stable and reliable sample acquisition with limited inter-sample variation.

An overview of the main tumor-infiltrating immune cells identified by mass cytometry showed a higher pro- portion of CD8$^+$ T cells in the PD-L1 treated group (24.1%) compared to the control group (16.1%) 8 days after first injection (Fig. 1D). Simultaneously, the frequency of the CD11b$^+$ myeloid compartment decreased after PD-L1 blockade. Thus, PD-L1 blockade empowers the increase of CD8$^+$ T cells and limits the infiltration of myeloid cells in the TME.

PD-L1 treatment increases selectively CD8$^+$ T-cell subsets expressing both activating and inhibitory receptors Because treatment with anti-PD-L1 has major effects on the expansion of the CD8$^+$ T-cell compartment, we ana- lyzed in detail the CD8$^+$ TIL subset at this timepoint and identified 48 different CD8$^+$ T-cell subsets (Fig. 2A). t-SNE clustering allowed distinction between naïve (e.g. cluster C28 expressing CD62L, CD27), effector (e.g. clus- ter C13 and C14 expressing CD54, CD38, CD27, CD44) and central-memory subsets (e.g. cluster C34 expressing CD54, CD62L, CD44, CD27). Remarkably, one cluster (cluster C4) displayed both activating (ICOS, CD69, CD43) and inhibitory receptors (PD-1, LAG-3, NKG2A). To visualize the distribution of each identified cluster, we displayed the abundance of each subset per treat- ment group (Fig. 2B). The t-SNE map overlaid with the expression of specific markers showed that the cluster C4 subset could be defined by the inhibitory molecule LAG-3 and the costimulatory receptor ICOS. Essentially, co-expression of ICOS and LAG-3 was highly specific to the PD-L1 blockade treated group (Fig. 2C, D). Further characterization of this subset also demonstrated up-regulation of the ectonucleotidase CD39, the early acti- vation marker CD69, the inhibitory NKG2A receptor, and the activation/exhaustion cell surface marker PD-1. The CD8$^+$ T-cell subset expressing both the activating and inhibitory molecules, referred hereafter as T_{AI} cells, represented approximately 17% of all the CD8$^+$ T cells across individual mice in the PD-L1 blockade group compared to 7% in the control group (Fig. 2E). Next, we

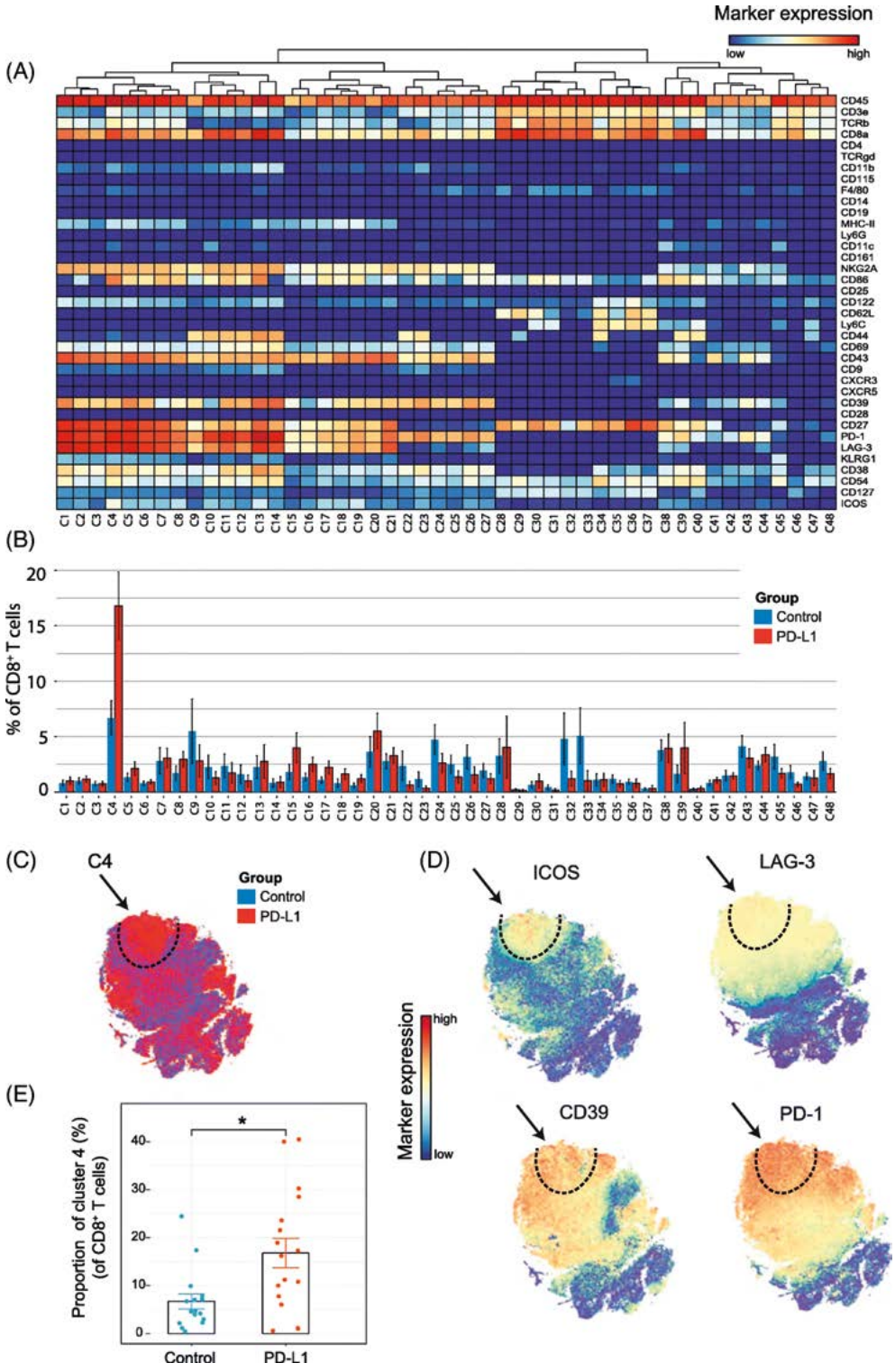
(A)
Marker expression
low
high
CD45
CD3e
TCRb
CD8a
CD4
TCRgd
CD11b
CD115
F4/80
CD14
CD19
MHC-II
Ly6G
CD11c
CD161
NKG2A
CD86
CD25
CD122
CD62L
Ly6C
CD44
CD69
CD43
CD9
CXCR3
CXCR5
CD39
CD28
CD27
PD-1
LAG-3
KLRG1
CD38
CD54
CD127
ICOS
C1 C2 C3 C4 C5 C6 C7 C8 C9 C10 C11 C12 C13 C14 C15 C16 C17 C18 C19 C20 C21 C22 C23 C24 C25 C26 C27 C28 C29 C30 C31 C32 C33 C34 C35 C36 C37 C38 C39 C40 C41 C42 C43 C44 C45 C46 C47 C48
(B)
% of CD8+ T cells
20
15
10
5
0
Group
Control
PD-L1
C1 C2 C3 C4 C5 C6 C7 C8 C9 C10 C11 C12 C13 C14 C15 C16 C17 C18 C19 C20 C21 C22 C23 C24 C25 C26 C27 C28 C29 C30 C31 C32 C33 C34 C35 C36 C37 C38 C39 C40 C41 C42 C43 C44 C45 C46 C47 C48
(C)
C4
Group
Control
PD-L1
(D)
ICOS
LAG-3
Marker expression
high
low
CD39
PD-1
(E)
Proportion of cluster 4 (%) (of CD8+ T cells)
*
40
30
20
10
0
Control
PD-L1

Figure 2. Identification of CD8⁺ T-cell clusters in Tumor Infiltrating T-cell populations (a) Heatmap of all CD8⁺ T-cell clusters identified at day 8 after the start of the PD-L1 treatment. Data shown is based on t-SNE plots, and is pooled from the control and PD-L1 treated group. Level of ArcSinh5-transformed expression marker is displayed by a rainbow scale. Dendrogram on the top represents the hierarchical similarity between the identified clusters. (b) Average and SEM in percentage of each CD8⁺ T-cell cluster among the CD8⁺ T-cell population of control (blue bars) and PD-L1 group (red bars). (c) t-SNE plot of respectively 0.32 × 10^6 and 0.35 × 10^6 CD8⁺ T cells from control (blue) and PD-L1 treated (red) group. (d) Same t-SNE plots as above now showing the level of expression marker by a rainbow scale. The arrow identifies the cluster of interest C4 (having a shared CD8⁺ LAG3⁺ ICOS⁺ phenotype). (e) Bar graph showing the mean frequency of cluster 4 (± SEM, unpaired t-test). Individual mice belonging to the control (blue) and PD-L1 treated (red) group are indicated

validated the presence of CD8⁺ T_{AI} cells by flow cytome- try. We isolated TILs from the TME and stained for the markers ICOS, LAG-3, CD69, CD39 and PD-1. The CD8⁺ T_{AI} subset (CD8⁺, LAG-3⁺, CD39⁺, PD-1⁺, ICOS⁺)

population could indeed be identified, and was more abundant following PD-L1 blockade therapy (mean = 22%, sd = 16%, *n* = 6) than in the untreated group (mean = 9%, sd = 8%, n = 6; p-value = 0.03 by Student's t- test). In addition, we confirmed our findings in the MCA205 sarcoma model. We identified the CD8⁺ T_{AI} cells by flow cytometry and observed that PD-L1 treat- ment increased this subset as compared to the control untreated group (Additional file 1: Figure S3A).

Identification of T_{AI} cell subsets in the tumor-infiltrated CD4⁺ T-cell compartment

We next analyzed whether PD-L1 blockade therapy-spe- cific subsets were also apparent in the CD4⁺ T-cell com- partment. The t-SNE algorithm identified 45 CD4⁺ T-cell subsets revealing the heterogeneous profile of the CD4⁺ T cells (Fig. 3A, B). Notably, as for the CD8⁺ T cells, one subset was identified that correlated with PD-L1 treatment (cluster C12) and displayed the activating molecule ICOS and the inhibitory molecule LAG-3. In addition, these CD4⁺ T_{AI} cells expressed CD27, CD39, CD43, CD44, CD54, KLRG1 and PD-1. The t-SNE map overlaid with the expression of specific markers showed that these sub- sets could also be defined by LAG-3, ICOS and CD39 and the co-expression of those markers was highly specific to the PD-L1 treated group (Fig. 3C, D). The T_{AI} subset of CD4⁺ T cells was also significantly more abundant, repre- senting about 17% of the total CD4⁺ T-cell population within the tumor infiltrated immune cells of the treated group compared to 8% in the control group (Fig. 3E). Also, in the MCA205 tumor model, the CD4⁺ T_{AI} cells were identified and were increased by PD-L1 treatment (Additional file 1: Figure S3B).

Differentiation relationships of the identified PD-L1 treatment-associated T-cell subsets

To corroborate the results obtained from the previous t- SNE analysis regarding the PD-L1 treatment-associated T-cell subsets, we used the PhenoGraph algorithm to identify cell clusters and their differentiation status (24). Similar T-cell metaclusters as those depicted by t-SNE earlier were indeed identified (Fig. 4A). The CD4 and CD8 T-cell

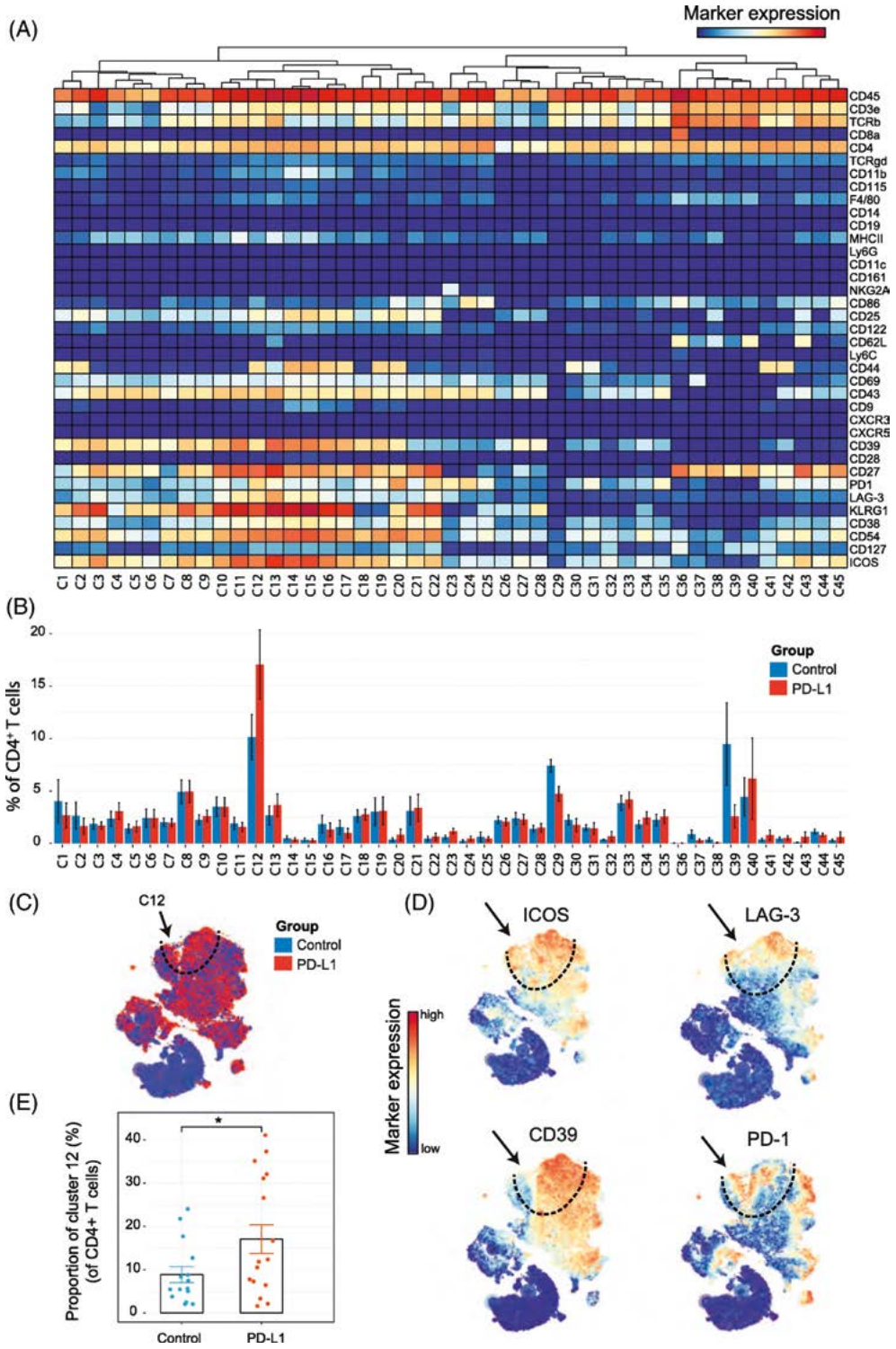
(A)
Marker expression
CD45
CD3e
TCRb
CD8a
CD4
TCRgd
CD11b
CD115
F4/80
CD14
CD19
MHCII
Ly6G
CD11c
CD161
NKG2A
CD86
CD25
CD122
CD62L
Ly6C
CD44
CD69
CD43
CD9
CXCR3
CXCR5
CD39
CD28
CD27
PD1
LAG-3
KLRG1
CD38
CD54
CD127
ICOS
C1 C2 C3 C4 C5 C6 C7 C8 C9 C10 C11 C12 C13 C14 C15 C16 C17 C18 C19 C20 C21 C22 C23 C24 C25 C26 C27 C28 C29 C30 C31 C32 C33 C34 C35 C36 C37 C38 C39 C40 C41 C42 C43 C44 C45
(B)
% of CD4+ T cells
20
15
10
5
0
Group
Control
PD-L1
C1 C2 C3 C4 C5 C6 C7 C8 C9 C10 C11 C12 C13 C14 C15 C16 C17 C18 C19 C20 C21 C22 C23 C24 C25 C26 C27 C28 C29 C30 C31 C32 C33 C34 C35 C36 C37 C38 C39 C40 C41 C42 C43 C44 C45
(C)
C12
Group
Control
PD-L1
(D)
ICOS
LAG-3
Marker expression
high
low
CD39
PD-1
(E)
Proportion of cluster 12 (%)
(of CD4+ T cells)
40
30
20
10
0
*
Control
PD-L1

Figure 3. Identification of CD4+ T-cell clusters in Tumor Infiltrating T-cell populations (a) Heatmap of all CD4+ T-cell clusters identified at day 8 after the start of the PD-L1 treatment. Data shown is based on t-SNE plots, and is pooled from the control and PD-L1 treated group. Level of ArcSinh5-transformed expression marker is displayed by a rainbow scale. Dendrogram on the top represents the hierarchical similarity between the identified clusters. (b) Average and SEM in percentage of each CD4+ T-cell cluster among the CD4+ T-cell population of control (blue bars) and PD-L1 group (red bars). (c) t-SNE plot of respectively 0.23×10^6 and 0.25×10^6 CD4+ T cells from control (blue) and PD-L1 treated (red) group. (d) Same t-SNE plots as above now showing the level of expression marker by a rainbow scale. The arrow identifies the cluster of interest 12 (having a shared CD4+ LAG3+ ICOS+ phenotype)(e) Bar graph showing the mean frequency of cluster 12 (± SEM, unpaired t-test). Individual mice belonging to the control (blue) and PD-L1 treated (red) group are indicated.

lineages could be distinguished into a resting phenotype (called *CD44^{low})*, an activated intermediate phenotype without inhibitory marker expression (called *CD44^{int}*), and the T_{AI} cells expressing both inhibitory and activation molecules (called *T_{AI}*). To investigate the relationship between those metaclusters identified by PhenoGraph, we used the diffusion map algorithm (28).

The two represented components defined gradual trends of variation (Fig. 4A) correlated with signatures for lineage and activation. Both CD4+ and CD8+ T cells could be distinguished on the diffusion map, showing the inde- pendent differentiation lineages of CD4+ and CD8+ T cells. The T_{AI} cells (CD39+, PD-1+, LAG-3+, ICOS+), more frequent in the PD-L1 treated group (Fig. 4B), could be derived from an intermediate phenotype, which was CD44^{int}. Thus, due to PD-L1 blockade treatment, T cells further differentiate into the more activated T_{AI} phenotype.

We next analyzed the level of expression of the indi- vidual activating and inhibitory molecules that were modulated upon anti-PD-L1 therapy. By displaying the diffusion map with the expression level (Fig. 4C), we ob- served that the expression of ICOS, LAG-3 and CD39 started to be upregulated on intermediate phenotypes but maximum expression of these molecules was reached on both CD4+ and CD8+ T_{AI} cells.

A summary of the phenotype of the three different clus- ters studied is represented by the evolution of the markers CD62L and CD44 (Fig. 4D). While PD-1 expression was more prominent on CD8+ T_{AI} cells, ICOS was more abundantly expressed on CD4+ T_{AI} cells (Fig. 4E). The in- hibitory and activating markers NKG2A, CD38 and CD43 were also found to be upregulated on the CD8+ T_{AI} cell subset (data not shown).

Early induction of CD4+ T_{AI} and CD8+ T_{AI} cells upon PD-L1 blocking

PD-L1 blocking treatment enhanced CD4+ and CD8+ T_{AI} cell subsets in the TME 8 days post therapy. To determine if the expansion of these compartments oc- curred already early after treatment, we analyzed the TME at day 3 post-treatment (i.e. 13 days after tumor inoculation). The expansion of the CD4+ T_{AI} cells started at an earlier stage, 3 days post-therapy, and continued over time. The presence of the CD8+ T_{AI} cells could also be observed 3 days after the start of the treatment, but these cells significantly increased

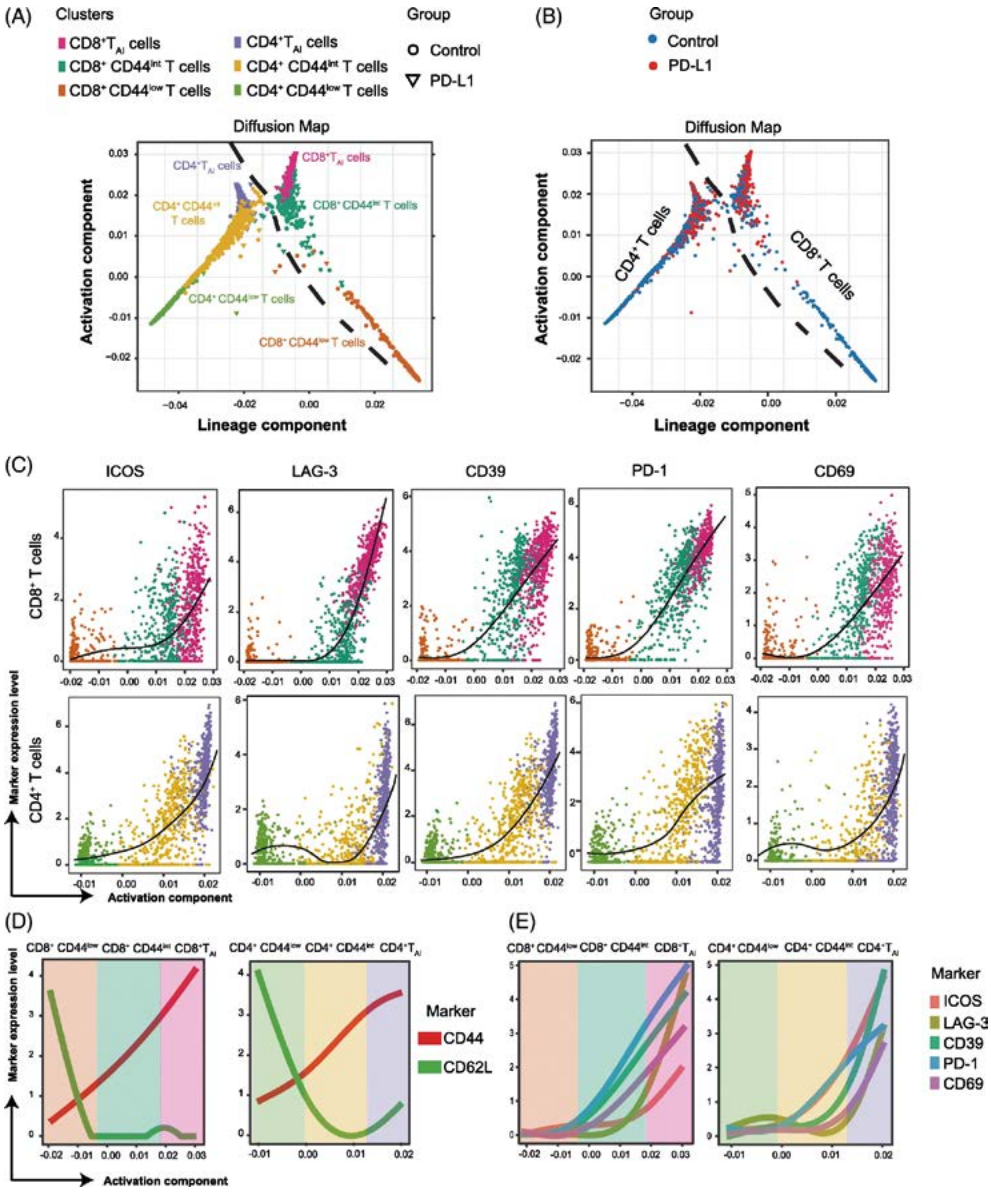
(A)
Clusters
CD8+TAI cells
CD8+ CD44int T cells
CD8+ CD44low T cells
CD4+TAI cells
CD4+ CD44int T cells
CD4+ CD44low T cells
Group
Control
PD-L1
(B)
Group
Control
PD-L1
Diffusion Map
Activation component
Lineage component
CD4+TAI cells
CD8+TAI cells
CD4+ CD44int T cells
CD8+ CD44int T cells
CD4+ CD44low T cells
CD8+ CD44low T cells
CD4+ T cells
CD8+ T cells
(C)
ICOS
LAG-3
CD39
PD-1
CD69
CD8+ T cells
CD4+ T cells
Marker expression level
Activation component
(D)
CD8+ CD44low CD8+ CD44int CD8+TAI
CD4+ CD44low CD4+ CD44int CD4+TAI
Marker expression level
Activation component
Marker
CD44
CD62L
(E)
CD8+ CD44low CD8+ CD44int CD8+TAI
CD4+ CD44low CD4+ CD44int CD4+TAI
Marker
ICOS
LAG-3
CD39
PD-1
CD69

Figure 4. Diffusion maps of the identified CD4⁺ and CD8⁺ subsets in the control and treated group. (a) Two-dimensional diffusion map of the CD4⁺ and CD8⁺ T cells present in the tumor at day 8 after the first PD-L1 treatment. Three different CD4⁺ and CD8⁺ T cell metaclusters have been identified by PhenoGraph. Continuity of the pattern reveals relationship between the different represented metaclusters (*n* = 5 mice per group). (b) Diffusion map of the CD4⁺ and CD8⁺ T_{AI} cell displayed by group origin (PBS in blue and PD-L1 in red). (c) Diffusion map of the CD4⁺ and CD8⁺ T_{AI} cell displayed by marker expression ICOS, LAG-3, CD39, PD-1 and CD69. (d) Expression levels of CD44 and CD62L on the metaclustered CD4⁺ and CD8⁺T cell populations. (e) Expression levels of ICOS, LAG-3, CD39, PD-1 and CD69 on the metaclustered CD4⁺ and CD8⁺T cell populations

over time (Fig. 5A). Essentially, the vast majority of the CD39⁺ PD1⁺ CD8⁺ T cells that are present in the TME produce copious amounts of granzyme B, revealing their cytotoxic potential (Fig. 5B).

Rational design of combinatorial immunotherapy targeting activating and inhibitory receptors

The data above indicate that the activity of anti-PD-L1 treatment could be mediated via the expansion of CD4⁺ and CD8⁺ T_{AI} cells that express activating receptors and inhibitory receptors. We assessed if we could further enhance the functionality of the T_{AI} cells by combining the PD-L1 blockade treatment with antibodies targeting inhibitory and stimulatory molecules. For the proof-of- principle, we performed co-treatment studies with blocking antibodies to the inhibitory receptor LAG-3 and with agonistic antibodies to ICOS during PD-L1 blockade (Fig. 6A).

PD-L1 blockade therapy in combination with LAG-3 blockade resulted in enhanced survival and tumor growth delay. Co-treatment with agonistic ICOS anti- body improved PD-L1 blockade therapy even further (Fig. 6B-C, Additional file 1:Figure S4).

Next, we aimed to examine whether induction of T_{AI} cells is linked to the improved survival rate observed in the PD-L1 plus ICOS targeting combination therapy. At day 8 after single and combined therapy, we analyzed the TME, and specifically analyzed the T_{AI} cell abundance in each tumor. Because, *in vivo* treatment with ICOS anti- bodies prevents ex vivo staining for ICOS, we defined the T_{AI} cells with the markers PD-1, CD39 and CD43. The percentage of CD8⁺ T_{AI} cells was significantly higher in the PD-L1 blockade treated group compared to the con- trol group. Importantly, significantly higher percentages of CD8⁺ T_{AI} cells were observed in mice treated by the com- bined ICOS and PD-L1 targeted therapy compared to control or PD-L1 blockade treated mice. Expansion of CD4⁺ T_{AI} cells upon single and combinatorial therapy was equivalent (Fig. 6D). Thus, combinatorial therapy target- ing ICOS and PD-L1 expands CD8⁺ T_{AI} cells and relates to improved survival of the treated mice.

Identification of T_{AI} cells in human colorectal cancer

To extrapolate our findings in preclinical models to clin- ical settings, we questioned whether the T_{AI} cells were present within tumor-infiltrated immune cell popula- tions in

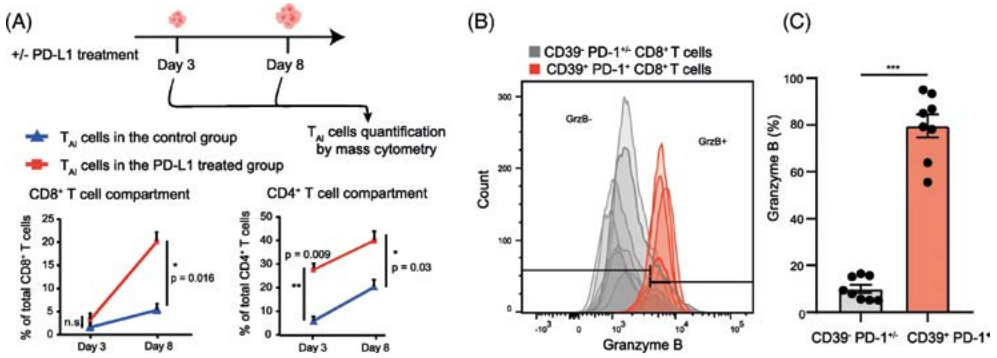

Figure 5. Quantification and cytotoxic capacity of the T_{AI} cells in the TME (a) Average percentage (and SEM) of T_{AI} cells within the CD8⁺ (left panel) and CD4⁺ (right panel) T-cell compartment at day 3 and 8 post PD-L1 blockade therapy in MC-38 tumor challenged mice. (b) Granzyme B expression of CD8⁺ T cell subsets at day 8 post PD-L1 treatment in MC-38 tumor bearing mice. The grey shaded histograms represent the CD39⁻ PD-1$^{+/-}$ CD8⁺ T cells and the red shaded histograms depict the CD39⁺ PD-1⁺ CD8⁺ T_{AI} cells of individual mice. (c) The percentage of granzyme B⁺ cells among the CD39⁺ PD-1⁺ CD8⁺ T_{AI} cells after 8 days of PD-L1 treatment in the MC-38 tumor model compared to the CD39⁻ PD-1$^{+/-}$ CD8 T cells

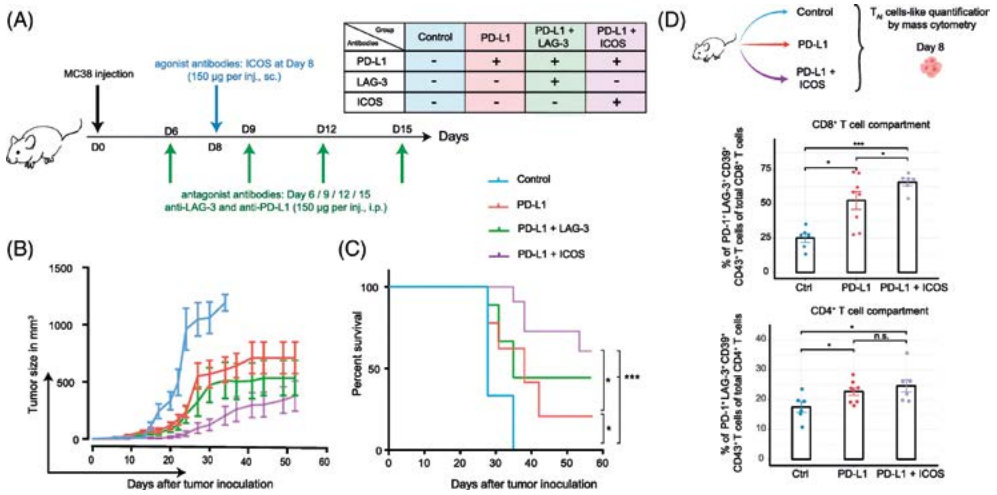

Figure 6. Correlation between the presence of T_{AI} cells in the TME and tumor growth. (a) Regimen scheme of (combinatorial) antibody treatment after tumor injection. (b) Comparison of tumor growth between control group (n = 9), PD-L1 antibody treated group (n = 9), PD-L1 and ICOS antibody treated group (n = 11), PD-L1 and LAG-3 antibody treated group (n = 10). (c) Survival curves for each treatment mentioned above. (d) Study of the tumor-microenvironment after control (n = 6), single therapy (PD-L1, n = 8) or combinatorial therapy (PD-L1 and ICOS, n = 6) of the CD8⁺ T_{AI}-like cells (left panel) and CD4⁺ T_{AI}-like cells (right panel) at day 8 (unpaired t-test) displayed on a per-mouse basis with mean ± SEM

human tumors. We investigated the phenotype of the TILs in colorectal tumors of five patients, who have not undergone any immunotherapy. To reflect the immunogenicity of the MC-38 model, we selected MMRd colorectal cancer patients (29). We designed our flow cytometry panel to characterize putative T_{AI} subsets within the tumor infiltrated $CD8^+$ and $CD4^+$ T cells. Hence, we included the activating receptors ICOS and CD69, also the inhibitory receptors like LAG-3 and CD39. We depicted the $CD8^+$ T cells phenotypic diver- sity by gating on $CD45^+$ $CD8^+$ $CD4^-$ cells and showed that a subset (cluster 8) with a similar phenotype ($CD69^+$ $ICOS^+$ and $LAG\text{-}3^+$) as identified in mice tu- mors could be found in human tumors (Fig. 7A). The $CD4^+$ T cell pool in human tumors contained a substan- tial fraction of cells with a $CD69^+$ $PD1^+$ phenotype, and within this population a $CD39^+$ $ICOS^+$ subset could be identified (Fig. 7B). Together, these results established that in tumors of mice and humans, $CD4^+$ and $CD8^+$ T_{AI} cell subsets are present.

DISCUSSION

Variance of clinical outcomes upon checkpoint blocking immunotherapy like PD-L1 antibody treatment reflects the diversity of the anti-tumor immune response. In the current work, we identified the expansion of $CD4^+$ and $CD8^+$ T-cell subsets that strikingly co-expressed both in- hibitory markers, like PD-1 and LAG-3, and activating markers like ICOS. These subsets, named T_{AI} cells, ex- panded over time, starting 3 days after therapy and were still visible 8 days after the start of the therapy. Since the PD-L1 blocking antibody we used does not induce anti- body-dependent cell-mediated cytoxicity (19), the expan- sion of the T_{AI} cells is most likely caused by blocking the PD-1 signaling pathways rather than e.g. depleting $PD\text{-}L1^+$ cells or reactions to the antibody itself.

The T_{AI} cells appear to play a central role in mediating tumor rejection, despite the expression of inhibitory re- ceptors. The variance seen in response to PD-L1 therapy could be explained by a variable expansion of T_{AI} cells in the TME and needs to be further explored. Our un- biased high dimensional immunophenotyping of the TME provides a deeper insight on the immune changes triggered by immune checkpoint blockade. By identifying a precise expansion of specific subsets in the TME, this strategy enabled us to rationally design immunothera- peutic combination treatments. We were able to en- hance the anti-tumor efficacy of PD-L1 blocking therapy by combining it with an agonist ICOS therapy or an an- tagonist LAG-3 therapy. The T_{AI} cells identified in our murine models shared a similar phenotype with colorec- tal cancer patients and therefore a similar effect of the combination therapy could be expected. Hence, this detection of the T_{AI} cells in human tumors could thus pave the path to clinically target these cells in colorectal cancer by e.g. combined PD-1/PD-L1 and ICOS targeted immunotherapy. We surmise that TIL analysis by mass cytometry might be a powerful tool for personal-guided combinatorial therapy for each individual patient.

Our mass cytometry panel only screened for certain immunomodulatory molecules of the CD28 superfamily. Upregulation of other molecules, as has been reported for

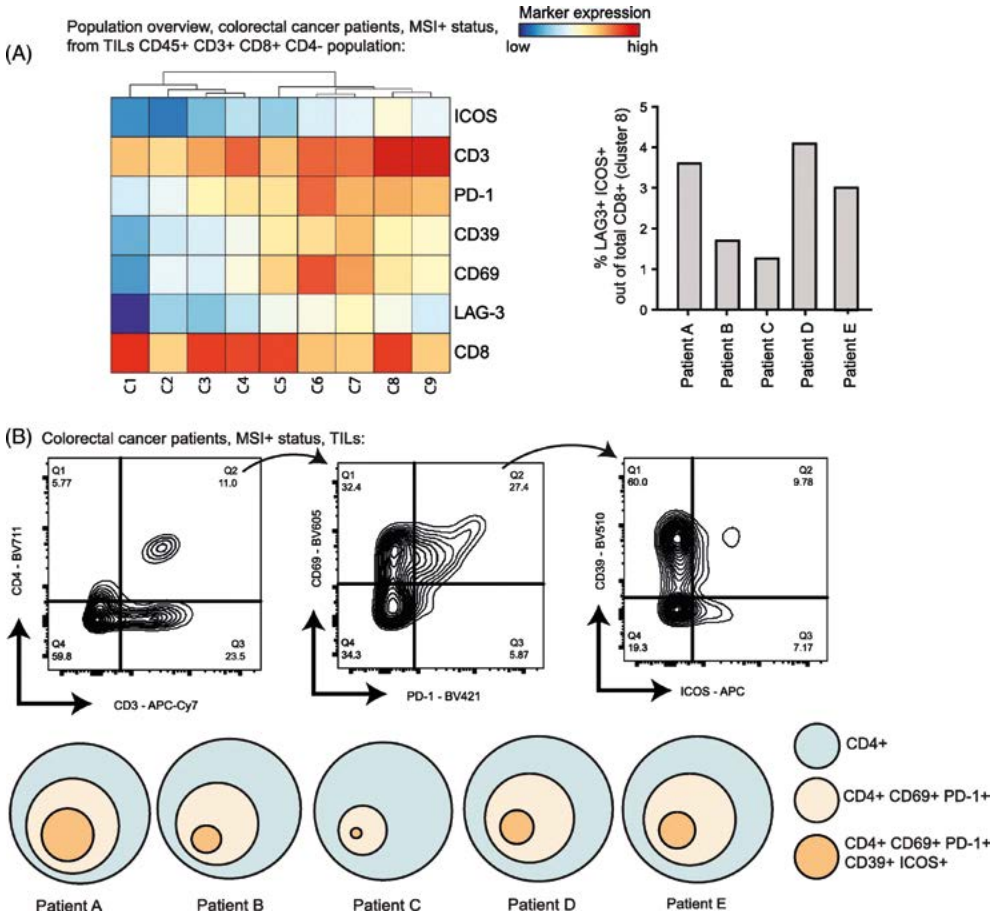

Figure 7. Identification of the T_{AI} cell subset in humans. (a) Heatmap of $CD8^+$ T-cell phenotypes (pre-gated on $CD45^+$ $CD3^+$ $CD4^-$ cells) in tumors of 5 human colorectal cancer (MMRd) patients. Dendrogram above shows the hierarchical similarity between the identified clusters. Right panel shows the frequency of $CD8^+$ $LAG3^+$ $ICOS^+$ cells (cluster 8) among total $CD8^+$ T cells across the 5 patients. (b) Gating strategy to identify the $CD4^+$ $CD69^+$ $PD1^+$ $CD39^+$ $ICOS^+$ population in human colorectal cancer. The abundance proportional to circle area is shown

CTLA-4 (30) or BTLA, might have occurred but were not analyzed due to the limitation of the number of markers in our designed mass cytometry panel. On the other hand, we have included other markers like LAG-3, CD39, CD38, NKG2A, CD43, CD54, ICOS, KLRG1, which have never been analyzed at once in mass cytometry on ex vivo TILs. A large percentage of the T_{AI} cells may be tumor-reactive and have encountered tumor-specific antigenic peptides (e.g. neo-antigens). The granzyme B expression within the T_{AI} cells under- lines this and is consistent with previous work showing that CD39 expression is a marker for cancer-related $CD8^+$ T cells in the TME (31). Consistently, $CD8^+$ T cells expressing PD-1 have also been shown to be more reactive against tumors (32).

Our study is in line with previous studies on other tumor models like the T3 methylcholanthrene-induced sarcomas showing that inhibitory markers like PD-1 and TIM-3 and activating receptors like ICOS are co- expressed on tumor-specific T cells (33). In addition, it was found that the expansion of $CD8^+$ T cells expressing PD-1 improves the efficacy of adoptive T-cell therapy (34) and T cells co-expressing CD39 and PD-1 or LAG- 3 and PD-1 were found to expand after anti-PD-1 ther- apy (7, 35).

Remarkably, in a viral setting, $CD8^+$ T cells that pro- vide the proliferative burst after PD-1 therapy are ex- pressing ICOS (36), suggesting that the T_{AI} cell expansion in the TME relies on the co-expression of ICOS and PD-1 markers. PD-1 and ICOS are also co- expressed on T cells in human bladder tumors (37). Our results can also explain the positive correlation between higher ICOS expression and a better overall survival in colorectal cancer patients (38). Together, this is strengthening the relevance of targeting the $PD\text{-}1^+$ $ICOS^+$ T_{AI} cells by the above-mentioned dual therapy targeting PD-L1 and ICOS. Interestingly, ICOS appears to be relatively higher expressed on $CD4^+$ T_{AI} cells than on $CD8^+$ T_{AI} cells, which we aim to further explore. The T_{AI} cells expanding after PD-L1 blocking therapy also co-expressed LAG-3, which might explain the betterefficiency of the combination of targeting PD-L1 and LAG-3. These findings are coherent with what has been previously reported in other studies (39, 40).

The T_{AI} cells are intratumorally present at an early stage, irrespective of the treatment and respond to immunother- apy as shown by an increase in the TME across time. This suggests that the T_{AI} cells are an identifiable unique subset among T cells, existing before immunotherapy, which can be further expanded by treatment. Tracking these cells in the TME warrants further investigation and would inform about their origin and the plasticity of their phenotype.

The expansion kinetics of the $CD4^+$ T_{AI} cells compared to the $CD8^+$ T_{AI} cells after PD-L1 treatment are dissimilar. In both relative abundance and absolute numbers $CD4^+$ T_{AI} cells are already strongly expanded at day 3 after treatment in contrast to $CD8^+$ T_{AI} cells, while at day 8 the $CD8^+$ T_{AI} cells are more expanded. This is in line with a restored early helper function of the CD4 compartment to stimulate expansion of effector $CD8^+$ T cells. Immunotherapy in the MC-38 model is fully dependent on $CD8^+$ T cells (41). Indeed, after 8 days of PD-L1 treatment, regression of tumor size becomes appar- ent. We could confirm that similar tumor infiltrating T- cell subsets exist in colorectal cancer patients. $CD4^+$ T_{AI} subsets co-expressing inhibitory PD-1 and activating ICOS as well as CD39 and CD69 were detectable in freshly resected colon tumor from MMRd colorectal cancer patients known to express neo-epitopes due to accumulated point-mutations. It would be interesting to study these T_{AI} subpopulations in patients upon treatment with checkpoint therapy or other immunotherapies.

The relevance of targeting simultaneously inhibitory and activating molecules is already transposed in humans. For example, three clinical trials ongoing (NCT02904226, NCT02723955 and NCT02520791) are meant to study the effect of anti-ICOS as monotherapy or in combination with anti-PD-1. Our preclinical study suggests

the syner- gistic effect of ICOS together with a blocking PD-L1 ther- apy. A systematic immunophenotyping of the TME should enable a better prediction of response to immunotherapy and a progress in development of rational immu- notherapeutic strategies.

Conclusion

This study described the expansion of a treatment-re- lated cell subset, named T_{AI} cells, which co-express acti- vating and inhibitory molecules. In preclinical mouse models, both $CD4^+$ and $CD8^+$ T_{AI} cells were higher in abundance in the TME upon PD-L1 therapy. Co-target- ing the inhibitory receptor LAG-3 or the activating receptor ICOS on the T_{AI} cells further enhanced this subset and resulted in improved tumor immunity. T_{AI} cells were also present in human colorectal tumors. We surmise that targeting the inhibitory and activating re- ceptors on these T_{AI} cells could lead to enhanced tumor immunity.

FUNDING

The authors acknowledge funding from the European Commission (Horizon 2020 MSCA grant under proposal number 675743; project acronym ISPIC) and from the Dutch Cancer Society (UL 2015–7817).

AVAILABILITY OF DATA AND MATERIALS

All data generated or analyzed during this study are included in this published article.

ETHICS APPROVAL AND CONSENT TO PARTICIPATE

The inclusion of patients has been conducted in accordance with the ethical principles set out in the Declaration of Helsinki. Patient inclusion was done with approval of the Leiden Medical Centre Medical Ethical Committee.

Written informed consent was obtained prior to data collection.

CONSENT FOR PUBLICATION

We confirm that the manuscript has been read and approved by all named authors and that there are no other persons who satisfied the criteria for authorship but are not listed. We further confirm that the order of authors listed in the manuscript has been approved by all of us.

We confirm that we have given due consideration to the protection of intellectual property associated with this work and that there are no impediments to publication, including the timing of publication, with respect to intellectual property. In so doing we confirm that we have followed the regulations of our institutions concerning intellectual property.

COMPETING INTERESTS

The authors declare no potential financial or commercial conflict of interest.

ABBREVIATIONS

AOF: Average Overlap Frequency; A-tSNE: Approximated t-distributed Stochastic Neighbor Embedding; HSNE: Hierarchical Stochastic Neighbor Embedding; MMRd: MisMatch Repair-deficient; TILs: Tumor Infiltrated Lymphocytes; TME: Tumor Micro-Environment; t-SNE: t-distributed Stochastic Neighbor Embedding

ACKNOWLEDGEMENTS

We would like to thank Sandra Laban for providing technical support, Tamim Abdelaal for his assistance in computational analysis, Camilla Labrie, Elham Beyranvand Nejad and Anke Redeker for their technical support in performing animal experiments and CyTOF processing, Sjoerd van der Burg for his critical review of the manuscript, Ferenc Scheeren for the characterisation of the PD-L1 antibodies (clone MIH5), and the LUMC flow cytometry facility for their support during CyTOF acquisition.

AUTHORS' CONTRIBUTIONS

GB conceived the study, performed the experiments, analyzed the data and wrote the manuscript. AY, EvdG, SvD and MC helped with tumor material processing and animal experiments. TH, VvU, FK, and AV developed Cytosplore and HSNE applications. NFM provided human tumor material. RA and FO designed the experiments, initiated and supervised the project and wrote the manuscript. All authors discussed the results and commented the manuscript. All authors read and approved the final manuscript.

REFERENCES

1. Brahmer JR, Tykodi SS, Chow LQ, Hwu WJ, Topalian SL, Hwu P, et al. Safety and activity of anti-PD-L1 antibody in patients with advanced cancer. N Engl J Med. 2012;366(26):2455–65. https://doi.org/10.1056/NEJMoa1200694.

2. Powles T, Eder JP, Fine GD, Braiteh FS, Loriot Y, Cruz C, et al. MPDL3280A (anti-PD-L1) treatment leads to clinical activity in metastatic bladder cancer. Nature. 2014;515(7528):558–62. https://doi.org/10.1038/nature13904.

3. Topalian SL, Hodi FS, Brahmer JR, Gettinger SN, Smith DC, McDermott DF, et al. Safety, activity, and immune correlates of anti-PD-1 antibody in cancer. N Engl J Med. 2012;366(26):2443–54. https://doi.org/10.1056/NEJMoa1200690.

4. Topalian SL, Taube JM, Anders RA, Pardoll DM. Mechanism-driven biomarkers to guide immune checkpoint blockade in cancer therapy. Nat Rev Cancer. 2016;16(5):275–87. https://doi.org/10.1038/nrc.2016.36.

5. McGranahan N, Furness AJ, Rosenthal R, Ramskov S, Lyngaa R, Saini SK, et al. Clonal neoantigens elicit T cell immunoreactivity and sensitivity to immune checkpoint blockade. Science. 2016;351(6280):1463–9. https://doi.org/1 0.1126/science.aaf1490.

6. Ahmadzadeh M, Johnson LA, Heemskerk B, Wunderlich JR, Dudley ME, White DE, et al. Tumor antigen-specific CD8 T cells infiltrating the tumor express high levels of PD-1 and are functionally impaired. Blood. 2009; 114(8):1537–44. https://doi.org/10.1182/blood-2008-12-195792.

7. Huang AC, Postow MA, Orlowski RJ, Mick R, Bengsch B, Manne S, et al. T-cell invigoration to tumour burden ratio associated with anti-PD-1 response. Nature. 2017;545(7652):60–5. https://doi.org/10.1038/nature22079.

8. Canale FP, Ramello MC, Nunez N, Furlan CLA, Bossio SN, Serran MG, et al. CD39 expression defines cell exhaustion in tumor-infiltrating CD8(+) T cells. Cancer Res. 2018;78(1):115–28. https://doi.org/10.1158/0008-5472.CAN-16-2684.

9. Jiang Y, Li Y, Zhu B. T-cell exhaustion in the tumor microenvironment. Cell Death Dis. 2015;6:e1792. https://doi.org/10.1038/cddis.2015.162.

10. Buchan SL, Fallatah M, Thirdborough SM, Taraban VY, Rogel A, Thomas LJ, et al. PD-1 blockade and CD27 stimulation activate distinct transcriptional programs that synergize for CD8+ T-cell driven anti-tumor immunity. Clin Cancer Res. 2018. https://doi.org/10.1158/1078-0432.CCR-17-3057.

11. Lichtenegger FS, Rothe M, Schnorfeil FM, Deiser K, Krupka C, Augsberger C, et al. Targeting LAG-3 and PD-1 to enhance T cell activation by antigen-presenting cells. Front Immunol. 2018;9:385. https://doi.org/10.3389/fimmu.2018.00385.

12. Sakuishi K, Apetoh L, Sullivan JM, Blazar BR, Kuchroo VK, Anderson AC. Targeting Tim-3 and PD-1 pathways to reverse T cell exhaustion and restore anti-tumor immunity. J Exp Med. 2010;207(10):2187–94. https://doi.org/10.1 084/jem.20100643.

13. Messenheimer DJ, Jensen SM, Afentoulis ME, Wegmann KW, Feng Z, Friedman DJ, et al. Timing of PD-1 blockade is critical to effective combination immunotherapy with anti-OX40. Clin Cancer Res. 2017. https://doi.org/10.1158/1078-0432.CCR-16-2677.

14. Beyrend G, Stam K, Hollt T, Ossendorp F, Arens R. Cytofast: a workflow for visual and quantitative analysis of flow and mass cytometry data to discover immune signatures and correlations. Comput Struct Biotechnol J. 2018;16: 435–42. https://doi.org/10.1016/j.csbj.2018.10.004.

15. Spitzer MH, Carmi Y, Reticker-Flynn NE, Kwek SS, Madhireddy D, Martins MM, et al. Systemic immunity is required for effective Cancer immunotherapy. Cell.

2017;168(3):487–502 e15. https://doi.org/10.1016/j. cell.2016.12.022.

16. Finck R, Simonds EF, Jager A, Krishnaswamy S, Sachs K, Fantl W, et al. Normalization of mass cytometry data with bead standards. Cytometry A. 2013;83(5):483–94. https://doi.org/10.1002/cyto.a.22271.

17. van Unen V, Li N, Molendijk I, Temurhan M, Hollt T, van der Meulen-de Jong AE, et al. Mass cytometry of the human mucosal immune system identifies tissue- and disease-associated immune subsets. Immunity. 2016;44(5):1227–39. https://doi.org/10.1016/j.immuni.2016.04.014.

18. Hollt T, Pezzotti N, van Unen V, Koning F, Eisemann E, Lelieveldt B, et al. Cytosplore: interactive immune cell phenotyping for large single-cell datasets. Comput Graph Forum. 2016;35(3):171–80. https://doi.org/10.1111/cgf.12893.

19. van der Schoot JMS, Fennemann FL, Valente M, Dolen Y, Hagemans IM, Becker AMD, Le Gall CM, van Dalen D, Cevirgel A, van Bruggen JAC, Engelfriet M, Caval T, Bentlage AEH, Fransen MF, Nederend M, Leusen JHW, Heck AJR, Vidarsson G, Figdor CG, Verdoes M, Scheeren FA, et al. Functional diversification of hybridoma-produced antibodies by CRISPR/HDR genomic engineering. Sci Adv. 2019;5:eaaw1822.

20. van Unen V, Hollt T, Pezzotti N, Li N, Reinders MJT, Eisemann E, et al. Visual analysis of mass cytometry data by hierarchical stochastic neighbour embedding reveals rare cell types. Nat Commun. 2017;8(1):1740. https://doi.org/10.1038/s41467-017-01689-9.

21. Pezzotti N, Lelieveldt BPF, Van Der Maaten L, Hollt T, Eisemann E, Vilanova A. Approximated and user steerable tSNE for progressive visual analytics. IEEE Trans Vis Comput Graph. 2017;23(7):1739–52. https://doi.org/10.1109/ TVCG.2016.2570755.

22. Nowicka M, Krieg C, Weber LM, Hartmann FJ, Guglietta S, Becher B, et al. CyTOF workflow: differential discovery in high-throughput high-dimensional cytometry datasets. F1000Res. 2017;(6):748. https://doi.org/10.12688/f1000research.11622.1.

23. Chen H, Lau MC, Wong MT, Newell EW, Poidinger M, Chen J. Cytofkit: a Bioconductor package for an integrated mass cytometry data analysis pipeline. PLoS Comput Biol. 2016;12(9):e1005112. https://doi.org/10.1371/ journal.pcbi.1005112.

24. Levine JH, Simonds EF, Bendall SC, Davis KL, el AD A, Tadmor MD, et al. Data-driven phenotypic dissection of AML reveals progenitor-like cells that correlate with prognosis. Cell. 2015;162(1):184–97. https://doi.org/10.1016/j. cell.2015.05.047.

25. Amir ED, Davis KL, Tadmor MD, Simonds EF, Levine JH, Bendall SC, et al. viSNE enables visualization of high dimensional single-cell data and reveals phenotypic heterogeneity of leukemia. Nat Biotechnol. 2013;31(6):545–52. https://doi.org/10.1038/nbt.2594.

26. Amir ED, Guo XV, Mayovska O, Rahman A. Average overlap frequency: a simple metric to evaluate staining quality and community identification in high dimensional mass cytometry experiments. J Immunol Methods. 2017. https://doi.org/10.1016/j.jim.2017.08.011.

27. Beyranvand Nejad E, van der Sluis TC, van Duikeren S, Yagita H, Janssen GM, van Veelen PA, et al. Tumor eradication by cisplatin is sustained by CD80/ 86-mediated Costimulation of CD8+ T cells. Cancer Res. 2016;76(20):6017– 29. https://doi.org/10.1158/0008-5472.CAN-16-0881.

28. Angerer P, Haghverdi L, Buttner M, Theis FJ, Marr C, Buettner F. destiny: diffusion maps for large-scale single-cell data in R. Bioinformatics. 2016;32(8): 1241–3. https://doi.org/10.1093/bioinformatics/btv715.

29. Banerjea A, Hands RE, Powar MP, Bustin SA, Dorudi S. Microsatellite and chromosomal stable colorectal cancers

demonstrate poor immunogenicity and early disease recurrence. Color Dis. 2009;11(6):601–8. https://doi.org/10.1111/j.1463-1318.2008.01639.x.

30. Wei SC, Levine JH, Cogdill AP, Zhao Y, Anang NAS, Andrews MC, et al. Distinct cellular mechanisms underlie anti-CTLA-4 and anti-PD-1 checkpoint blockade. Cell. 2017. https://doi.org/10.1016/j.cell.2017.07.024.

31. Simoni Y, Becht E, Fehlings M, Loh CY, Koo SL, Teng KWW, et al. Bystander CD8(+) T cells are abundant and phenotypically distinct in human tumour infiltrates. Nature. 2018. https://doi.org/10.1038/s41586-018-0130-2.

32. Gros A, Robbins PF, Yao X, Li YF, Turcotte S, Tran E, et al. PD-1 identifies the patient-specific CD8(+) tumor-reactive repertoire infiltrating human tumors. J Clin Invest. 2014;124(5):2246–59. https://doi.org/10.1172/JCI73639.

33. Fehlings M, Simoni Y, Penny HL, Becht E, Loh CY, Gubin MM, et al. Checkpoint blockade immunotherapy reshapes the high-dimensional phenotypic heterogeneity of murine intratumoural neoantigen-specific CD8+ T cells. Nat Commun. 2017;8(1):562. https://doi.org/10.1038/s41467-017-00627-z.

34. Fernandez-Poma SM, Salas-Benito D, Lozano T, Casares N, Riezu-Boj JI, Mancheno U, et al. Expansion of tumor-infiltrating CD8+ T cells expressing PD-1 improves the efficacy of adoptive T-cell therapy. Cancer Res. 2017; 77(13):3672–84. https://doi.org/10.1158/0008-5472.CAN-17-0236.

35. Edwards J, Wilmott JS, Madore J, Gide TN, Quek C, Tasker A, et al. CD103+ tumor-resident CD8+ T cells are associated with improved survival in immunotherapy naive melanoma patients and expand significantly during anti-PD1 treatment. Clin Cancer Res. 2018. https://doi.org/10.1158/1078- 0432.CCR-17-2257.

36. Im SJ, Hashimoto M, Gerner MY, Lee J, Kissick HT, Burger MC, et al. Defining CD8+ T cells that provide the proliferative burst after PD-1 therapy. Nature. 2016;537(7620):417–21. https://doi.org/10.1038/nature19330.

37. Wong YNS, Joshi K, Khetrapal P, Ismail M, Reading JL, Sunderland MW, et al. Urine-derived lymphocytes as a non-invasive measure of the bladder tumor immune microenvironment. J Exp Med. 2018. https://doi.org/10.1084/jem.20181003.

38. Zhang Y, Luo Y, Qin SL, Mu YF, Qi Y, Yu MH, et al. The clinical impact of ICOS signal in colorectal cancer patients. Oncoimmunology. 2016;5(5): e1141857. https://doi.org/10.1080/2162402X.2016.1141857.

39. Woo SR, Turnis ME, Goldberg MV, Bankoti J, Selby M, Nirschl CJ, et al. Immune inhibitory molecules LAG-3 and PD-1 synergistically regulate T-cell function to promote tumoral immune escape. Cancer Res. 2012;72(4):917– 27. https://doi.org/10.1158/0008-5472.CAN-11-1620.

40. Huang R-Y, Eppolito C, Lele S, Shrikant P, Matsuzaki J, Odunsi K. LAG3 and PD1 co-inhibitory molecules collaborate to limit CD8+ T cell signaling and dampen antitumor immunity in a murine ovarian cancer model. Oncotarget. 2015;6(29):27359–77. https://doi.org/10.18632/oncotarget.4751.

41. Kleinovink JW, Marijt KA, Schoonderwoerd MJA, van Hall T, Ossendorp F, Fransen MF. PD-L1 expression on malignant cells is no prerequisite for checkpoint therapy. Oncoimmunology. 2017;6(4):e1294299. https://doi.org/10.1080/2162402X.2017.1294299.

ADDITIONAL FILE

(A)

Immune context	
CD45	Pan immune
TCR γδ	γδ T cells
TCRβ	T cells
CD3ε	T cells
CD8α	Cytotoxic T cells
CD4	Helper T cells
CD19	B cells
CD115	MCSF-1R
MHCII	Antigen presenting cells
CD161	NK cells
CD11c	Dendritic cells
Ly6C	Monocytes
Ly6G	Neutrophiles
F4/80	Macrophages

Differentiation / activation markers	
CD69	Glycoprotein
CD43	Glycoprotein
CD27	TNF R.
CD28	B7.1R. B7.2R.
CD86	B7.2 protein
CD14	LPS receptor

Immunomodulatory molecules	
PD-1	Co-inhibitory R.
PD-L1	Ligand of PD-1
KLRG1	Glycoprotein
ICOS	Co-stimulatory R.
LAG-3	Co-inhibitory R.

Cyto/Chemokine receptors	
CXCR3	Chemokine R.3
CXCR5	Chemokine R.5
CD25	IL-2Rα
CD122	IL-2Rβ
CD127	IL-7Rα

Adhesion molecules	
CD54	ICAM-1
CD9	Tetraspanin
NKG2A	C-type lectin R.
CD44	HCAM
CD62L	L-selectin
CD11b	Integrin

Ectoenzymes	
CD38	cADP ribose hydrolase
CD39	E-NTPDase

(B) **CD45+ live tumor cells, day 8 post-therapy**

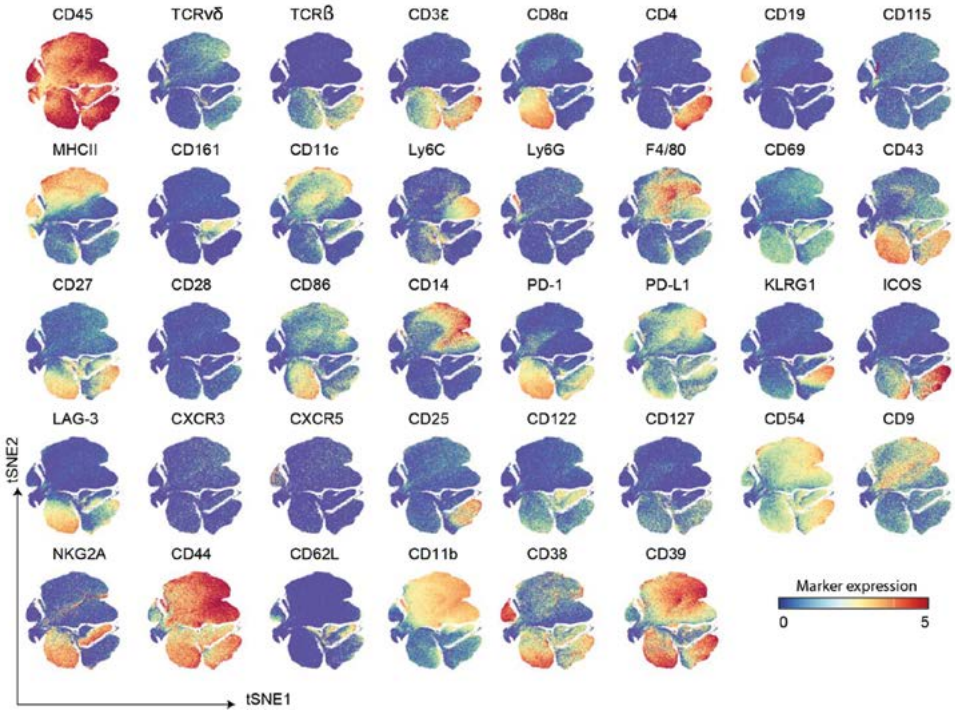

Figure S1. Mass cytometry panel and marker expression. (A) Description of the mass cytometry panel. (B) t-SNE-based two-dimensional maps showing ArcSinh5-transformed marker expression patterns (rainbow scale) of each antibody on live CD45$^+$ cells (4.0×10^4) present in MC-38 tumors, 8 days post PD-L1therapy. Each dot represents a single cell.

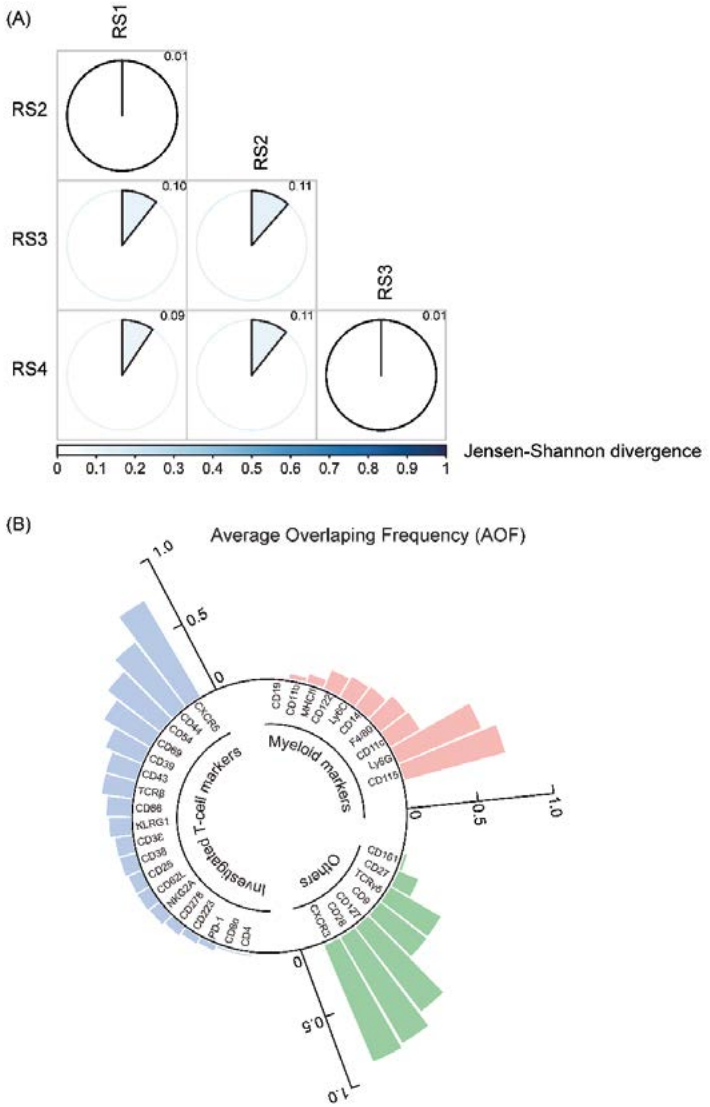

Figure S2. Quality control assessment of the data generated by mass cytometry. (A) Matrix displaying the Jensen-Shannon divergence of the reference standard measured at regular intervals. All values are low, showing consistency between all measurements. (B) Bar plots representing the Average Overlap Frequency values for CD3⁺ events in the TME (myeloid markers shown in pink, T-cell markers in blue and others in green). In bold are highlighted the markers discussed in Figure 3. Values close to zero indicates a clear separation between the positive and negative peaks.

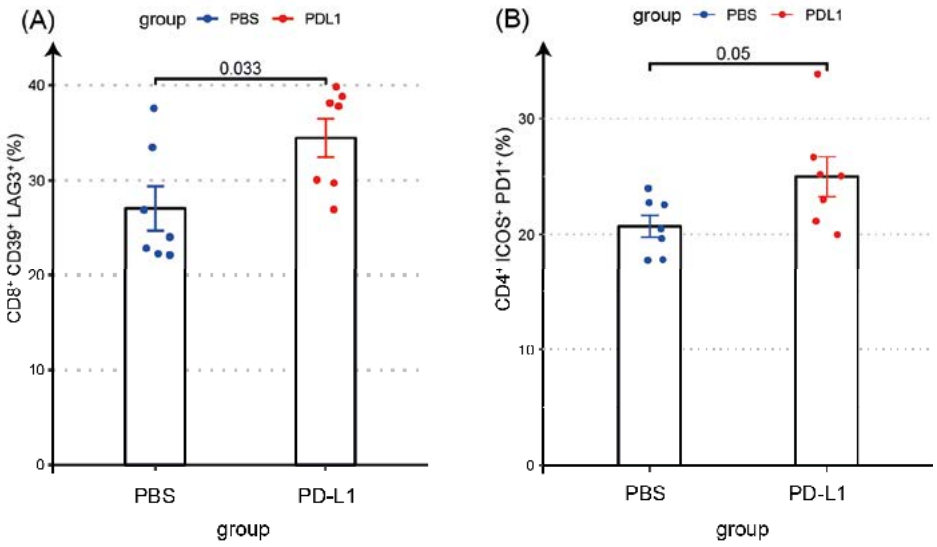

Figure S3. Cytotoxic capacity of CD8⁺ T_{AI} cells and identification of CD4⁺ and CD8⁺ T_{AI} cells in the MCA205 sarcoma model. (A) Bar graph showing the percentage of CD8⁺ T_{AI} cells in the MCA205 tumor model. CD8⁺ T_{AI} cells were identified by CD39 and LAG-3 expression at day 8 post treatment (control (blue) and PD-L1 treated group (red)). (B) Bar graph showing the percentage of CD4⁺ T_{AI} cells in the MCA205 tumor model. CD4⁺ T_{AI} cells were identified by ICOS and PD-1 expression at day 8 post treatment (control (blue) and PD-L1 treated group (red)).

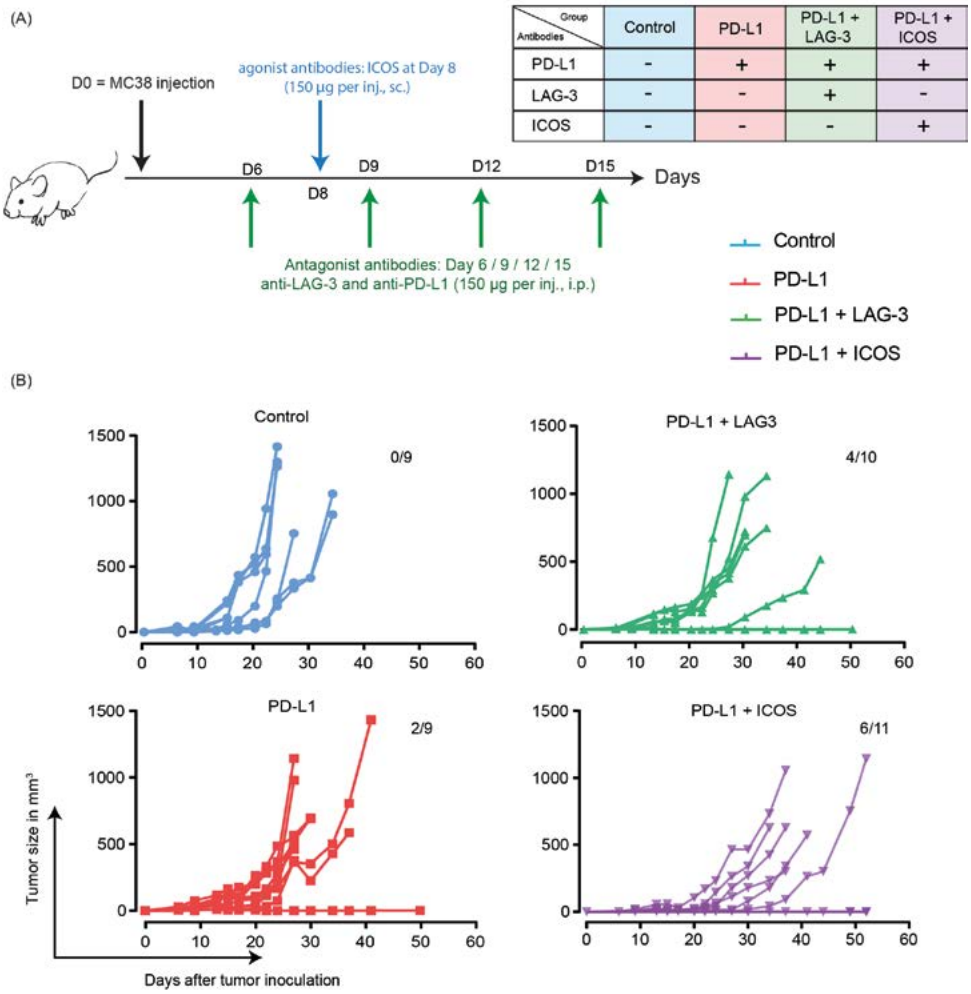

Figure S4. Synergy of combination immunotherapy. (A) Schematic of (combination) treatment after tumor challenge. (B) Individual tumor growth curves of control (PBS, n=9), PD-L1 treated (n=9), PD-L1 and LAG-3 treated (n=10), and PD-L1 and ICOS treated mice (n=11). At day 32, mice from the combination groups PD-L1 + LAG-3 and PD-L1 + ICOS presented smaller tumors compared to the control group (respectively p=0.02 and p <0.0001, unpaired t-test) or compared to the single therapy PD-L1 (respectively p=0.08 and p<00.6, unpaired t-test).

Table S1. FACS panels used in the study.

Antibodies	Clone	Color	Manufacturer	Reference
FACS panel for mouse studies				
CD4	RM4-5	BV605	BD Biosciences	563151
CD8	53-6.7	Alexa 700	BioLegend	100730
CD45	104	FITC	BD Biosciences	553772
7AAD	7AAD	PerCP5.5	ThermoFisher	A1310
CD3	500A2	BV500	BD Biosciences	550277
ICOS	7E.17G9	PE	BioLegend	117406
LAG3	C9B7W	PE-Cy7	BioLegend	125226
CD25	PC61	APC	BioLegend	102012
FACS panel for human studies				
CD45	30-F11	FITC	BD Biosciences	345808
LAG3	FAB2319P	PE	R&D	FAB100A
ICOS	ISA-3	APC	ThermoFisher	17-9948-41
CD8	RPA-T8	PE-Cy7	BD Biosciences	557746
CD3	17A2	APC eFluor	ThermoFisher	47-0038-41
PD1	EH12.2H7	BV421	Biolegend	329919
CD39	A1	BV510	Sony Biotechnology	2241095
7AAD	7AAD	Per-CP5.5	ThermoFisher	A1310
CD4	SK3	BV711	BD Biosciences	563033
CD69	FN50	BV605	Biolegend	310937

DISCOVERY OF CIRCULATING EFFECTOR T CELL STATES CONNECTED TO EFFECTIVE IMMUNE CHECKPOINT THERAPY

5

ABSTRACT

Immune checkpoint therapy (ICT) has the potency to eradicate cancer but the characteristics and mechanisms of effective *versus* non-effective therapy-induced immune responses remain to be elucidated. Here, using high-dimensional single-cell profiling we define T cell states that develop in response to effective ICT eradicating syngeneic mouse tumors. Unbiased assessment of transcriptomic alterations of therapy-responsive T cells in the circulation by single-cell RNA sequencing and system-wide profiling of cell-surface protein expression by mass cytometry revealed unique effector CD4$^+$ and CD8$^+$ T cell states. The therapy-responsive CD4$^+$ and CD8$^+$ effector T cells displayed distinct NK cell receptors and chemokine receptors, and these cells were system-wide existing. Functional targeting of these molecules in tumor-bearing mice showed their functional importance for therapy-induced anti-tumor immunity. Moreover, NK cell receptor-expressing effector T cells were also present in the peripheral blood of immunotherapy-responsive cancer patients. These findings provide a better understanding of ICT and highlight the use of biomarkers on effector CD4$^+$ and CD8$^+$ T cells to improve cancer immunotherapy.

Manuscript in preparation

Guillaume Beyrend[1], Esmé T.I. van der Gracht[1*], Tetje C. van der Sluis[1*], Tamim Abdelaal[2,3], Simon Jochems[4], Bob Belderbos[5], Tom Wesselink[1], Suzanne van Duikeren[1], Anke Redeker[1], Elham Beyranvand Nejad[6], Marcel Camps[1], Adriaan Bins[7], John BAG Haanen[8], Joachim G Aerts[5], Ferry Ossendorp[1], Ramon Arens[1]

[1] Department of Immunology, Leiden University Medical Center, Leiden, The Netherlands
[2] Pattern Recognition and Bioinformatics, Delft University of Technology, Delft, The Netherlands
[3] Leiden Computational Biology Centre, Leiden University Medical Centre, Leiden, The Netherlands
[4] Department of Parasitology, Leiden University Medical Centre, Leiden, The Netherlands
[5] Department of Pulmonary Diseases, Erasmus Medical Center, Rotterdam, The Netherlands
[6] Department of Medical Oncology, Leiden University Medical Centre, Leiden, The Netherlands
[7] Department of Department of Medical Oncology, Amsterdam UMC, location AMC, Amsterdam, the Netherlands.
[8] Division of Molecular Oncology and Immunology, Netherlands Cancer Institute, Amsterdam, the Netherlands
*shared authorship

INTRODUCTION

Immunotherapy has become an important treatment against cancer, but a deeper understanding of factors governing immune responses in cancer is required to extend clinical efficacy to the majority of patients. Many studies have focused on profiling intratumoral CD8 T^+ cells, however recent studies have demonstrated that systemic anti-tumor immune responses are essential for immunotherapeutic efficacy (1). A comprehensive description of how immunotherapy during cancer development affects the systemic T cell states is lacking.

Regression of solid tumors is generally positively correlated with T cells infiltrating the tumor tissue (2). Expression of inhibitory molecules including PD-1 and CTLA-4 on these T cells, however, associate with impaired function such as diminution of the cytotoxic and proliferative potential (3). To counteract the cancer-associated T-cell inhibition, successful therapies were developed that were able to antagonize such T-cell inhibition leading to durable responses (4, 5). This type of immunotherapy, named immune checkpoint therapy (ICT), provides currently an established treatment option for several types of cancer. However, long-term survival can only be achieved in a minority of patients, which warrants to determine the probability of clinical response rates and the development of more efficacious treatment options. In this respect, a better understanding of the cellular mechanisms that mediate tumor rejection could support both the clinical prospects as the design of optimal treatment modalities (6). Non-invasive screening methods with predictive biomarkers related to effective therapy are highly desired, especially, in light of the many clinical trials that incorporate novel (combinatorial) immunotherapeutic approaches that are on-going (7).

The application of single-cell RNA sequencing (sc-RNA-seq) to cancers has provided unprecedented insights into the tumor microenvironmental heterogeneity. Deep immunophenotyping using other single-cell technologies such as high-dimensional cytometry has also been instrumental in understanding how the tumor micro-environment was shaped upon immunotherapy (8-10). For example, by using these single-cell technologies it was shown that the intratumoral T cells have different states of functionality ranging from functional cytotoxicity to exhausted states. Cancer immunity has also been investigated on a systemic level, showing key roles for T cells, NK cells (11), monocytes (12) and macrophage (13) subsets (14-16).

In this study, we analyzed the T cell response to different types of immunotherapeutic regimens, representing different response levels of the immune system towards murine tumors. We used two forms of high-dimensional single-cell profiling—single-cell RNA sequencing (17) and mass cytometry (CyTOF) (18)—to assess transcriptional and proteomic changes of responding T cell populations. We found specific effector T cell subsets in the blood, characterized by specific biomarkers (e.g. transcription factors, chemokines and NK cell markers), which connected functionally to the treatment and the related tumor rejection. System-wide analysis revealed that the therapy-responsive T

cells were not limited to the blood but connected to other main immune compartments like the spleen, bone marrow and lymph nodes. Finally, we extrapolated the results to human settings by analyzing peripheral blood mononuclear cells shortly after therapy, and found T cell states in the blood that correlated with the clinical response rate. Together, this study reveals heretofore unrecognized dynamic cellular changes occurring during ICT, and the role of a set of biomarkers, which are of importance in tumor immunity and could be used in screening to assess the level of immunotherapy efficiency.

MATERIALS AND METHODS

Mice and tumor cell lines

C57BL/6 female mice were obtained from Janvier Laboratories (Le Genest-Saint-Isle, France). At the start of the experiments, mice were 6 to 8 weeks old. $Spn^{-/-}$ mice (*Spn*^{em1Lumc}) on a C56BL/6 background were generated using CRISPR-Cas9-mediated targeting of zygotes, which resulted in deletion of the coding sequence of Exon 2 of the Spn (Cd43) gene. Mice were housed in individually ventilated cages (IVC) under specific pathogen-free (SPF) conditions in the animal facility of Leiden University Medical Centre (LUMC, The Netherlands). All mouse experiments were controlled by the animal welfare committee (IvD) of the Leiden University Medical Center and approved by the national central committee of animal experiments (CCD) under the permit number AVD116002015271, in accordance with the Dutch Act on Animal Experimentation and EU Directive 2010/63/EU.

Tumor challenge models

Treatment schedule of experiments are indicated in the respective figures and legends. In tumor experiments, mice were inoculated in the flank with 0.3×10^6 MC-38 (subcutaneously) or HCMel12 (intra-dermally) tumor cells in respectively 200 µL or 30 µL PBS containing 0.2% BSA on day 0. Tumor outgrowth was measured by caliper in three dimensions, until mice had to be sacrificed due to tumor burden, according to local ethical guidelines. Briefly, mice were euthanized when tumor size reached 1000 mm^3 in volume or when mice lost over more than 20% of their total body weight (relative to initial body mass).

In vivo antibody usage

OX40 (clone OX86) was injected subcutaneously next to the tumor together with anti-CpG 6 days after tumor inoculation to agonistically target OX40 and CpG. αPD-L1 (clone MIH5) blocking antibodies were administered intraperitoneally 10, 13 and 16 days after tumor inoculation.

$CD4^+$ (clone GK1.5) and $CD8^+$ (clone 2.43) T cell depleting monoclonal antibodies were produced in the LUMC and administered intraperitoneally twice weekly (respectively 150 µg/mouse first injection followed by 150 µg/mouse injections) for 2 weeks. $CD8^+$ T

cell depletion was started 4 days before tumor challenge. Depletion was checked by staining for CD3, CD4 and CD8 marker expression followed by flow cytometric analysis.

CXCR3 and NKG2D depleting antibodies were purchased from BioXCell and administered intraperitoneally three times a week for a total of 4 injections. Correct blocking of CXCR3 and NKG2D receptors was verified by flow cytometry using CXCR3 and NKG2D antibodies in the antibody mix presented **in Figure S1** and used in **Figure 4**.

MACS sorting and debris removal

To purify mouse T cells extracted from the blood, the Pan T Cell Isolation Kit I for mouse (130-095-130, Miltenyi Biotec) was used two consecutive times to reach a high level of T cell purity, consequently check by flow cytometry after blood lysis step. A consecutive step to remove debris from the blood was performed by using the Debris Removal Solution (130-109-398) from Miltenyi Biotec according to the manufacturer protocol. Results by flow cytometry (7AAD, CD4 - FITC, CD8 -APC, CD3 -BV510) showed a purity of more than 95% (data not shown) and was then sequenced for single-cell-RNA-sequencing.

Organ processing

Tumor-bearing mice were sacrificed, and transcardially perfused with 30 mL of PBS/EDTA (2 mM) to eliminate blood contamination of tumor material mainly. Tumors were minced, incubated with 2.5 mg/mL Collagenase D and DNAse (Roche) for 20 minutes at 37°C and single-cell suspensions were made using 70-µm cell strainers (BD Biosciences). For further processing with mass cytometry, tumor infiltrating lymphocytes were purified with a 40/60/80/100 Percoll (GE Healthcare) gradient. Spleen and lymph nodes were minced through a 70-µm cell strainers, bone marrow was extracted from the bones by flushing with medium 8% FBS. On all samples, red blood cells were lysed for 2 minutes with a lysis buffer. Samples were then washed with medium 8% FBS and analyzed by flow or further processed for analysis by mass cytometry.

Flow cytometry analysis

Samples obtained from the organ processing steps were rinsed with flow cytometry buffer (PBS with 2% FBS). Mouse Fc-Receptors were blocked with anti-mouse CD16/32 (clone 2.4G2) and 10% naïve mouse serum for 15 minutes before antibody staining. Cells were then stained using combinations of antibodies as shown in **Figure S1**. Samples were acquired on a Fortessa (BD) and analyzed using FlowJo software (Tree Star).

Mass cytometry (CyTOF)

Single cell suspensions of mouse tumors were prepared identically as for flow cytometry, as described above. In addition, debris, tumor cells and aggregates were removed using a 100/60/40/30-percent gradient of Percoll (GE HealthCare) in RPMI 1640 (Lonza), resuspending pelleted single cells in the 40% fraction. This procedure did not skew

the abundance of macrophage subsets as assessed by flow cytometry of the same tumor samples with and without using the Percoll gradient (data not shown). Approximately 3 million cells were then taken for antibody staining. Metal-conjugated antibodies were purchased from Fluidigm Sciences, other antibodies were conjugated in-house using the MaxPar X8 antibody labeling Kit (Fluidigm Sciences) according to manufactures instructions. For all non-cadmium metals or with the Maxpar MCP9 for cadmium metals, and respectively stored in Antibody Stabilization Buffer (Candor Bioscience GmbH) or HRP-Protector™ peroxidase stabilizer (Boca Scientific) was used.

Mass cytometry staining

All reagents were purchased from Fluidigm Sciences unless stated otherwise. In short, samples were incubated with 1 μM Cell-ID intercalator-103Rh to identify dead cells, followed by blockage of mouse serum (2%) and Fc blocking anti-mouse CD16/32 (clone 2.4G2, BD Biosciences: 5%). Then, the metal-conjugated antibody mix was added, and cells were incubated overnight up to 48 hours with 125 nM Cell-ID Intercalator-Ir in MaxPar Fix and Perm. Prior to acquisition on a Helios mass cytometer, samples were centrifuged and resuspended in MilliQ and measured directly. Data were normalized using EQ Four Element Calibration Beads with the reference EQ passport P13H2302. Data analysis was performed by pre-gating live singlet $CD45^+$ cells using FlowJo software (Tree Star), followed by non-supervised clustering based using the hierarchical t-SNE (HSNE) function of Cytosplore with 5 levels.

Single-Cell RNA Sequencing Library Generation

Droplet-based 3′ end massively parallel single-cell RNA sequencing (scRNAseq) was performed by encapsulating sorted live CD45+ tumor infiltrating cells into droplets and libraries were prepared using Chromium Single Cell 3′ Reagent Kits v1 according to manufacturer's protocol (10x Genomics). The generated scRNAseq libraries were sequenced using an Illumina HiSeq2500.

Preprocessing Analysis with Seurat Package

Downstream analysis was performed using the Seurat R package (34). Briefly, for each sample (OX40, PDL1, PDOX and untreated), mitochondrial, ribosomal and hemoglobin genes were excluded. Further, cells expressing less than 200 genes, and genes that were expressed in less than 3 cells were excluded. Next, all samples were pooled together into one dataset, and outlier cells expressing more than 2900 genes were excluded, which resulted in a dataset of 5260 cells Next, the dataset was log1p normalized with a scaling factor of 10,000. Next, the set of 1709 highly variable genes were selected for further analysis. Dataset was preprocessed using principal component analysis. Using the top 15 principle components, the dataset was clustered using Louvain (graph-based community detection) and visualized using tSNE (35). Differentially expressed genes (DEgenes) were

identified between different cell groups, using Wilcoxon rank sum test with Bonferroni multiple test correction. DEgenes were visualized using violin plots, where statistically significant genes had adjusted P-value < 0.05. Within the CD4+ and CD8+ T cells separately, cells expressing the Cxcr3, Klrk1 and Klrc1 genes were compared. DE genes were obtained between positive and negative groups of cells expressing these genes (expression > 1 was considered positive, otherwise negative).

Statistics

All *in vivo* and *ex vivo* data are presented as mean and SEM unless stated otherwise. Statistical comparison of groups was performed using an ANOVA and unpaired two-tailed Student's t test (two-tailed). A minimum of three biological replicates was used in all experiments, as specified in figure legends. Differences were considered statistically significant at $p < 0.05$.

RESULTS

Identification of circulating immunotherapy-responsive T cell subsets by sc-RNA-seq

To analyze T cell states associated with efficient immune checkpoint therapies, we challenged wild-type mice with syngeneic MC38 colorectal tumors (19), and then treated tumor-bearing mice with αPD-L1 antibody, blocking the inhibitory checkpoint pathway PD-1/PD-L1, and with agonistic antibodies stimulating the costimulatory receptor OX40 on tumor-specific T cells **(Figure 1A)**. The blockade of the PD-1-PD-L1 axis resulted in delayed tumor outgrowth and cure in 30% of the mice, whereas anti-OX40 treatment resulted in a non-significant delay of tumor outgrowth. However, addition of the TLR9 ligand CpG augmented the antitumoral actions of anti-OX40 (**Figure S1**), which is in line with a previous report (20). Strikingly, the combination of αPD-L1 blockade and anti-OX40/CpG induced cure in the majority of mice **(Figure 1B)**. The combination of the two immunotherapeutics (αPD-L1 and anti-OX40/CpG), referred hereafter as PDOX, was correspondingly most effective against established syngeneic HCMel12 melanoma tumors (21) **(Figure 1C)**.

To identify circulating T cell subsets that respond to effective checkpoint therapy, we isolated $CD4^+$ and $CD8^+$ T cells from the peripheral blood at day 18 post tumor challenge. Per condition >1,000 cells were analyzed by single-cell RNA sequencing (sc-RNA-seq) with a coverage of 60.000 reads per cell. The subpopulation structure of the circulating T cells was defined by pooling data from the different treatment groups representing 5,600 cells total and using the Seurat package analysis to identify transcriptional clusters (**Figure 1D, Figure S2B**). Six distinct T cell clusters could be identified consisting of three $CD4^+$ and three $CD8^+$ T cell clusters **(Figure 1E)**. Two clusters (CD4-T3, CD8-T3) were over-represented in the PDOX group **(Figure 1F)**, and these clusters were characterized by *Id2* and *Lgals1* transcripts encoding for the transcription factor ID2 and Galectin-1,

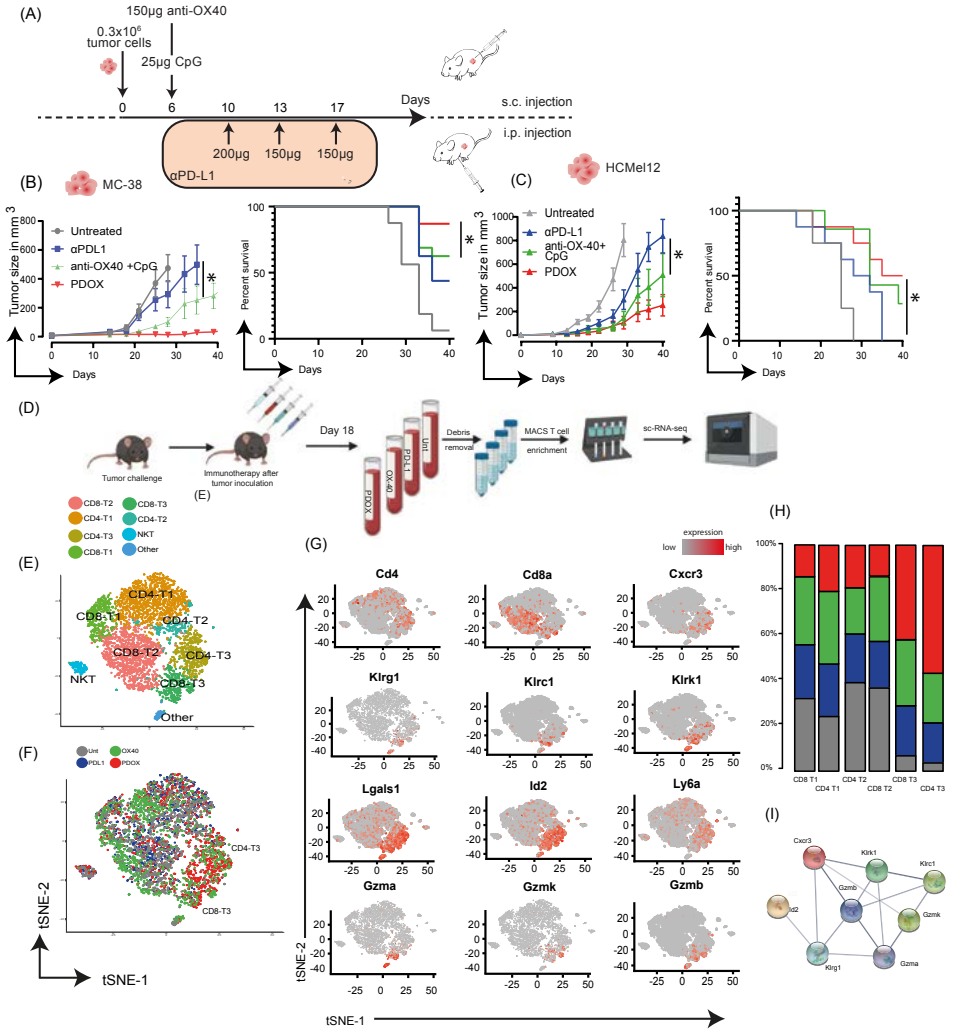

Figure 1. Synergy of immunotherapy targeting inhibitory and activating immune checkpoints. (A) Schematic summary of the therapy regimen. (B) Left panel: comparison of mean (+/- SEM) of MC38 tumor growth between the untreated (grey), OX40 + CpG (green), PD-L1 (blue), combination PDL1 and OX-40, named PDOX group (red), n=16 mice per group. Right panel: Survival of MC38-tumor bearing mice (C) Same as in (B), HCMel12 tumor, n=8 mice per group. (D) Protocol of blood isolation on tumor-bearing mice receiving immunotherapy or left untreated meant for sc-RNA-sequencing analysis. One mouse from each group are submitted to the same antibody regimen as explained in (B). 18 days after tumor inoculation, mice are sacrificed, blood is collected and purified for its T cell compartment using MACS separation. Cells are then sequenced by 10X Genomics Reader. (E) tSNE plot of cells color coded by identified subsets (F) Same as in (E), color coded by group, as explained in (B). (G) Same as in (E) color coded by the expression of the relative gene (Cd4, Cd8a, Cxcr3, Klrg1, Klrc1, Klrk1, Lgals1, Id2, Ly6a, Gzma, Gzmk, Gzmb) from grey to red. (H) Bar graph representing the percentage of the all the 6 subsets according to their group (Untreated in grey, PD-L1 in blue, OX40 in green or PDOX in red).

respectively **(Figure 1G)**. Other gene transcripts overrepresented in both CD4-T3 and CD8-T3 cells were *Cxcr3* (coding for the chemokine receptor CXCR3) and *Ly6a* (coding for Sca-1). Transcripts linked to NK cell markers and cytotoxicity including *Klrk1* (coding for NKG2D protein), *Klrc1* (coding for NKG2A), *Klrg1* (coding for KLRG1), *Nkg7* (coding for NKG7), *Ccl5* (coding for CCL5), *Gzma*, *Gzmb*, and *Gzmk* (coding for Granzyme A, B, K) were enriched in CD8-T3 (**Figure 1H**). *Klrk1* and *Klrc1* transcripts were also found in the CD4-T3 cluster. The upregulated genes upon combination therapy are linked to each other, highlighting the *Klr* relationship evolving around cytotoxicity power (**Figure 1I**).

Transcriptional profiling of immunotherapy-responsive T cell subsets

The CD4-T3 and CD8-T3 clusters were characterized by a high level of *Id2* transcripts (**Figure 2A**), and this connected closely to *Lgals1* transcripts (**Figure S2B**). To search for cell-surface markers associated with these genes we identified the effector T cell-associated glycoform of sialoforine (CD43) using the 1B11 mAb, given the association of ID2 with effector T cell formation (22) and of the association of Galectin-1 with different CD43 glycoforms (23). The antibody clone S11, recognizing CD43 regardless of glycosylation, was not useful in this respect as it identifies CD43 expression on virtually on all T cells being activated or not **(Figure S3)**. Strikingly, the majority of the $ID2^+$ $CD8^+$ T cells expressed the hyperglycosylated CD43 isoform while only a minority of the $ID2^-$ $CD8^+$ T cells expressed this CD43 isoform (**Figure 2B**), and similar results were found for $CD4^+$ T cells (data not shown). Moreover, CD43 positivity correlates closely to PDOX treatment (**Figure 2C**).

To functionally test whether CD43 is implicated in the efficacy of effective checkpoint therapy, we challenged mice deficient in the *Spn* gene (coding for CD43) with MC38 tumor cells, and treated these mice with PDOX. Whereas CD43 proficient mice showed therapeutic efficacy of PDOX upon tumor challenge, the mice deficient in CD43 could not control MC38 tumors despite PDOX treatment (**Figure 2D**). Moreover, PDOX treatment efficacy was highly dependent on $CD8^+$ T cells (**Figure 2E**), suggesting that mainly the effector-type $CD8^+$ T cells characterized by the activation-associated glycoform of CD43 are crucial. In line with this, an increased percentage of $CD43^+CD8^+$ T cells was found in blood and tumors upon PDOX treatment **(Figure 2F)**. Furthermore, the vast majority of tumor-specific $CD8^+$ T cells recognizing the neoantigen Adpgk expressed by MC38 tumors, were positive for CD43 **(Figure 2G)**.

To accurately define the signature of the circulating $CD43^+CD8^+$ and $CD43^+CD4^+$ T cells subsets we performed bulk mRNA sequencing on FACS sorted $CD43^-$ and $CD43^+$ T cells from tumor-challenge PDOX treated mice. The circulating $CD43^+CD8^+$ and $CD43^+CD4^+$ T cells had overlapping gene signatures as the genes expressed in the CD4-T3 and CD8-T3 clusters (e.g. *Id2*, *Lgals1*, *Klrc1*, *Klrg1*, *Klrk1*, *Ly6a*, *Cxcr3*, *Gzmb*) as detected by single cell RNA sequencing **(Figure 2H)**.

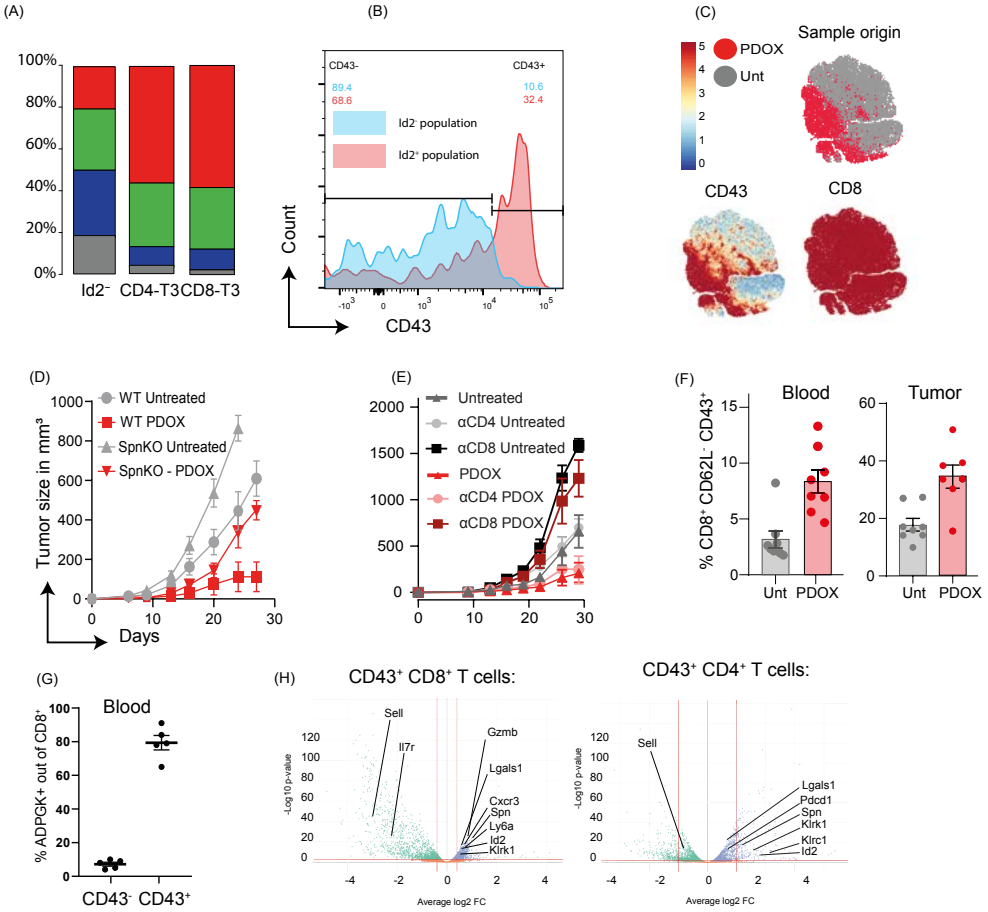

Figure 2. Transcriptional profiling identifies unique effector CD4 and CD8 T cell subsets enriched during effective immunotherapy. Bar graph representing the cell origin per group: untreated (grey), PD-L1 (blue), OX-40 (green), PDOX (red). Representative flow cytometry plot of an ID2⁻ and ID2⁺ population regarding their CD43 expression from a PDOX treated mouse. tSNE plots of flow cytometry data shown per sample group (untreated in grey and PDOX in red), or by the CD8 and CD43 expression (in a blue-to-red scale). Histograms showed a higher expression of CD43 on combined treatment group (mean represented, n=8 samples per group). Average of tumor growth of wild type tumor mice (WT Untreated, round grey), wild type mice receiving PDOX treatment (WT PDOX, square red) Spn$^{-/-}$ mice untreated (SpnKO Untreated, triangle grey) and Spn$^{-/-}$ treated with combination of antibodies (SpnKO – PDOX, triangle red), n=8 mice per group. Average of tumor growth of wild type mice (Untreated, triangle grey), CD4 depleted mice untreated (αCD4 Untreated, grey circle), CD8 depleted mice untreated (αCD8 Untreated, black square), wild type mice treated with PDOX treatment (red, triangle), CD4 depleted mice treated with PDOX treatment (αCD4 PDOX, pink circle), CD8 depleted mice treated with PDOX treatment (αCD8 PDOX, dark red square). Histogram showing the difference of CD8⁺ CD62L⁻ CD43⁺ % in blood and tumor between untreated (Unt) and combination group (PDOX). Proportion of ADGK⁺ cells in blood which are CD43⁻ or CD43⁺. Bulk RNA-seq experiments of sorted CD43⁺ CD8⁺ T cells and CD43⁺ CD4⁺ T cells from wild type mice treated after 8 days of PDOX treatment.

Functional characterization of immunotherapy-responsive T cell subsets

A subset of the CD43$^+$ T cells exhibited NK cell-associated gene expression including *Klkr1* and *Klrc1*. These genes are key molecules related to the effector capacity of NK cells as well as T cells. In the CD8$^+$ lineage, the *Klrk1*$^+$ cells associated to expression of other *Klr* family receptors (*Klrc1*, *Klrc2*, *Klre1*), to the metabolic receptors *Lgals1* and *Lgals3*, to the chemokine ligand *Ccl5* and to chemokines receptor Cxcr3. These cells also expressed *Granzyme A* and *Granzyme B*, emphasizing their cytotoxic capacity. *Klrc1*$^+$ cells presented a similar pattern with upregulation of the *Klrk* family gene members (*Klrk1*, *Klrc2*), upregulation of the transcription factor *Id2*, the chemokine *Ccl5* and granzyme A and B. Compared to other treatments, PDOX treatment triggered the highest increase of Klrk1$^+$, Klrc1$^+$ and Cxcr3$^+$ cells **(Figure 3A)**.

The gene product of *Klrk1*, NKG2D, is known as a molecule with the capacity to provide costimulatory signals to T cells, whereas NKG2A is identified as an inhibitory receptor. Blockade of NKG2D could thus alleviate the positive effect of PDOX treatment on tumor control. To interrogate this hypothesis, we designed *in vivo* experiments in which blockade of NKG2D, using neutralizing antibodies, was combined with PDOX treatment (**Figure 3B**). Whereas NKG2D blockade by itself had no consequence, the effectivity of the PDOX treatment on controlling tumor outgrowth was reduced by the addition of the αNKG2D blocking antibodies **(Figure 3C)**. Remarkably, αNKG2D blockade combined with PDOX treatment did not affect the number of CD43$^+$ CD8$^+$ T cells or tumor antigen-specific CD8$^+$ T cells in the blood but the effect of αNKG2D blockade related to a diminution of CD43$^+$ CD8$^+$ T cells in the tumor-micro-environment. Thus, αNKG2D blockade seem to interfere with recruitment of effector T cells into the TME. To test whether blocking of adhesion receptors expressed on the CD43$^+$ subset had similar effects we blocked the chemokine receptor CXCR3. Blockade of CXCR3 using blocking antibodies resulted in lower CD43$^+$ CD8$^+$ T cells in the TME while the CD43$^+$ CD8+ T cells and tumor-specific CD8$^+$ T cells even accumulated in the blood **(Figure 3D and 3E)**.

Early effector T cell response kinetics as predictors for immunotherapy

To gain insight into the dynamics of the therapy-responsive T cell subsets, we longitudinally followed the CD43$^+$ T cells in the blood of tumor-bearing mice. Anti-OX40/CpG treatment but not αPD-L1 treatment increased the CD43$^+$CD8$^+$ T cell subset at day 13 post-tumor challenge. PDOX treatment however resulted in a further amplification of the CD43$^+$CD8$^+$ T cells, which peaked at day 18 post-tumor challenge **(Figure 4A)**. In non-tumor bearing mice, anti-OX40/CpG and PDOX treatment increased the CD43$^+$CD8$^+$ T cells similarly, indicating that the synergy between anti-OX40/CpG and αPD-L1 blockade to induce the effective treatment-associated T cells is likely driven by the tumor. The kinetics of the CD43$^+$ CD8$^+$ T cells achieved its peak already thirteen days after tumor challenge. Also here, PDOX treatment induced the highest level of CD43$^+$ CD4$^+$ T cells compared to other treatment groups (anti-OX40/CpG, αPD-L1) and untreated mice. These higher

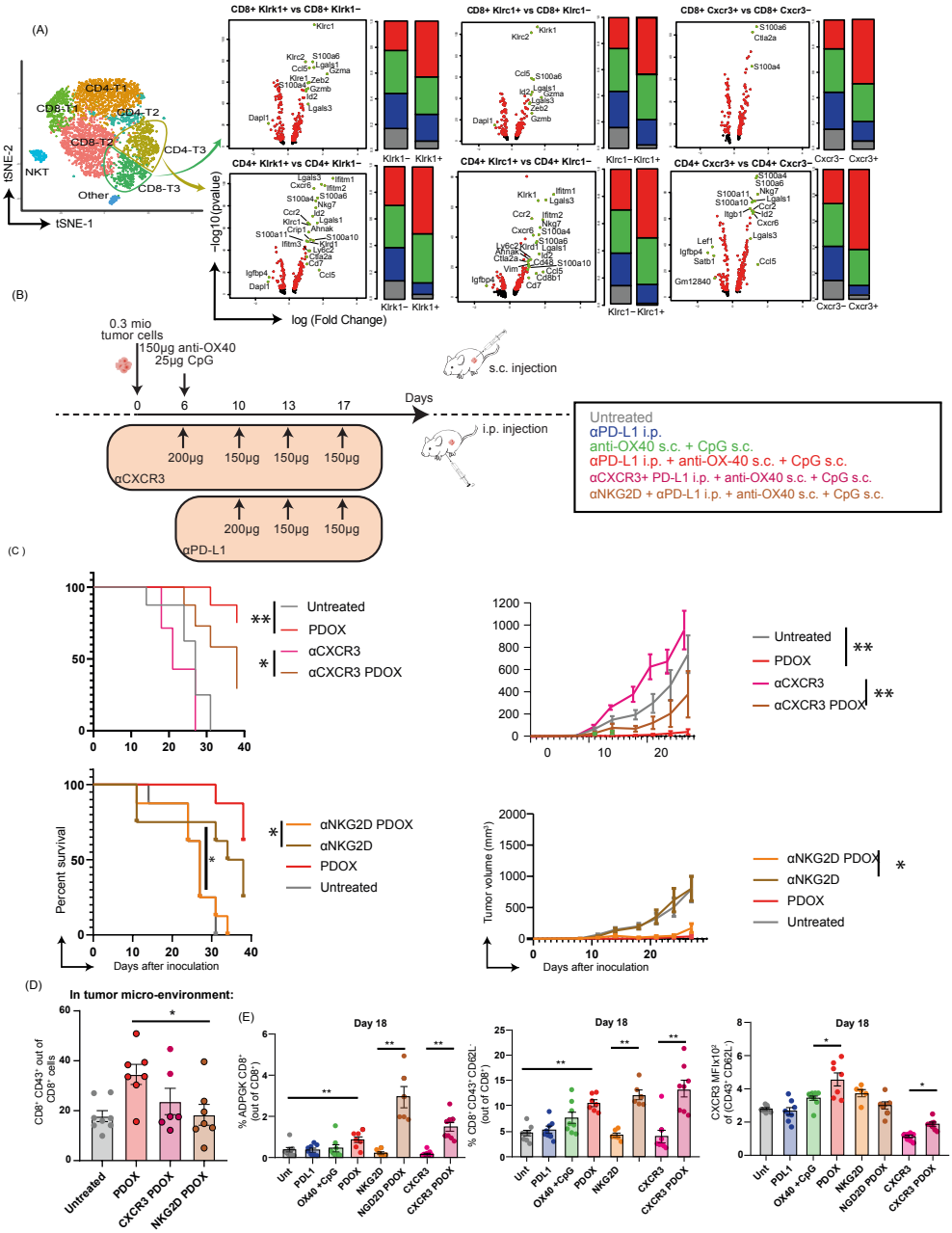

Figure 3. (A) Volcano plots from gated Klrk1+, Klrc1+, Cxcr3+ from either CD4 or CD8 T cells identified on the tSNE map, illustrating the log2 fold change (FC) in gene expression on the x-axis and unadjusted P values from Student t tests on the y-axis between the groups indicated above each plot. A bar graph represents the percentage of the cell origin according to their group (Untreated in grey, PD-L1 in blue, OX40 in green or PDOX in red). Black points: genes with adjusted P-value > 0.05, red points: genes with adjusted P-value < 0.05 and absolute average log2 Fold-Change < 1, green points with gene name label: genes with adjusted P-value < 0.05 and absolute average log2 ▸

Fold-Change > 1. (B) Design of the experiment to characterize the kinetics of the CD62L$^-$ CD43$^+$ T cells. Blood is analyzed 18 days after tumor challenge and mice are treated in four different ways (n=8 per group) as shown. (C) Comparison of the survival and the mean (+/- SEM) of tumor growth between the groups described in (B), n=8 mice per group. (D) Study of the TME after 18 days as indicated on the bar graphs in a sub-optimal treatment (all injections delayed of 2 days). The amount of CD8$^+$ CD43$^+$ cells are shown and compared between the different groups at day 18, (untreated n=8 mice, PDOX n= 7 mice, CXCR3 PDOX n= 6 mice, NKG2D PDOX n= 7 mice) with the same color code as above displayed on a per-mouse basis with mean +/- SEM. (E) Study of the blood after 18 days. The percentage of ADPGK out of CD8$^+$ T cell (%), CD8+ CD43+ CD62L- cell (%), the MFI of CXCR3 and Sca-1 are represented across eight different groups, n=8 mice per group.

CD43$^+$ CD4$^+$ T cell levels lasted until day 25 and was only observed in tumor-bearing mice **(Figure 4B)**.

To correlate the level of CD43$^+$CD8$^+$ T cells to tumor progression, the percentage of CD8$^+$ CD62L$^-$ CD43$^+$ was ranked for all groups and the clinical outcome indicated. The vast majority of the mice with a percentage of CD43$^+$ CD8$^+$ T cells greater than 3% in the blood controlled MC38 tumor outgrowth, whereas none of the mice presenting a percentage of lower than 3% could clear the tumor. This threshold of 3% was even more pronounced in mice challenged with HCMel12 tumors. Altogether, these data suggest that specific effector T cell subsets expand and contract, and this phenomenon correlates to tumor immunity **(Figure 4C)**. Similar results could be determined while studying the expression of Sca-1 on CD8$^+$ CD43$^+$, correlating with tumor immunity as well **(Figure 4D)**.

System-wide characterization of immunotherapy-responsive T cell subsets by CyTOF

To interrogate the system-wide effect of effective ICT, we dissected the blood and other lymphoid compartments including the spleen, bone marrow, lymph nodes by mass cytometry (**Figure 5A**). We developed a 38-marker panel based on our previous data sets including the markers CD43, Sca-1, KLRG-1 (**Figure S4A**). As anticipated, in the blood compartment clusters expressing CD43 are more abundant in the PDOX treated group compared to other groups (16.3 % for PDOX, < 8.6% for other groups) **(Figure 5B)**. Moreover, certain clusters (e.g. cluster CD8-11) are co-expressing markers like CD38, CD39, CD54, KLRG1, and NKG2A. The spleen also contained CD8$^+$ T cells co-expressing CD43 and other activation markers upon PDOX treatment (cluster 8, PDOX: 5%, others: less than 1%). The lymph node compartment contained more CD43$^+$ICOS$^+$CD38$^+$ CD4$^+$ T cells in the PDOX group. In the bone marrow two CD43$^+$ CD4$^+$ T cell subsets were identified as more abundant upon efficient therapy (18% in PDOX vs < 11% in other therapies), and these cells co-expressed PD-1, LAG-3, ICOS and CD54.

Next, we integrated the identified immune cell clusters across all tissues in one immune-systemwide analysis to highlight the correlation between all subsets

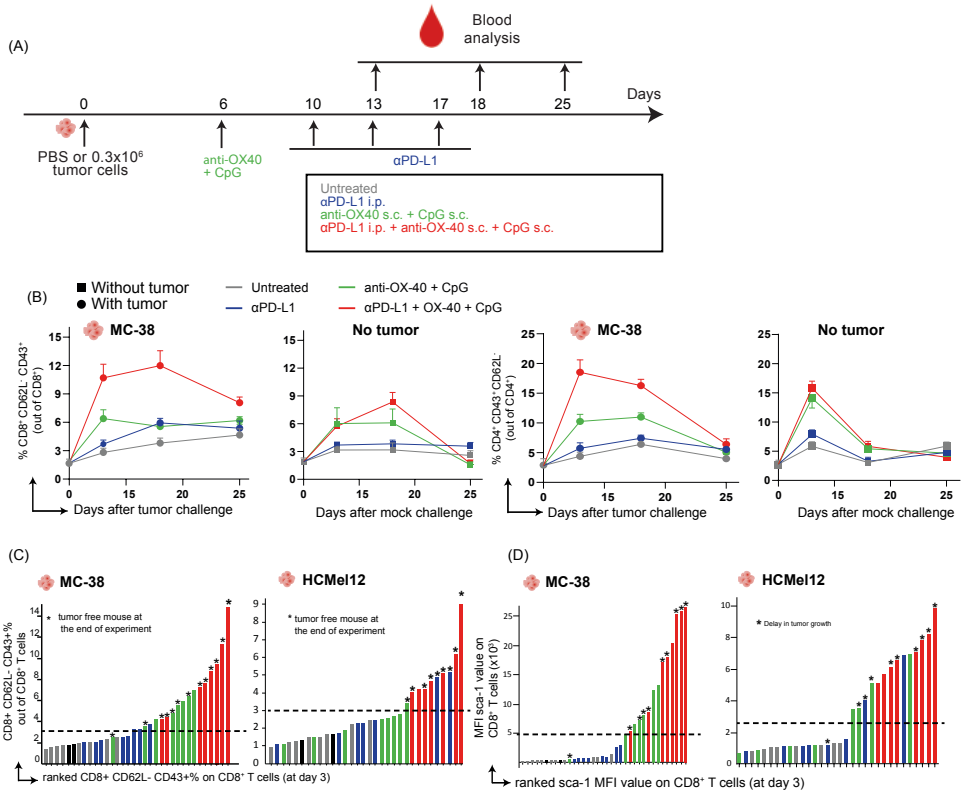

Figure 4. Kinetic study of a CD62L- CD43+ subset and correlation with tumor free survival mice. (A) Design of the experiment to characterize the kinetics of the CD62L$^-$ CD43$^+$ T cells. Blood is analyzed 13 and 18 days after tumor challenge and mice are treated in four different ways (n=8 per group) as shown, naïve mice showing a percentage CD62L$^-$ CD43$^+$ T cells at Day 13 below 1%. (B) Kinetics of the CD43$^+$ T cells across days at three different timepoints (13, 18 and 25 days after tumor injection) investigated by flow cytometry according to their treatment anti-PD-L1 (blue), anti-OX40 (green), combination (red) treatment or if left untreated (grey). Mice are either injected with tumor (round symbol) or left without tumors (square symbols). (C) Correlation between tumor-free rate and CD62L$^-$ CD43$^+$ T cell percentage at Day 25 for each individual MC38-bearing-mice (left panel) or HCMel12-bearing-mice (right panel). (D) Correlation between tumor-free rate and Sca-1 expression on CD62L$^-$ CD43$^+$ T cell percentage at Day 25 for each individual MC38-bearing-mice (left panel) or HCMel12-bearing-mice (right panel).

(Figure 5B). Spearman correlation revealed the relationships between the immune cell subsets in the tissues. The therapy-responsive T cell subsets in the blood are most closely connected to those in the spleen and bone marrow, whereas the lymph node T cell subsets are connected to the spleen. System-wide immunity may thus involve the bone marrow, lymph nodes, spleen and the blood to enable efficient tumor immunity. Altogether, these data show the identification of therapy-responsive effector T cell subsets that are not only existing in the blood compartment but omnipresent in basically all tissues of the immune system.

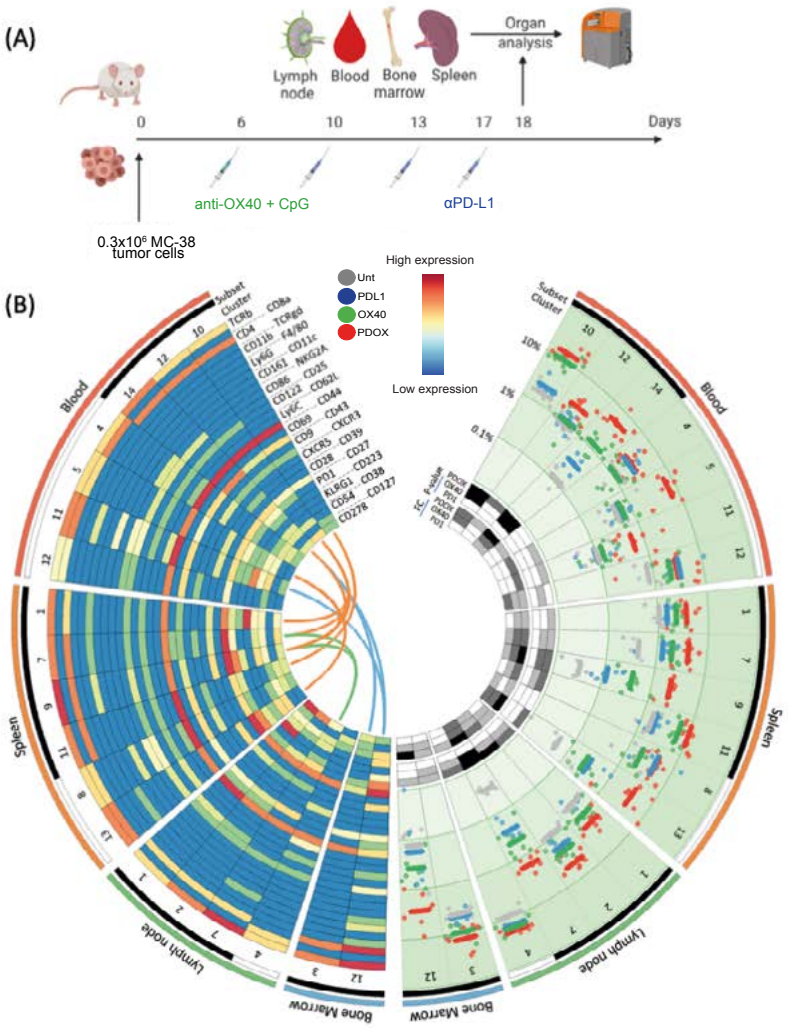

Figure 5. Systemic CyTOF analysis following immunotherapy. (A) Schematic of CyTOF mass cytometry experiment investigating the systemic effect of four different immunotherapies. (B) Circle diagram showing 19 CD4 and CD8 T cell clusters in blood, spleen, lymph nodes or bone marrow. Clusters are mirrored with phenotypic information on the left and abundance in mouse groups on the right. From outside in: CD8 T cell (white bars) and CD4 T cell (black bars) clusters are indicated with cluster number given below. On the left, a heatmap for 32 markers measured by CyTOF depicts normalized expression for each marker per cluster. Clusters that are highly correlated (r>0.8) between compartments are connected by lines, which are colored according to their compartment. On the right, frequency of a subsets within its parent (CD4 or CD8 T cells) is given per cluster on a log-scale. Each dot represents one animal treated with either PDOX (red, n=7-8), OX40 (green, n=8), PD1 (blue, n=5) and untreated (grey, n=5). Mean values per group are indicated by diamonds. Multiple-testing corrected p-values for each of the 3 treated groups compared to the control group are shown, with p>0.01 (white), p<0.01 (light grey), p<0.001 (dark grey), p<0.0001 (black). P-values were based on t-test on log-transformed frequencies and corrected by Benjamini-Hochberg correction. Then means of fold changes (FC) of log-transformed values of groups over the untreated group are shown with FC<2 (white), FC>2 (light grey), FC>4 (dark grey), FC>16 (black).

Systemic immunity is transposable to the human settings in melanoma or NSCLC cancers

We next investigated if the blood compartment could inform on the therapeutic efficacy of immunotherapeutic treatments like PD-1 blockade. We gathered 4 NSCLC (2 responders and 2 non-responders) and 9 melanoma (5 responders and 4 non-responders) cancer patients and added 4 healthy donors in our cohort for a quality check. Blood was collected before treatment and after 2 weeks and analyzed using a 44 mass-cytometry antibody panel **(Figure S4B)**. An analysis of all the detectable CD8⁺ T cell subsets has been performed by HSNE and significant clusters (CTL-24 and -17) are phenotypically described **(Figure 6A)** and associated with the corresponding abundance of each cluster in the responder and non-responder group **(Figure 6B)**. These two subsets were present

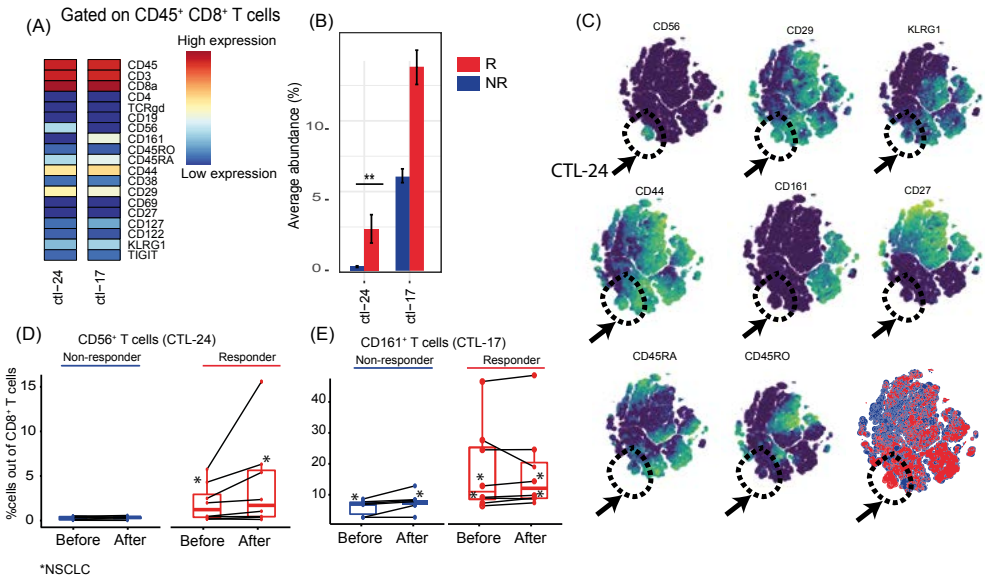

Figure 6. Identification of CD8⁺ T-cell clusters in blood from melanoma patients. (A) Heatmap of all CD8⁺ T-cell clusters identified at baseline or after 2 weeks of PD-1 therapy. Data shown is based on t-SNE plots and is pooled from the responder, non-responder and control groups. Level of ArcSinh5-transformed expression marker is displayed by a rainbow scale. Dendrogram on the top represents the hierarchical similarity between the identified clusters. (B) Average and SEM in percentage of each CD8⁺ T-cell cluster among the CD8⁺ T-cell population of control (blue bars), responder (green bars) and non-responder group (red bars). (C) Bar graph showing the mean frequency of cluster CTL-24 (± SEM, paired t-test on the left panel; unpaired t-test on the right panel) between before and after PD-1 therapy for both responder (green) and non-responder (red) groups. (D) Bar graph showing the mean frequency of specifically mentioned CD161⁺ T cell clusters (± SEM, paired t-test) comparing responder (green) and non-responder (red) groups. (E) Bar graph showing the mean frequency of specifically mentioned CD161⁺ T cell clusters (± SEM, unpaired t-test) comparing healthy donor (blue), responder (green) and non-responder (red) groups. (F) tSNe plot where one dot represents one cell showing the level of expression marker by a rainbow scale from blue to green. The arrow identifies cluster of interest CTL- 24.

in a higher abundance in the responder group compared to the non-responder group. CTL-24 and -17 had the specificity to respectively express CD56 and CD161, making those two markers relevant for immunotherapy screening, a t-SNE map colored per group showed the specificity of CD56 for the responder group **(Figure 6C)**. Over time, within two weeks PD-1 blockade triggered a higher amount of CTL-24 in the responder groups (from 1 to 3%) whereas it remains absent in the non-responder group **(Figure 6D)**. There is however not a specific pattern regarding PD-1 therapeutic effect on the abundance of CD161^{+} cells **(Figure 6E)**, those being more abundant at baseline, correlating with favorable clinical outcome.

DISCUSSION

Immunotherapy has placed itself firmly as an important treatment option amongst conventional therapies such as radiotherapy and chemotherapy in the clinic but oftentimes the clinical responses are partial and variable. Given the substantial variability regarding immunotherapy response, identification of biomarkers in an accessible immune compartment like the blood is necessary to allow for discrimination between responders and non-responders. Such an approach allows tailoring of the treatment to individual patients that are unlikely to respond.

Our work demonstrated a systemic T cell response upon efficient immunotherapy that is characterized by a unique gene and phenotypic signature with similarities to NK cell receptor-expressing T cells that appear upon infection. In two different murine models HCMel12 (uveal melanoma) and MC-38 (colorectal carcinoma), the tumoricidal activity of monotherapy was limited, whereas the combination of an anti–PD-L1 antagonist and an anti-OX40 agonist was exceptionally efficient in eradicating progressing tumors. These data show the importance of using combinatorial treatment of already used therapeutics in patients, i.e. anti-OX40 (24) and anti-PD-L1 (25), and emphasized the potential of this combination as also observed in other mouse tumor models recently (26, 27). The synergic effect of the combinatorial treatment was deciphered by complementary high-dimensional single-cell technology platforms. Both scRNA-seq and mass cytometry highlighted functionally active effector T cell states that were dynamic in their kinetics and characterized by NK receptor expression and expression of adhesion/migration receptors. The kinetics of these effector cells showed an expansion followed by a retraction phase, that is typical for acute infection, and may reflect the temporal activation.

The expression of CD43 on CD8^{+} T cells was a strong marker for these cells as an indicator for effector function based on the co-expression of the NK cell receptors and granzymes. The co-expression of the stemness marker Sca-1 indicated that these cells are antigen-experienced cells (28). In line with our previous findings, it could be suggested that those cells are in a proliferative state and correspond in the tumor environment to a T_{AI} cell phenotype as described recently (29, 30). Interestingly in humans, mass cytometry analysis revealed that the CD62L^{low} CD4^{+} T cell subset expressed T-bet^{+} and CXCR3^{+}, indicative of a Th1 subpopulation (31). These results are also in line with our functional

study, which identified the importance in tumor immunity of the Klr family genes, among them NKG2D, but also chemokines like CXCR3.

Our study indicated that the efficiency of immunotherapeutic treatment is mirrored by the induction of specific peripheral T cells. Here, we identified several markers on $CD8^+$ T cells in the blood, of which some are closely linked to the effectiveness of immunotherapy. For example, ICOS is one of the upregulated molecules upon PDOX treatment, and this marker is linked to effective immunotherapy in mice (32) but also in responsive patients (33).

Altogether, we have provided evidence for an effective-related-treatment immune signature. Future studies entailing a systematic and multicenter cohort of patients with different cancer types for which a PDOX treatment is approved remains needed. A prediction signature might then be directly used in clinical practice to stratify different levels of effectiveness of treatments.

CONTRIBUTIONS

GB conceived the study, performed the experiments, analyzed the data and wrote the manuscript. EvdG, TW, EBN, MC, SvD and MC helped with tumor material processing and animal experiments. TA provided sc-RNA-sequencing analysis. RA designed the experiments, initiated and supervised the project and wrote the manuscript. FO reviewed the manuscript and provided scientific advice. All authors discussed the results and commented the manuscript. All authors read and approved the final manuscript.

ACKNOWLEDGMENT

We would like to thank Camilla Labrie and Iris Pardieck for their technical support in performing animal experiments and CyTOF processing, and the LUMC flow cytometry facility for their support during CyTOF acquisition.

FUNDING

The authors acknowledge funding from the European Commission (Horizon 2020 MSCA grant under proposal number 675743; project acronym ISPIC) and from the Dutch Cancer Society (UL 2015–7817).

REFERENCES

1. Spitzer MH, Carmi Y, Reticker-Flynn NE, Kwek SS, Madhireddy D, Martins MM, et al. Systemic Immunity Is Required for Effective Cancer Immunotherapy. Cell. 2017;168(3):487-502 e15.
2. Galon J, Costes A, Sanchez-Cabo F, Kirilovsky A, Mlecnik B, Lagorce-Pages C, et al. Type, density, and location of immune cells within human colorectal tumors predict clinical outcome. Science. 2006;313(5795):1960-4.
3. Pardoll DM. The blockade of immune checkpoints in cancer immunotherapy. Nat Rev Cancer. 2012;12(4):252-64.
4. Robert C, Schachter J, Long GV, Arance A, Grob JJ, Mortier L, et al. Pembrolizumab versus Ipilimumab in Advanced Melanoma. N Engl J Med. 2015;372(26):2521-32.
5. Robert C, Ribas A, Schachter J, Arance A, Grob JJ, Mortier L, et al. Pembrolizumab versus ipilimumab in advanced melanoma (KEYNOTE-006): post-hoc 5-year results from an open-label, multicentre, randomised, controlled, phase 3 study. Lancet Oncol. 2019;20(9):1239-51.
6. Benedict CA, Ware CF. Virus targeting of the tumor necrosis factor superfamily. Virology. 2001;289(1):1-5.
7. Infante JR, Hansen AR, Pishvaian MJ, Chow LQM, McArthur GA, Bauer TM, et al. A phase Ib dose escalation study of the OX40 agonist MOXR0916 and the PD-L1 inhibitor atezolizumab in patients with advanced solid tumors. Journal of Clinical Oncology. 2016;34(15_suppl):101-.
8. Gubin MM, Zhang X, Schuster H, Caron E, Ward JP, Noguchi T, et al. Checkpoint blockade cancer immunotherapy targets tumour-specific mutant antigens. Nature. 2014;515(7528):577-81.
9. Newell EW, Sigal N, Nair N, Kidd BA, Greenberg HB, Davis MM. Combinatorial tetramer staining and mass cytometry analysis facilitate T-cell epitope mapping and characterization. Nat Biotechnol. 2013;31(7):623-9.
10. Hartmann FJ, Babdor J, Gherardini PF, Amir ED, Jones K, Sahaf B, et al. Comprehensive Immune Monitoring of Clinical Trials to Advance Human Immunotherapy. Cell Rep. 2019;28(3):819-31 e4.
11. Subrahmanyam PB, Dong Z, Gusenleitner D, Giobbie-Hurder A, Severgnini M, Zhou J, et al. Distinct predictive biomarker candidates for response to anti-CTLA-4 and anti-PD-1 immunotherapy in melanoma patients. J Immunother Cancer. 2018;6(1):18.
12. Krieg C, Nowicka M, Guglietta S, Schindler S, Hartmann FJ, Weber LM, et al. High-dimensional single-cell analysis predicts response to anti-PD-1 immunotherapy. Nat Med. 2018.
13. Gubin MM, Esaulova E, Ward JP, Malkova ON, Runci D, Wong P, et al. High-Dimensional Analysis Delineates Myeloid and Lymphoid Compartment Remodeling during Successful Immune-Checkpoint Cancer Therapy. Cell. 2018.
14. Manjarrez-Orduno N, Menard LC, Kansal S, Fischer P, Kakrecha B, Jiang C, et al. Circulating T Cell Subpopulations Correlate With Immune Responses at the Tumor Site and Clinical Response to PD1 Inhibition in Non-Small Cell Lung Cancer. Front Immunol. 2018;9:1613.
15. Nixon AB, Schalper KA, Jacobs I, Potluri S, Wang IM, Fleener C. Peripheral immune-based biomarkers in cancer immunotherapy: can we realize their predictive potential? Journal for ImmunoTherapy of Cancer. 2019;7(1):325.
16. Takeuchi Y, Tanemura A, Tada Y, Katayama I, Kumanogoh A, Nishikawa H. Clinical response to PD-1 blockade correlates with a sub-fraction of peripheral central memory

CD4+ T cells in patients with malignant melanoma. Int Immunol. 2018;30(1):13-22.

17. Sade-Feldman M, Yizhak K, Bjorgaard SL, Ray JP, de Boer CG, Jenkins RW, et al. Defining T Cell States Associated with Response to Checkpoint Immunotherapy in Melanoma. Cell. 2018;175(4):998-1013.e20.

18. Spitzer MH, Gherardini PF, Fragiadakis GK, Bhattacharya N, Yuan RT, Hotson AN, et al. IMMUNOLOGY. An interactive reference framework for modeling a dynamic immune system. Science. 2015;349(6244):1259425.

19. Corbett TH, Griswold DP, Jr., Roberts BJ, Peckham JC, Schabel FM, Jr. Tumor induction relationships in development of transplantable cancers of the colon in mice for chemotherapy assays, with a note on carcinogen structure. Cancer Res. 1975;35(9):2434-9.

20. Sagiv-Barfi I, Czerwinski DK, Levy S, Alam IS, Mayer AT, Gambhir SS, et al. Eradication of spontaneous malignancy by local immunotherapy. Science translational medicine. 2018;10(426):eaan4488.

21. Kilian MM, Loeffler KU, Pfarrer C, Holz FG, Kurts C, Herwig MC. Intravitreally Injected HCmel12 Melanoma Cells Serve as a Mouse Model of Tumor Biology of Intraocular Melanoma. Curr Eye Res. 2016;41(1):121-8.

22. Omilusik KD, Nadjsombati MS, Shaw LA, Yu B, Milner JJ, Goldrath AW. Sustained Id2 regulation of E proteins is required for terminal differentiation of effector CD8(+) T cells. J Exp Med. 2018;215(3):773-83.

23. Hernandez JD, Nguyen JT, He J, Wang W, Ardman B, Green JM, et al. Galectin-1 binds different CD43 glycoforms to cluster CD43 and regulate T cell death. J Immunol. 2006;177(8):5328-36.

24. Wang R, Gao C, Raymond M, Dito G, Kabbabe D, Shao X, et al. An Integrative Approach to Inform Optimal Administration of OX40 Agonist Antibodies in Patients with Advanced Solid Tumors. 2019.

25. Brahmer JR, Tykodi SS, Chow LQ, Hwu WJ, Topalian SL, Hwu P, et al. Safety and activity of anti-PD-L1 antibody in patients with advanced cancer. N Engl J Med. 2012;366(26):2455-65.

26. Messenheimer DJ, Jensen SM, Afentoulis ME, Wegmann KW, Feng Z, Friedman DJ, et al. Timing of PD-1 Blockade Is Critical to Effective Combination Immunotherapy with Anti-OX40. Clin Cancer Res. 2017.

27. Ma Y, Li J, Wang H, Chiu Y, Kingsley CV, Fry D, et al. Combination of PD1 Inhibitor and OX40 Agonist Induces Tumor Rejection and Immune Memory in Mouse Models of Pancreatic Cancer. Gastroenterology. 2020.

28. Kaech SM, Hemby S, Kersh E, Ahmed R. Molecular and functional profiling of memory CD8 T cell differentiation. Cell. 2002;111(6):837-51.

29. Li H, van der Leun AM, Yofe I, Lubling Y, Gelbard-Solodkin D, van Akkooi ACJ, et al. Dysfunctional CD8 T Cells Form a Proliferative, Dynamically Regulated Compartment within Human Melanoma. Cell. 2019;176(4):775-89.e18.

30. Beyrend G, van der Gracht E, Yilmaz A, van Duikeren S, Camps M, Höllt T, et al. PD-L1 blockade engages tumor-infiltrating lymphocytes to co-express targetable activating and inhibitory receptors. Journal for ImmunoTherapy of Cancer. 2019;7(1):217.

31. Kagamu H, Kitano S, Yamaguchi O, Yoshimura K, Horimoto K, Kitazawa M, et al. CD4+ T-cell immunity in the peripheral blood correlates with response to anti-PD-1 therapy. 2019:canimm.0574.2019.

32. Beyrend G, van der Gracht E, Yilmaz A, van Duikeren S, Camps M, Hollt T, et al. PD-L1 blockade engages tumor-infiltrating lymphocytes to co-express targetable activating and inhibitory receptors. J Immunother Cancer. 2019;7(1):217.

33. Friedman CF, Postow MA. Emerging Tissue and Blood-Based Biomarkers that may Predict Response to Immune Checkpoint Inhibition. Curr Oncol Rep. 2016;18(4):21.

34. Butler A, Hoffman P, Smibert P, Papalexi E, Satija R. Integrating single-cell transcriptomic data across different conditions, technologies, and species. Nat Biotechnol. 2018;36(5):411-20.

35. van der Maaten L, Hinton, G. Visualizing Data using t-SNE. Journal of Machine Learning Research. 2008.

ADDITIONAL FILE

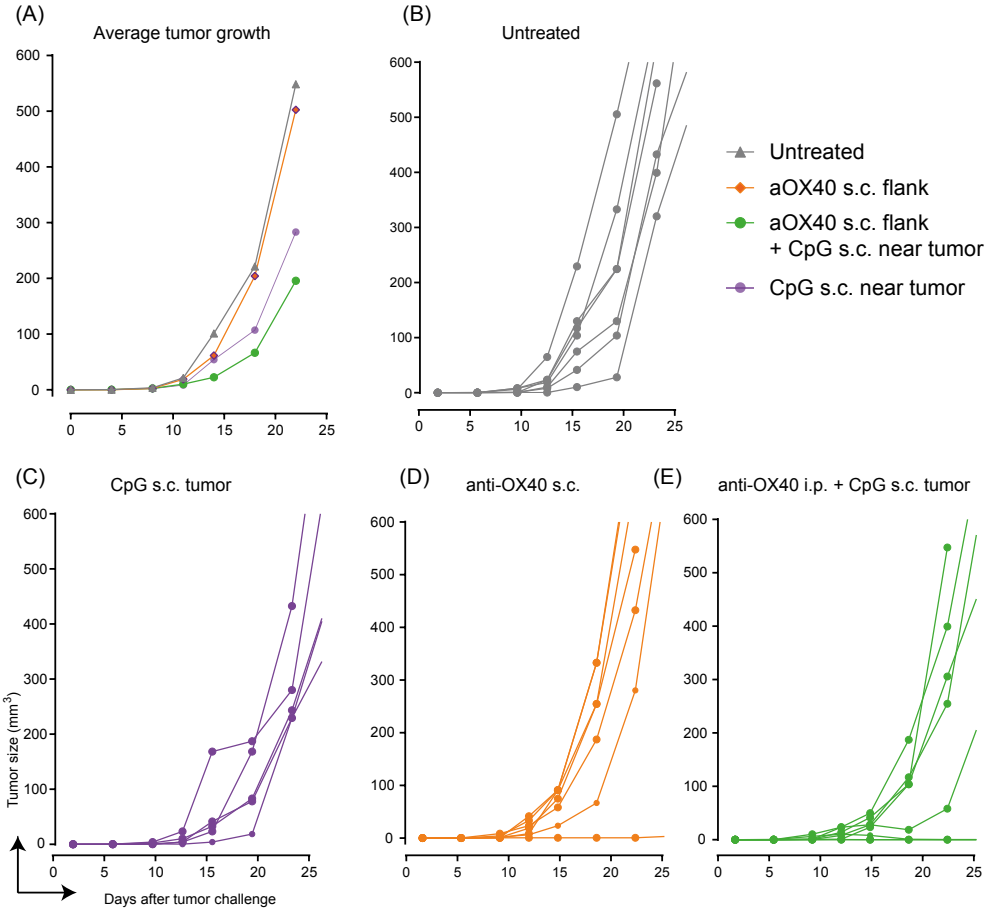

Figure S1. (A) Average of tumor growth of mice different treatments. (B) Tumor growth of individual mice left untreated. (C) Tumor growth of individual mice treated with CpG only near the tumor subcutaneously. (D) Tumor growth of individual mice treated with anti-OX40 only near the tumor subcutaneously. (E) Tumor growth of individual mice treated with anti-OX40 and CpG near the tumor subcutaneously.

(A)

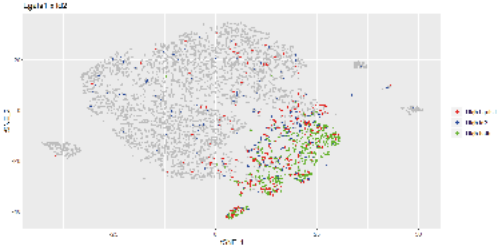

(B)

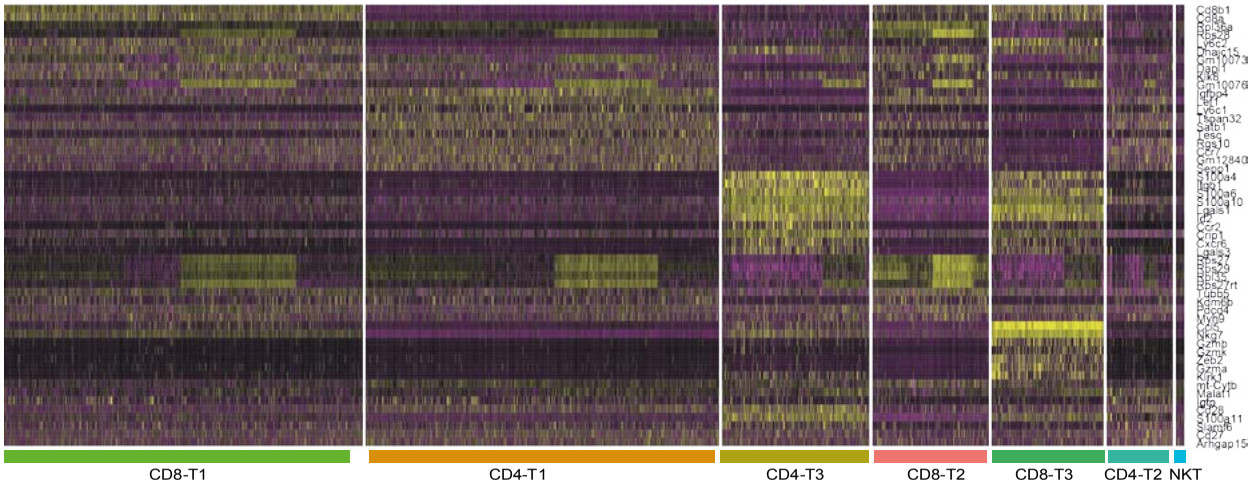

Figure S2. Volcano plots of single cell RNA-sequencing analysis showing high co-expression of Id2 and Lgals1 in T3 subset.

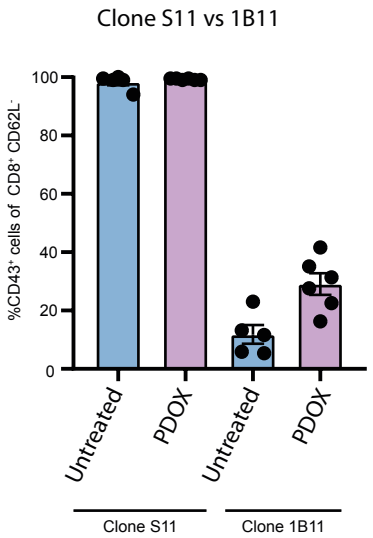

Figure S3. Flow cytometry panels. (A) Flow cytometry panel consisting of 11 extracellular markers to analyze mouse blood. (B) Flow cytometry panel consisting of 8 extracellular markers and 2 tetramers to analyze mouse blood. (C) Flow cytometry panel consisting of 8 extracellular and 2 intracellular markers to analyze mouse tumor-micro-environment. (D) CD43 positive cells in percentage found in the blood at day 18 after PDOX treatment or left untreated, n= 6 mice per group.

Mouse panel		
Antigen	**Clone**	**Company**
CD3e	145-2C11	eBiosciences
CD4	RMA45	Fluidigm
CD8A	53-6.7	Fluidigm
CD9	eBioKMC8	eBiosciences
CD11B	M1/70	Fluidigm
CD11C	N418	eBiosciences
CD14	Sa14-2	BioLegend
CD19	6D5	Fluidigm
CD25	3C7	Fluidigm
CD27	LG.3A10	eBiosciences
CD28	37.51	Fluidigm
CD38	90	eBiosciences
CD39	24DMS1	eBiosciences
CD43	1B11	BioLegend
CD44	IM7	eBiosciences
CD45	30-F11	Fluidigm
ICAM-1	YN1/1.7.4	BioLegend
L-selectin	MEL-14	BioLegend
CD69	H1.2F3	Fluidigm
B7-2	GL-1	eBiosciences
C-FMS	AFS98	Fluidigm
CD122	TM-b1	BioLegend
CD127	A7R34	Fluidigm
NK1.1	PK136	eBiosciences
CXCR3	CXCR3-173	eBiosciences
CXCR5	L138D7	BioLegend
LAG-3	eBioC9B7W	eBiosciences
PDL1	10F.9G2	BioLegend
ICOS	7E.17G9	BioLegend
PD1	29F.1A12	eBiosciences
F4/80	BM8	eBiosciences
KLRG1	2F1	eBiosciences
Ly6C	HK1.4	eBiosciences
Ly6G	1A8	Fluidigm
MHC II	M5/114.15.2	eBiosciences
NKG2A	20d5	eBiosciences
TCRab	H57-597	BioLegend
TCRgd	eBioGL3	eBiosciences

Human panel		
Antigen	**Clone**	**Company**
CD38	HIT2	BioLegend
CD45RO	UCHL1	Fluidigm
CD45RA	HI100	BioLegend
CD44	IM7	Fluidigm
CD45	HI30	Fluidigm
CD49b	P1E6-C5	BioLegend
CD39	A1	BioLegend
HLA-DR	L243	Fluidigm
CD29	TS2/12	BioLegend
CD11b (Mac-1)	ICRF44	Fluidigm
TCRgd	11F2	Dianova
CD274 (PD-L1)	29E.2A3	Fluidigm
CD8a	RPA-T8	Fluidigm
CD278/ICOS	C398.4A	Fluidigm
CD103	Ber-ACT8	BioLegend
CD49A	SR84	BD Biosciences
CD27	L128	Fluidigm
CD127 (IL-7Ra)	A019D5	Fluidigm
CD25 (IL-2R)	2A3	Fluidigm
CD3	UCHT1	Fluidigm
CD4	RPA-T4	Fluidigm
TIGIT	MBSA43	eBioscience
CXCR5	MAB190	RnDsytems
CD62L	DREG-56	BioLegend
CD69	FN50	BioLegend
CD86	IT2.2	Fluidigm
CD154 (CD40L)	24-31	ThermoFischer
CD134 (OX40)	ACT35	BD Biosciences
CD161	HP-3G10	Fluidigm
CD335 (NKp46)	BAB281	Fluidigm
KLRG1	SA231A2	BioLegend
CD223/LAG-3	11C3C65	Fluidigm
CD20	2H7	BioLegend
CD14	Tük4	ThermoFischer
CD56	5.1H11	BioLegend
CD150	A12	BioLegend
CD244	2-69	BioLegend
CD160	BY55	BioLegend
CCR6	GE034E3	BioLegend
CD122	Tu27	BioLegend
4-1BB	4B4-1	BioLegend
CXCR6	KE041E5	BioLegend
NKG2A	131411	RnDsytems
PD-1	EH12.2H7	Fluidigm

Figure S4. Mass cytometry panels. (A) Mouse cytometry panel used to analyze the blood, spleen, lymph nodes and bone marrow from mice. (B) Human mass cytometry panel used to analyze the blood of patients or healthy controls. **Figure S4:** sc-RNA-seq recap

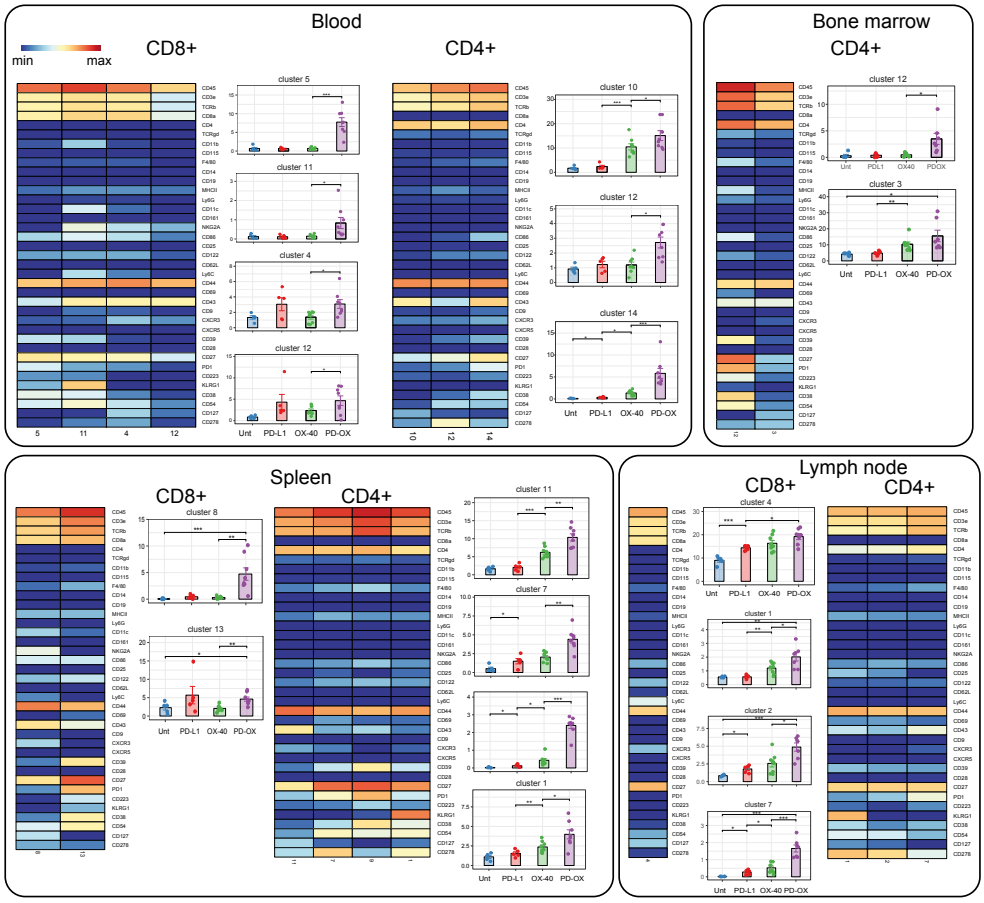
Blood
CD8+
CD4+
min
max
cluster 5
cluster 11
cluster 4
cluster 12
cluster 10
cluster 12
cluster 14
Unt
PD-L1
OX-40
PD-OX
Bone marrow
CD4+
cluster 12
cluster 3
Spleen
CD8+
CD4+
cluster 8
cluster 13
cluster 11
cluster 7
cluster 1
Lymph node
CD8+
CD4+
cluster 4
cluster 1
cluster 2
cluster 7

Figure S5.

T CELLS IN BLOOD: WITNESSES AND EXECUTERS OF IMMUNOTHERAPY IN CANCER

6

ABSTRACT

Immunotherapy has revolutionized the treatment of many cancers, exerting the cytotoxic power of T cells against tumor cells. Specifically, blockade of immune checkpoint markers like programmed cell death protein-1 (PD-1) or cytotoxic T-lymphocyte antigen-4 (CTLA-4) has been found to be effective for the treatment of melanoma or other cancer types with high mutation load. While a better understanding of the composition of tumor infiltrates may help tailoring immunotherapy, tumor inaccessibility often hampers proper analysis. The recent advances in single cell technologies have led to identification of several new biomarkers and immune cell subset definition in the blood which correlate with disease progression and clinical outcome. In depth immunophenotyping of blood of cancer patients may reveal relevant information regarding immunotherapeutic efficiency. Here, we discuss how peripheral immune-based biomarkers can predict the efficacy of immunotherapeutic agents. We review the current knowledge of T cell subsets and their fates can contribute to improve immunotherapy efficacy.

Manuscript in preparation

Guillaume Beyrend[1], Ramon Arens[1], Ferry Ossendorp[1]

[1] Department of Immunology, Leiden University Medical Center, Leiden, Netherlands

INTRODUCTION

From the first study conducted in cutaneous melanoma more than two decades ago (1), it is now well-established that a correlation exists between the tumor infiltrating lymphocytes (TILs) landscape and overall survival (OS). In 1996, 285 primary cutaneous melanoma cases have been analyzed and the presence of TILs had a very strong predictive value regarding OS. Ten years later, it has been demonstrated that detailed characterization of tumor-infiltrating immune cells by flow cytometry better reflected the prognosis of colorectal patients than histopathological methods currently used to stage colorectal cancer (2, 3). This observation led to the development of "Immunoscore", becoming a reference in classification of malignant tumors (4) by implying relative few immunological markers (CD3, CD8, CD45RO) (5). This approach gave more insight in the role of the immune system in different cancer types and helped to predict treatment efficacy (6). In parallel, cancer therapies have been developed to target the immune system rather than only targeting tumor growth. The last decade, immune checkpoint blocking antibodies have been increasingly used in the clinic. Specifically, two main immunotherapeutic agents blocking two inhibiting markers called programmed cell death protein 1 (PD-1) and cytotoxic T-lymphocyte antigen-4 (CTLA-4) have been developed, unleashing the cytotoxic power of T cells. PD-1 is expressed by T cells and its natural function is to inhibit the activation and function of potential pathogenic (self-reactive) cytotoxic and helper T cells but also suppressing desirable cancer-reactive T cells (7). CTLA-4 binds competitively with CD28 to CD80 or CD86 and break the activation signal of T cells (8). CTLA-4 belongs to the immunoglobulin superfamily, is mainly expressed by activated T cells and transmits an inhibitory signal to T cells. In a similar way as PD-1, such signal potentially dampens the reactivity of T cells towards cancer cells.

Blocking those molecules by immune checkpoint blockers (ICB) show significant but variable clinical outcome in cancer patients (9, 10) which coincides with unwanted immune-related adverse events (11) by breaking T cell tolerance. To avoid unnecessary exposure to potentially hazardous agents, there is an urging need for biomarkers that correlate with clinical activity and can predict immunotherapeutic efficacy in individual patients.

The recent development of deep phenotyping technologies such as mass cytometry (12), single-cell RNA sequencing (13) or TCR sequencing revealed undiscovered specific immune cell subsets. The advances of single-cell technology highlighted specific intratumoral subsets undergoing immunological changes when treated by ICB (14). Such changes can help guiding therapeutic alternatives (15) and tailoring precision treatments.

Investigation of the cellular composition of the tumor microenvironment often requires invasive surgery which strongly delays decision making for therapeutic options. Peripheral bio-markers are therefore highly needed to adjust or confirm treatment strategy in the clinic. To enhance a routinely monitoring system, we propose a review of immune parameters detectable in the blood, at different timepoints, which may predict efficiency of a potential immunotherapeutic treatment strategy. By focussing on studies involving

patients with solid tumors, we will evaluate the effects of ICB on the immune cell subsets in the blood over time and review the importance of an early based-blood investigation for a better prediction of adequate immunotherapy for individual patients.

QUANTIFICATION OF THE MAJOR LEUKOCYTE LINEAGES IS INFORMATIVE FOR ICB EFFICIENCY

One of the first basic parameters studied for efficacy prediction was the concentration of leukocytes in the blood at different timepoints before and during ipilimumab therapy (anti-CTLA-4) of melanoma. In two different studies (16, 17), a threshold of 1000 lymphocytes/ µL has been described to be associated with a better survival of melanoma patients. Ku *et al.* confirmed that the absolute lymphocyte count after 2 treatments, at week 7, correlated with validated clinical benefits later (18). Delyon *et al.* studied the eosinophil count, for which an increase of >100/ µL between the first and second infusion surprisingly correlated with an improved OS in melanoma. A possible explanation could rely on the release of cytotoxic granules from eosinophils in the tumor microenvironment (TME) (19). A more recent study (20) on large cohort of 615 melanoma patients validated these previous findings and similarly concluded that a high relative lymphocyte count is associated with a better clinical outcome.

By extending their investigation to the myeloid compartment, the same authors showed that a lower absolute monocyte counts correlates as well with a better OS. The baseline values of the parameters studied by Martens *et al.* are sufficient to predict the efficacy of ipilimumab treatment. Finally, a more recent study from 2018 (21) focused on baseline level of derived neutrophil-to-lymphocyte ratio of 720 melanoma patients in blood and showed a threshold of 3, for which survival rates is decreasing beyond this value. These results were confirmed in a larger study, involving patients treated with ipilimumab and pembrolizumab-treated (anti-PD-1) patients (22), by showing the baseline parameters of the relative eosinophil count ≥1.5% and relative lymphocyte count ≥17.5 were associated with favourable OS. These early findings were later confirmed on other cancer types like the non-small cell lung cancer (NSCLC). In NSCLC patients treated with anti-PD-1 antibodies (Nivolumab mainly) it was reportedthat a higher baseline of absolute neutrophil or monocyte count was correlated with worse clinical outcome. The same holds true for the myeloid to lymphocyte ratio and the neutrophils to lymphocyte ratio, both correlated with worse outcome in patients who underwent anti-PD-1 treatment.

Combination therapy of anti-CTLA-4 and anti-PD-1 showed significant independent variables for favourable OS including high relative levels ofeosinophils, high relative levels of basophils, low absolute numbers of monocytes, low LDH, and a low neutrophil-to-lymphocyte ratio (23).

The above results suggest that an overall count of the main blood cell lineages, without requiring complex staining or specific immune marker of the immune system during the first weeks of treatment can be indicative of a good efficiency of both anti-CTLA-4 or

anti-PD-1 treatments. Briefly, a high lymphocyte and eosinophil count are correlated to a better overall survival, whereas a high basophil, neutrophil and monocyte count have the opposite effect (Figure 1). These results might be explained by the cytotoxic power of the lymphocytes or eosinophils. The role of eosinophils has not been clearly unraveled but their potential cytotoxic power might have an effect on decreasing the tumor burden (19). The other myeloid lineages basophils and neutrophils might release anti-inflammatory cytokines in the tumor micro-environment, which has an unwanted effect on promoting tumor growth over time.

CENTRAL AND EFFECTOR MEMORY T CELL COMPARTMENTS ARE MODULATED UPON IMMUNOTHERAPY

As reviewed above, the main immune blood cell lineages can predict, to a certain level, the baseline efficiency of immunotherapy. This suggests that more specific categories of immune cells belonging to these major lineages are responsible for modulating the treatment efficiency.

In melanoma following ipilimumab treatment, during the two first cycles of therapy increases were observed in the central and effector memory T cell compartments (24). Similarly, anti-CTLA-4-treated responders presented a higher level of effector memory T cells (T_{EM}) and central memory T cells (T_{CM}) in metastatic melanoma setting (25). The authors could not demonstrate similar changes in patients treated with nivolumab (anti-PD-1). The baseline of $CD8^+$ T_{CM} cells by itself might also be predictive of ipilimumab efficiency (26). A higher presence of $CD8^+$ T_{CM} cells and elevated $CD8^+$ activated T-cells is associated with clinical response. A year later, confirmation study on ipilimumab-treated melanoma patients (27) showed that a higher level of $CD27^+$ $CD28^+$ $CD8^+$ T_{EM} cells in the blood correlated with a positive clinical outcome.

Following the studies with ipilimumab in melanoma, a year later it was demonstrated that nivolumab-treated cancer patients, who present high CM/Effector T cell ratios, are more likely associated to a higher inflammatory signature and therefore had longer progression-free survival 3 months after the treatment initiation (28) regardless of the tumor type. Interestingly, in their study, the authors also showed that the treatment did not trigger major changes in CM/Effector T cell ratios as suggested earlier by the previous authors (25). In other words, only the ratio CM/Effector cells before the treatment starts was predictive of the clinical outcome. The treatment itself had limited effect on the ratio.

In a nutshell, these studies show that the levels of T_{CM} and T_{EM} in blood are associated with immunotherapy clinical outcome, in some cases the latter can be modulated upon treatment, but often already determined before the treatment itself (Figure 1). This would suggest that immunotherapy can enhance a pre-existing T cell pool and therefore its efficiency can be predicted based on the T cell presence at baseline. These results indicate a primary response already exists in cancer patients and that ICB can promote anti-tumor responses and not create these *de novo*.

THE CENTRAL AND EFFECTOR MEMORY T CELLS MARKERS CD45RA AND CD45RO AND IMMUNOTHERAPY EFFICIENCY

The recent development of single cell technology allowed a systemic approach with a larger screening of immune cell subsets detected by mass cytometry or single-cell RNA sequencing. Such characterisation is helpful in the development of new targeting strategies, for example to enhance modulation of specific immune populations.

Following anti-CTLA-4 therapy in melanoma patients, an increase of $CD4^+$ T cells, especially activated $CD45RO^+$, $CD45RO^+TBET^+EOMES^+CD4^+$ and $CD45RO^+ICOS^+PD\text{-}1^+CD4^+$ effector T cells was shown (29). Tremelimumab (anti-CTLA-4) administered to 12 melanoma patients led to an increase in CD45RO on $CD4^+$ T cells after 3 doses and significantly differentiated responders from non-responders (30). Similarly, the hypothesis of an early detection of such cell subsets has been supported by another study showing that baseline levels of $CD45RO^+CD8^+$ T cells correlate with response and longer survival to ipilimumab (31).

Other studies have highlighted CD45RA as a determinant marker for immunotherapy responsiveness. A stronger intensity of CD45RA on T cells is indicative of non-responders receiving anti-CTLA-4, whereas responders display lower frequencies of $CD45RA^+$ at baseline (25). Low abundance of peripheral $CD45RA^+CD8^+$ T_{EM} cells associates with favorable clinical outcome (27). These studies enlighten the role of Th1-like $CD4^+$ T cells in tumor immunity in melanoma, especially after anti-CTLA4 treatment.

Surprisingly, a recent study focussing on evaluating the effect of Nivolumab (anti-PD-1) in 71 NSCLC patients (32) presented unexpected results that $CD8^+$ T cell compartment in responders patients displayed a higher abundance of $CD45RA^+$ T_{EM} and $CD95^+$ or $CD69^-$ T cells and lack stimulatory receptors (ICOS, CD40L, CD28, OX40, 4-1BB) only after 1 or 2 cycles. Such findings might be specifically valid for NSCLC and was not validated in other cancers. On the opposite, in 8 melanoma patients receiving anti-PD-1 treatment, an increase of $CD45RA^-CD4^+$ T_{CM} cells after treatment in long-term survivors, but not in non-responder, has been measured by mass cytometry (33). These studies might benefit from a validation cohort to corroborate their results.

It is not the first time that a crucial role for $CD4^+$ T cells has been reported. A central role of $PD\text{-}1^-CD127^{low}$ $CD4^+$ T cells has already been highlighted on a systemic level and associated with effective therapy (34). Deficient $CD4^+$ T cell help has been reported to reduce the response of CTLs and conversely a maximizing $CD4^+$ T cell help was seen to improve outcomes in cancer immunotherapy strategies (35). Altogether, these studies support the idea that immunotherapy benefits from the expansion of a Th1-like CD4 effector T cell subset, but is thus far not consistently reported across all tumor types and immunotherapeutic agents (Figure 1).

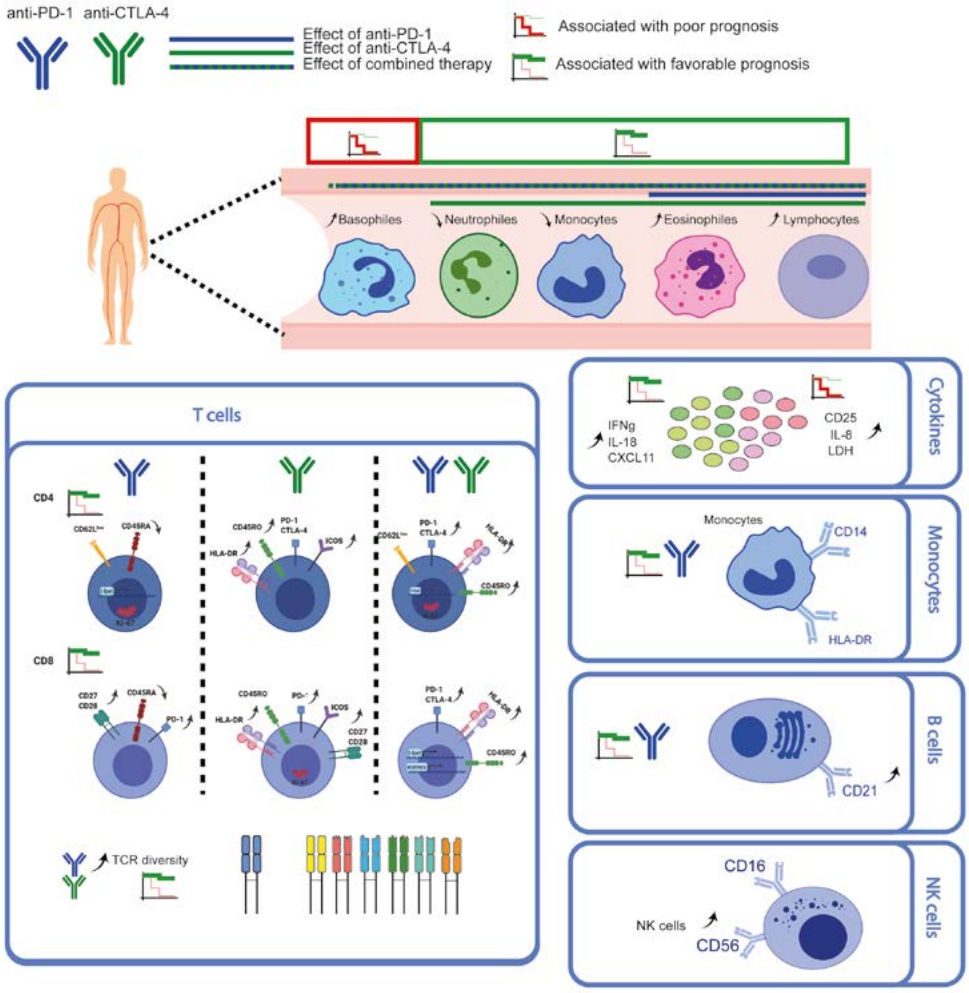

Figure 1. Graphical abstract

IPILIMUMAB SPECIFICALLY LEADS TO EXPANSION OF AN ICOS$^+$ T CELL SUBSET IN BLOOD

Further characterisation on the therapy-associated Th1-like CD4$^+$ T effector memory cell subset was performed to by detailed flow cytometry more than 10 years ago. An ICOS$^+$ Th1 subset has been discovered in 6 ipilimumab-treated-bladder cancer patients (36) and in 10 ipilimumab-treated prostate cancer patients (37), where it has been shown that therapy is correlated with an increase of CD4$^+$ICOS^{hi} T cells in the blood together with IFN-γ expression. A year later, same evidence was brought for bladder and melanoma ipilimumab-treated patients (38). CD4$^+$ICOS^{hi} T cells were sustained over a period of 12 weeks of therapy but already present 3 weeks after treatment. Another anti-CTLA-4 agent, tremelimumab, used on 26 hormone responsive breast cancer patients, was

reported to have the same effect (39). In this study conducted on 197 ipilimumab-treated patients, increases of activated ICOS$^+$ CD4$^+$ T cells at an early stage of the treatment, week 4 and 7, revealed a rapid immunomodulation upon the first infusion. These findings have been validated later on 36 anti-CTLA-4 treated melanoma and prostate cancer patients (40) and more recently on 26 melanoma cancer patients (41), where it was demonstrated that ipilimumab led to a higher ICOS$^+$ CD4$^+$ T cells in blood after two or three infusions. In brief, these reports show that the ICOS$^+$ T cell subset is present across multiple tumor types but present in patients specifically treated with anti-CTLA-4 agents (Figure 1).

Beyond the ICOS upregulation on CD4$^+$ T cells, similar increase has been detected on other subsets, like Gata3 on CD4$^+$. ICOS expression is not limited to CD4$^+$ T cells. Its activity has been shown on CD8$^+$ T cells at 6-month post-ipilimumab on 55 melanoma treated patients (42). The increase in ICOS expression might be linked to CD8$^+$ T cell cytotoxicity. These findings, in apparent contradiction with other studies showing no increase on ICOS CD8$^+$ T cells after therapy (24), illustrate the complexity and the dynamics of the immune response where the timing of analysis may play a crucial role. A possible explanation is a transient increase of ICOS expression which can be detected only at an early stage.

These studies showing ICOS upregulation have been confirmed in several murine models (43, 44), showing the importance of the ICOS pathway signalling in CTLA-4 therapy. The kinetic of Th1 subset shows an expansion at an early timepoint, meaning that the effect can be monitored at the start of therapy.

On the opposite, PD-1 blockade did not trigger such a clear upregulation of ICOS molecules on T cells. The populations found to be expanded after PD-1 were limited to an exhausted-like CD8$^+$ T cell phenotype. (45).

In conclusion, anti-CTLA-4 therapy but not anti-PD-1 is triggering an upregulation of ICOS on T cells, explaining a more activated phenotype against tumor cells, underlying the potential efficiency of CTLA-4 related therapies. ICOS is a stimulatory marker related to T cell immunity, and its presence in the blood reveals a tumor-reactive T cell phenotype.

ACTIVATED AND PROLIFERATIVE PHENOTYPE ON T CELLS UPON CHECKPOINT INHIBITORS

A deeper characterisation of the Th1-like CD4$^+$ cells revealed a functional feature of this subset, especially regarding their proliferative and active potential through the detection of respectively Ki-67 and HLA-DR. Ipilimumab upregulated both ICOS and Ki-67 expression on CD4$^+$ and CD8$^+$ T cells at both 3- and 6-month post therapy in melanoma patients (42). At baseline, low ICOS$^+$Ki-67$^+$EOMES$^+$CD8$^+$ T cells were associated with relapse. Some other activation markers can be expressed like HLA-DR as shown by the study conducted on 197 melanoma patients treated with ipilimumab (24). At an early stage of the treatment, week 4 and 7, patients showed a greater activated HLA-DR$^+$ CD4$^+$ and CD8$^+$ T cells with concomitant decreases in naive CD4$^+$ and CD8$^+$ T cells confirmed later in similar settings (31). Ipilimumab activates CD8$^+$ T cells by increasing HLA-DR$^+$CD25$^-$ phenotype,

implying non-specific antigen stimulation. These proliferating cells were also detected upon tremelimumab therapy in melanoma patients (30).

The ICOS$^+$ proliferative cells express inhibitory markers like CTLA-4 or PD-1 (46, 47). These cells can co-express inhibitory and activating receptors (ICOS, HLA-DR, CTLA-4, and PD-1) and are expanding after ipilimumab therapy, but no association with response could be established. These later studies would suggest that PD-1$^+$ cells expanding upon ipilimumab are not exhausted cells but can be tumor-reactive cells, as already suggested in our previous work (48).

A recent mass cytometry study on melanoma patients (49) with the aim to compare the effect of both anti–PD-1 and CTLA-4 monotherapies showed similar patterns. In both therapies, a strong enrichment of Ki-67$^+$ proliferative cells in PD-1$^+$ versus PD-1$^-$ CD8$^+$ T cells was noted. An investigation (50) on the phenotype from the blood of 29 treated NSCLC patients, revealed that therapy triggered an increase in effector-like phenotype Ki-67$^+$ PD-1^{hi+} ICOS$^+$ CD8$^+$ T cells and found out that these cells were also HLA-DR$^+$, CD38$^+$, Bcl-2^{low} and CD28$^+$, CD27$^+$ in 70% of patients, with most responses seen within 4 weeks. Conversely, 70% of patients with disease progression had either a delayed or absent PD-1$^+$ CD8$^+$ T-cell response, whereas 80% of patients with clinical benefit exhibited PD-1$^+$ CD8$^+$ T-cell responses within 4 weeks of treatment initiation. The kinetics of such subsets were further examined on patients with stage IV melanoma treated with pembrolizumab (51). The frequency of Ki-67$^+$ CD8$^+$ T cells was increased after only 3 weeks after treatment and then declined in most patients. Briefly, this study shows that Ki-67$^+$ (HLA-DR$^+$CD38$^+$) T cells in the blood are reinvigorated by anti-PD-1 therapy. Another study (52) suggests that the changes occurs even earlier than 3 weeks after treatment, by looking at the blood only one week after treatment. It was concluded from the blood of 79 NSCLC treated with anti-PD-1 agents that Ki-67$^+$ cells among PD-1$^+$CD8$^+$ T cells can predict durable clinical benefit already 7 days after the first dose. PD-1 has an immediate effect on blood cells as shown on 22 nivolumab or pembrolizumab treated patients (53), where the responder group showed higher expressions of PD-1 on CD4$^+$ T cells than the non-responder group after the first cycle of immunotherapy. The kinetics of other markers reveals a lower expression of CTLA-4, GITR, and OX40 after the second cycle of immunotherapy. Elevation of key biomarkers after the first cycle of immunotherapy, followed by a decrease in their expression after the second cycle, was associated with a better outcome from immunotherapy at an early stage of treatment of cancer. These studies underscore the importance of the timing of blood phenotyping and highlight the dynamical changes in the blood in response to therapy, often occurring within the first weeks of treatments, regardless the treatment or the tumor type (Figure 1).

Similar findings were extended by targeting PD-L1 with atezolizumab in a study investigating the blood of 14 patients suffering from metastatic bladder cancer (54). By comparing the blood at baseline and after treatment, it was eventually concluded that HLA$^-$DR$^+$Ki-67$^+$ CD8$^+$ T cells increased after atezolizumab injections. This has been validated the same year in 185 patients in other cancer types (RCC, NSCLC, melanoma,

cutaneous, mucosal and ocular) in anti-PD-L1 therapy where HLA^{-}DR^{+}Ki-67^{+} CD8^{+} T cells increase was detected (55) after only one treatment, at early stage. Therefore, blocking PD-1 or its ligand PD-L1 might lead eventually to the same cellular effects.

To summarize, these studies highlight the upregulation of activating markers on T cells, including ICOS, HLA-DR and proliferative markers like Ki-67. The possible transient upregulation of those markers demonstrates the importance of kinetic analysis of the systemic immune response and that a correct timing is crucial for accurate immune correlation. These results emphasized the very rapid effect of PD-1 on systemic immunity. PD-1^{+} expression on T cells does not only delineate exhaustive cells but can also point to an ongoing cellular response.

THE SYNERGIC EFFECT OF PD-1 AND CTLA-4 COMBINED TREATMENT

In 2017, a study showed that higher PD-L1 expression on peripheral T cells, was correlated with worse progression-free survival on ipilimumab-treated patients (56). This leads to the conclusion that PD-L1 is still playing an inhibiting role which cannot be overcome by anti-CTLA-4 alone. A combination therapy might be the answer for a better prognostic, by modulating the immune system. As described earlier, the proliferating CD4^{+} and CD8^{+} T cells expressing HLA-DR, ICOS and/or Ki-67 have been found after combined therapy on the two main lineages CD4^{+} and CD8^{+} T cells (57) and of terminally differentiated TBET^{+}EOMES^{+}CD8^{+} T cells (49). The combination blockade leads to nonoverlapping (Ki-67, granzyme A/B, IL-8 and HLA-DR, IFNγ) expression changes with monotherapy (46) highlighting their synergistic effect (58). The number of studies studying the blood compartment in patients treated with the combination PD-1/PD-L1 together with CTLA-4 is still limited, especially due to its increased toxicity(59).

ARE REGULATORY T CELLS IMPACTED BY ICB?

Anti-CTLA-4 and anti-PD-1 therapy efficiency can be partially explained by the expansion of effector subsets. However, these immunotherapies might have an independent effect by reducing the number of T regulatory cells, thereby indirectly enhancing tumor immunity. The absence of impact of CTLA-4 blockade on regulatory T cells has already been proposed in melanoma patients (60), where no decrease in the expression of CD25^{+} CD4^{+} T cells in whole PBMC, nor a decrease in FoxP3 gene expression in the CD4^{+} or purified CD25^{+} CD4^{+} T cell populations post-treatment was shown. These results were confirmed in a larger study involving 197 ipilimumab-treated melanoma patients (24) and 12 tremelimumab-treated patients (30). Low pre-treatment frequencies of regulatory T cells were also found to be associated with a better clinical outcome (61), suggesting that T_{regs} are not a potential target of anti-CTLA-4 therapy and that this treatment does not deplete FoxP3 as recently demonstrated (62). However, contradictory results have been reported (63) where, following anti-CTLA-4 treatment, a greater increase in T_{regs} (CD25^{hi+} Foxp3^{+} CD4^{+}) was unexpectedly associated with improved progression-free survival (PFS). Finally,

findings were reported where baseline frequencies of $CD25^+FoxP3^+$ $CD4^+$ $T_{regs} \geq 1.5\%$ were associated with favourable prognosis after initiation of ipilimumab (20). It might be that T_{regs} represent target cells of ipilimumab due to their CTLA-4 expression. Therefore, a high baseline frequency might render patients more susceptible to anti–CTLA-4 antibodies. This hypothesis is strongly supported by the observed correlation between decreasing levels of circulating T_{regs} during ipilimumab and favorable outcome (18).

In summary, the potential impact of ICB regarding T_{regs} still needs to be defined. If in some cases, no depletion of T_{regs} can be measured, it might be possible that the regulatory potential of the T cells is modulated upon anti-CTLA-4 therapy, due to its constitutive expression on T_{regs} or that the T_{regs} are not measurable in the blood but be present in other compartments, like in the tumor or the lymph nodes.

A CROSS-TALK BETWEEN IMMUNE CELL LINEAGES

PD-1 and CTLA-4 expression is not restricted to T cells and the blocking effect of ICB is not limited to the T cells. In 2014, a study on ipilimumab therapy on melanoma patients showed a decrease in circulating monocyte MDSC $Lin^-/HLA\text{-}DR^-/CD33^+/CD11b^+$ cells was associated with improved PFS (63). The same year, it was also demonstrated that monocytic-MDSC frequencies were inversely correlated with peripheral $CD8^+$ T-cell expansion following ipilimumab treatment in melanoma (64, 65). Myeloid cell frequencies could be correlated to the $CD8^+$ T cell frequencies and therefore play a role in tumor immunity through their impact on $CD8^+$T cells.

An extensive study was performed later to define more precisely the myeloid subsets predicting PD-1 blockade effect. Before commencing therapy, a strong predictor of progression-free and overall survival in response to anti-PD-1 immunotherapy was the high frequency of $CD14^+CD16^-HLA\text{-}DR^{hi}$ monocytes (66). On the opposite, it has been shown that the $CD14^+CD16^-$ monocyte subsets before therapy were higher in the resistance group (67)

Following immunotherapy checkpoint blockade, it was noticed that in anti-PD-1 treated melanoma patients but not in anti-CTLA-4 treated patients, $CD69^+$ NK cells are correlated with clinical response (25). Melanoma patients responding to immunotherapy had a higher frequency of NK cells and CD56- $CD16^{hi}$ T cells (67) and showed higher expressions of PD-1 on NK cells than the non-responder group after the first cycle of immunotherapy (53). In peripheral blood of PD-1 treated patients, an unusual population of immune blood cells expressing CD56, HLA-DR, $CD14^{mid}$ and $CD4^{mid}$ increased by 9-fold from the patients with a response to therapy (68). Lastly, B cells are also subject to changes. Anti-PD-1 therapy led to decline in circulating B cells and an increase in $CD21^{low}$ B cells (with higher PD-1 expression and higher clonality) and plasmablasts. Interestingly, patients with early B cell changes experienced higher rates of grade 3 or higher IRAEs 6 months after immunotherapy (69) (Figure 1).

The presence of these cells might be connected to effector T cells and the lymph nodes are enhancing such cross-talks. A recent study (70) showed that lymph nodes are critical for successful PD-1 therapy.

CONCLUSION AND DISCUSSION

The use of an increasing number and combinations of immunotherapeutic agents against cancer results in a large offer of treatments, which needs to be optimized by increasing its efficacy and minimizing adverse events. Blood is an easily accessible compartment where relevant information can be extracted to tailor treatment on an individual patient-basis.

All studies conducted with checkpoint blockers and monitoring changes in the different blood immune cell subsets showed that baseline parameters at the start of therapy should be taken in account to predict the outcome of the specific therapeutic agent. The presence of specific immune cell subsets at baseline has an impact on immunotherapy efficiency, explaining potential resistance of different individuals. Timing should be considered during immunomonitoring, changes might be transient and only detectable during first weeks of treatment.

The prediction potential of the blood has been realized with the venue of the new single cell technology like mass cytometry, single cell RNA-sequencing, epigenetic analysis, multianalyte serum immunoassays, metabolic analysis or glycoprotein modification analysis; and the importance of other components, like the microbiome (41) has been recently evaluated. Other immune compartments like lymphoid organs and bone marrow are also part of the systemic immune response and might play an additional role in immunotherapy efficiency.

ACKNOWLEDGEMENTS

The authors acknowledge funding from the European Commission (Horizon 2020 MSCA grant under proposal number 675743; project acronym ISPIC).

LIST OF ABBREVIATIONS

OS	Overall survival
TME	Tumor Microenvironment
TIL	Tumor Infiltrating lymphocyte
PD-1	Progammed cell death protein-1
CTLA-4	Cytotoxic T-lymphocyte antigen-4
ICB	Immune checkpoint blocker
LDH	Lactate dehydrogenase
TCM	T central memory cell
TEM	T effector memory cell
NSCLC	Non-small cell lung cancer

Table 1. Summary of the findings on peripheral biomarkers

Study	Year	Timing	Immunotherapy
(Ferrucci, Ascierto et al. 2018)	2018	Baseline, week 12 and every 12 week thereafter	Ipilimumab i.v. 3mg/kg every 3 weeks for 4 infusions
(Martens, Wistuba-Hamprecht et al. 2016)	2016	Baseline	Ipilimumab: treatment with at least one dose at 3 or 10 mg/kg
(71)	2018	Baseline and each cycle	11 patients treated with pembrolizumab 2 mg/kg every 21 days and 146 with nivolumab 3 mg/kg every 14 days
(Ku, Yuan et al. 2010)	2010	Week 7 (after 2 doses of ipilimumab)	Ipilimumab 10 mg/kg every 3 weeks for 4 doses
(Delyon, Mateus et al. 2013)	2013	Baseline, after 1st and 2nd treatment	Ipilimumab 4 doses every 3 weeks 3mg/kg
Rosner, Kwong et al. 2018	2018	Baseline	Nivolumab + Ipilimumab
(Simeone, Gentilcore et al. 2014)	2014	baseline and Weeks 4, 7, 10 and 12	Patients received ipilimumab 3 mg/kg every 3 weeks for four doses
(Weide, Martens et al. 2016)	2016	Baseline	pembrolizumab
(Kelderman, Heemskerk et al. 2014)	2014	Baseline, week 6	4 cycles of 3 mg/kg ipilimumab every 3 weeks
(Liakou, Kamat et al. 2008)	2008	Baseline, week 3 (before 2nd dose) and week 7	Ipilimumab at 3 mg/kg, every 3 weeks, for total of 2 doses
(Fan, Quezada et al. 2014)	2014	N/A	CTLA-4, ICOSL, CTLA-4 + ICOSL, CTLA-4 at D3/6/9/12

Cancer type	Peripheral findings
720 advanced melanoma patients	In blood at baseline: neutrophil-to-lymphocyte ratio > 3 means prognosis worsened.
Advanced Melanoma: 209 patients (identification and confirmation cohort), validation cohort (406).	Low baseline LDH, absolute monocyte counts (AMC), Lin(-)CD14(+) HLA-DR(-/low)-MDSC frequencies, and high absolute eosinophil counts (AEC), relative lymphocyte counts (RLC), and CD4(+)CD25(+)FoxP3(+)-Treg frequencies are associated with better survival
157 patients non-small cell lung cancer	Higher baseline absolute neutrophil count (ANC), AMC, ANC: ALC ratio and myeloid to lymphoid ratio correlated with worse clinical outcomes in patients who underwent anti-PD-1 treatment
51 refractory melanoma patients	Patients with an absolute lymphocyte count (ALC) ≥1000/μL after 2 ipilimumab treatments had a improved clinical benefit rate and median OS compared with those with an ALC <1000/μL
73 melanoma patients	A lymphocyte count >1000/mm^3 at the start of the second course and an increase in the eosinophil count >100/mm^3 between the first and second infusions were correlated with an improved OS
209 unresectable stage III ou IV melanoma	High relative eosinophils, high relative basophils, low absolute monocytes, low LDH, and a low neutrophil-to-lymphocyte ratio correlated with improved OS
95 melanoma patients	Survival was significantly associated with decreasing levels of lactate dehydrogenase, C-reactive protein and FoxP3/regulatory T cells, and increasing absolute lymphocyte count, between baseline and the end of dosing (Week 12)
616 patients	Relative eosinophil count (REC) ≥1.5%, relative lymphocyte count (RLC) ≥17.5%, ≤2.5-fold elevation of LDH, and the absence of metastasis other than soft-tissue/lung were associated with favorable OS
230 cutaneous melanoma patients	Long-term benefit of ipilimumab treatment was unlikely for patients with baseline serum LDH greater than twice the upper limit of normal
bladder cancer (6) Healthy donor (10)	Th1 CD4$^+$ ICOS$^+$ T cells are increased after CTLA-4 immunotherapy in blood and produce IFNγ and recognize the tumor antigen NY-ESO-1
B16 model mouse (melanoma and prostate cancer)	Concomitant CTLA-4 blockade and ICOS engagement by tumor cell vaccines engineered to express ICOS ligand enhanced antitumor immune responses in melanoma and prostate cancer in mice.

Table 1. (continued)

Study	Year	Timing	Immunotherapy
(Ng Tang, Shen et al. 2013)	2013	Baseline, week 3 before 2nd dose, and week 7	Ipilimumab at 3 mg/kg, every 3 weeks, for total of 2 doses
(Metzger, Long et al. 2016)	2016	2 weeks after tumor implantation	Treated on days 9, 13, and 16
(Chaput, Lepage et al. 2017)	2017	Baseline and before each treatment	Ipilimumab 3 or 10 mg/kg every 3 weeks then every 12 weeks
(Vonderheide, LoRusso et al. 2010)	2010	Baseline, 4 and 8 weeks	tremelimumab (3-10 mg/kg) every 28 days or every 90 days plus exemestane 25 mg daily
(Wang, Yu et al. 2012)	2012	Baseline, after 2 and 4 doses (3 and 6 months)	resected stage IIIC/IV melanoma received ipilimumab with or without a peptide vaccine.
(Carthon, Wolchok et al. 2010)	2010	Baseline, after 1/2 dose and after 2/4 doses	Ipilimumab at 3 or 10 mg/kg/ dose
(Weber, Hamid et al. 2012)	2012	Baseline, week 4, 7 and 12	Ipilimumab 3 mg/kg (n=40) or 10 mg/kg (n=42) every 3 weeks for 4 doses (induction) and vaccines.
(Chen, Liakou et al. 2009)	2009	Baseline and after treatment	2 doses 3 mg/kg or 10 mg/kg of ipilimumab with a 3-week interval
(Wei, Anang et al. 2019)	2019	From 6 to 184 days In average: anti-CTLA-4 (39), anti-PD-1 (25), combo (52), donor (3)	anti-PD-1 and anti-CTLA-4
(Callahan, Horak et al. 2013)	2013	Not specified	Combination nivolumab and ipilimumab

Cancer type	Peripheral findings
10 controls, 36 anti-CTLA-4 patients, 10 gp100 DNA vaccine (melanoma and prostate)	$ICOS^+$ CD4 T cells increase after ipilimumab treatment
CT26-bearing mice	Anti-OX40 efficacy was impaired with ICOS-L blockade. OX40 stimulation alone was sufficient to drive an increase in the frequency of ICOS expression among all T-cell subsets
26 patients with MM treated with ipilimumab	Baseline gut microbiota enriched with Faecalibacterium associated with beneficial clinical response to ipilimumab. Ipilimumab led to a higher ICOS CD4+ T cells in blood and higher CD25 in serum.
26 hormone responsive breast cancer	Treatment was associated in most patients with increased peripheral $CD4^+$ and $CD8^+$ T cells expressing inducible costimulator (ICOS) and a marked increase in the ratio of $ICOS^+$ T cells to $FoxP3^+$ regulatory T cells
55 melanoma patients	Ipilimumab up-regulated Ki-67 and ICOS on $CD4^+$ and $CD8^+$ T cells at both 3- and 6-month post ipilimumab. At baseline, low Ki-67+EOMES+CD8+ T cells were associated with relapse
12 urothelial carcinoma bladder cancer patients and 14 melanoma patients	In melanoma and bladder cancer patients: increase in $CD4^+ICOS^{hi}$ T cells. $CD4^+ICOS^{hi}$ T cells, sustained over a period of 12 weeks of therapy, correlates with increased of clinical benefits Melanoma patients: no significant differences in ICOS expression on T cells from frozen samples as compared with fresh samples.
197 melanoma patients	At week 7, most patients showed greater humoral responses relative to baseline titers and increases in the percent of activated $HLA\text{-}DR^+$ $CD4^+$ and $CD8^+$ T cells with concomitant decreases in naive $CD4^+$ and $CD8^+$ T cells Increases from week 4 observed in central memory, effector memory, and activated $ICOS^+$ $CD4^+$ T cells, but not in $ICOS^+$ $CD8^+$ T cells or in $FoxP3^+$ $CD4^+$ regulatory T cells.
7 treated patients	Increase in the frequency of $CD4^+ICOS^{hi}$ T cells in the blood following treatment
PBMC from melanoma patients: ipilimumab therapy (13), anti-PD-1 monotherapy (22), combo (13), donor (3)	Following anti–PD-1 or CTLA-4 monotherapy: strong enrichment of Ki-67^+ proliferative cells in PD-1^+ versus PD-1^- $CD8^+$ T cells anti-CTLA-4: increase of $CD4^+$ T cells, activated $CD45RO^+$ and $CD45RO^+$ $TBET^+$ $EOMES^+$ $CD4^+$ effector T cell, $CD45RO^+$ $ICOS^+$ PD-1^+ $CD4^+$ effector T cell Combination therapy: increase in overall frequency of $CD8^+$ T cells and increase of frequency of a terminally differentiated $TBET^+$ $EOMES^+$ $CD8^+$ T cells
35 patients advanced melanoma	T-cell subsets, including increases in the percentage of CD4 and CD8 expressing HLA-DR, ICOS and/or Ki-67 were seen with combination therapy

Table 1. (continued)

Study	Year	Timing	Immunotherapy
(Yi, Ready et al. 2017)	2017	Baseline and end of treatment	Ipilimumab, neoadjuvant chemotherapy, paclitaxel
(Kamphorst, Pillai et al. 2017)	2017	Baseline and every treatment cycle.	anti–PD-1 or anti–PD-L1 blocking antibodies
(Huang, Postow et al. 2017)	2017	Baseline and before each treatment	pembrolizumab (2mg/kg) infusion every 3 weeks for 12 weeks.
(Das, Verma et al. 2015)	2015	Before and after (not specified)	anti-PD-1, anti-CTLA-4, combination
(Kagamu, Kitano et al. 2019)	2019	Baseline, between 12 and 92 weeks.	Nivolumab 3 mg/kg body weight every two weeks
(61)	2013	Baseline and every 4 weeks	Ipilimimuab and GVAX vaccine
(Manjarrez-Orduno, Menard et al. 2018)	2018	Baseline, 8 and 12 weeks	Nivolumab
(Takeuchi, Tanemura et al. 2018)	2018	Before and after (timelines not specified)	Nivolumab (3 m/kg) every 2 weeks .Pembrolizumab (2 m/kg) every 3 weeks
(Subrahmanyam, Dong et al. 2018)	2018	Baseline	anti-CTLA-4 and anti-PD-1 therapies according to FDA protocol for metastatic melanoma

Cancer type	Peripheral findings
24 NSCLC	Increased of ICOS, HLA-DR, CTLA-4, and PD-1 on T cell after ipilimumab, but no association with response.
29 NSCLC patients	Following therapy: increase in effector-like phenotype Ki-67^{+} PD-1^{hi+} CD8^{+} T cells (also HLA-DR^{+}, CD38^{+}, Bcl-2^{lo} and CD28^{+}, CD27^{+}, ICOS^{+}) following therapy in ~70% of patients, most responses seen within 4 weeks. 70% of patients with disease progression had either a delayed or absent PD-1^{+} CD8^{+} T-cell response, whereas 80% of patients with clinical benefit exhibited early PD-1^{+} CD8^{+} T-cell responses
Patients with stage IV melanoma	Frequency of Ki-67^{+} CD8^{+} T cells was increased at 3 weeks after pembrolizumab treatment and then declined in most patients. Ki-67^{+} (HLA-DR^{+}CD38^{+}) T cells in the blood are reinvigorated by anti-PD-1 therapy and contain T-cell clones that are also present in the tumour
Cancer patients: anti–PD-1 (n = 24), anti–CTLA-4 (n = 9) or combination therapy (n = 12).	CTLA-4 blockade: induces a proliferative signature in T_{EM} (Ki-67, CTLA-4 and ICOS, IFNγ) PD-1 blockade: changes in genes implicated in cytolysis (granzyme A/B, FCRL3 and KLRF1, IFNγ) Combination blockade: leads to nonoverlapping (Ki-67, granzyme A/B, IL-8 and HLA-DR, IFNγ) changes
non-small lung cancer discovery cohort (40) and validation cohort (86)	Blood: Higher CD62L^{low} CD4^{+} (T-bet^{+}, CD27^{-}, FOXP3^{-} and CXCR3^{+}: Th1) % T cells prior to PD-1 blockade (correlated with long-term survival in NSCLC patients). CD25^{+}FOXP3^{+} CD4^{+} % T cells were significantly higher in non-responders.
28 prostate cancer patients	Significantly prolonged overall survival (OS) was observed for patients with high pre-treatment frequencies of CD4+CTLA-4+, CD4+PD-1+ or low pre-treatment frequencies of differentiated CD4+ or regulatory T cells.
22 patients	Patients with, at baseline, high CM/Eff T cell ratios (associated with higher inflammatory signature), had longer progression-free survival (PFS) 3 months after the initiation of nivolumab but treatment did not show major changes in CM/Eff T cell ratios
8 malignant melanoma patients (4 as exploratory and 4 as validation).	Anti-PD-1 mAb treatment: increase of CD4T CM (CD27+FAS-CD45RA-CCR7+) after treatment in long-term survivors, but not in non-responders.
67 melanoma patients	Anti-CTLA-4: In non-responders: stronger intensity of CD45RA (in CD4^{+} and CD8^{+} T cells) In responders: lower frequencies of CD45RA+ (in CD4+ and CD8+ T cells) higher T_{CM} and T_{EM} cells In anti-PD-1: CD69+ NK cells correlated with clinical response

Table 1. (continued)

Study	Year	Timing	Immunotherapy
(Kunert, Basak et al. 2019)	2019	Baseline, 2 weeks (after 1st dose), 4 weeks (2nd dose)	NSCLC patients treated with 3 mg/kg of nivolumab (intravenously every 2 weeks)
(Wistuba-Hamprecht, Martens et al. 2017)	2017	Baseline, 2nd dose (D 19–23), 3rd dose (D 40–44) and thereafter (>D45)	104 patients received 4 doses of ipilimumab, whereas in the remaining patients, the treatment was stopped after 1 to 3 doses.
(Herbst, Soria et al. 2014)	2014	Day 1, D2, D8 after cycle 1, first day after each cycle	PD-L1 MPDL3280A, clinical activity was seen from 1 to 20 mg kg, treatment every 3 weeks for 16 cycles
(Pirozyan, McGuire et al. 2020)	2020	Baseline (36), week 6 (39), 1 year (18).	Prembolizumab or Nivolumab
(Spitzer, Carmi et al. 2017)	2017	3 and 8 days after immunotherapy	anti-PD-1, IFNg + antiCD40 + CD1 alloIg, IFNg + antiCD40 + B6 alloIg
(Comin-Anduix, Lee et al. 2008)	2008	Baseline and at each dose	At least 2 doses of tremelimumab (up to 24) 10 mg/kg monthly
(Tietze, Angelova et al. 2017)	2017	Baseline, and 1-2 days and at each cycle	treated with ipilimumab (n = 21) and pembrolizumab (n = 9)
(Jacquelot, Roberti et al. 2017)	2017	Baseline	ipilimumab

Cancer type	Peripheral findings
71 NSCLC patients Healthy control samples were obtained from 15 donors	In partial response patients: $CD8^+$ T cells at baseline and during treatment is similar to healthy controls, but 2 times higher than in patients with PD or SD. CD8 in PR have more % of TEMRA (CD45RA) and $CD95^+$ or $CD69^-$ and lack stimulatory receptors (ICOS, CD40L, CD28 OX40, 4-1BB).
137 late-stage melanoma patients.	Higher levels of CD8 T_{EM} $CD27^+$ $CD28^+$ cells in blood are predictive for good outcome Low abundance of peripheral CD8 T_{EMRA} cells associate with good outcome.
RCC (56), NSCLC (n=53), Melanoma (11), Cutaneous (n=33), Mucosal (n=5), Ocular (4), Others (23)	Increase in IL-18, CXCL11 and CD8+HLA-DR+Ki-67+ T cells and IFN-γ during the first cycle of treatment IL-6 level decreases cycle 2, day 1. Changes not correlated to response or progression.
42 from melanoma patients prior to beginning anti-PD-1 treatment 39 from 6 weeks post-treatment and 18 from the 1-year time point	Responders had a higher frequency of NK and CD56-expressing $CD16^{hi}$ T cells. Patients in the primary resistance group had a higher frequency of classical monocytes.
Mice	A $CD4^+$ T cell subset from the periphery is sufficient to mediate anti-tumor immunity. Specific clusters PD-1-$CD127^{low}$ PD-1^{low} $CD4^+$ T cells were significantly elevated in responders compared to non-responders at both time points
12 patients advanced melanoma. Cohort of HLA-A*0201-positive patients with MART1-positive melanoma	Tremelimumab does not increase the number or function of antigen-specific $CD8^+$ T cells in peripheral blood nor decrease FoxP3 transcripts But increase in CD45RO on $CD4^+$ T cells after 3 doses and increase in HLA-DR on $CD8^+$ T cells after 2 doses significantly differentiated responders from non-responders.
30 melanoma patients	Baseline levels of $CD45RO^+CD8^+$ T cells correlate with response and longer survival to ipilimumab. ipilimumab: activates $CD8^+$ T cells by increasing $HLA\text{-}DR^+CD25^-$ phenotype, implying antigen non-specific stimulation.
190 patients metastatic melanoma	Higher the PD-L1 expression on peripheral T cells the worst regarding progression-free survival. Detectable CD137 on circulating $CD8^+$ T cells was associated with the disease-free status of resected stage III melanoma patients after adjuvant ipilimumab + nivolumab (but not nivolumab alone)

Table 1. (continued)

Study	Year	Timing	Immunotherapy
(Hiniker, Reddy et al. 2016)	2016	Baseline, 4 weeks after the last dose of ipilimumab	Ipilimumab every 3 weeks and local radiotherapy
(Du, Hu et al. 2018)	2018	Baseline, D21 and D42	nivolumab (3 mg/kg) or pembrolizumab (2 mg/kg) alone or with chemotherapy in each of cycles.
(Cha, Klinger et al. 2014)	2014	Baseline and after 1 month of treatment	Ipilimumab: up to 4 doses (1.5 to 10 mg/kg) every 4 weeks and GM-CSF daily (250 mg/ m2) the first 2 weeks of cycles. Tremelimumab: 15mg/kg every 3 month
(Robert, Tsoi et al. 2014)	2014	Baseline and 30 to 60 days	tremelimumab. Administered at 15 mg/kg every 3 months
(Rizvi, Hellmann et al. 2015)	2015	Baseline, D21, D44, D63, D256, D297	pembrolizumab, treated at 10mg/kg every 2-3 weeks
(Baitsch, Baumgaertner et al. 2011)	2011	Mean of 96 days after vaccination	Monthly s.c. 100 ug Melan-A/ MART-1 peptide and CpG (500 ug) in IFA (300–600 ul Montanide)
(Kvistborg, Philips et al. 2014)	2014	Baseline, post treatment (from 7 to 54 days)	ipilimumab
(Yuan, Adamow et al. 2011)	2011	Baseline; Week 7, 2, 24	Patients received ipilimumab at 0.3 mg/kg (n = 1), 3 mg/kg (n = 4), or 10 mg/kg (n = 139) every 3 wk for four treatments
(Powles, Eder et al. 2014)	2014	Baseline and after treatment	15 mg kg–1 every 3 weeks of atezolizumab
(Ribas, Shin et al. 2016)	2016	Baseline and 74 days (mean)	Pembrolizumab: 0 mg/kg every 2 weeks, or 2 mg/kg or 10 mg/kg every 3 weeks

Cancer type	Peripheral findings
9 melanoma patients	Higher baseline CD8 T_{CM} cells, transient on-treatment increases in MIP-1α and β, and sustained increases in IP-10 and MIG associated with CR/PR. Analysis of immune response data suggested a relationship between elevated CD8-activated T-cells and response
22 different cancer patients	Responder group showed higher expressions of PD-1 on CD4+ and NK cells than the non-responder group after the first cycle of immunotherapy, and lower expression of CTLA-4, GITR, and OX40 after the second cycle of immunotherapy.
25 metastatic castration-resistant prostate cancer patients treated with ipilimumab and GM-CSF, 21 metastatic melanoma patients treated with tremelimumab, 9 controls.	Treatment increase TCR diversity. Number of clonotypes that increased with treatment was not associated with clinical outcome. Improved overall survival was associated with maintenance of high-frequency clones at baseline.
21 patients metastatic melanoma	CTLA-4 blockade diversifies the peripheral T-cell pool
1 patient had stage IV non-small cell lung cancer (NSCLC)	Anti–PD-1-induced neoantigen-specific T cell reactivity in blood
A*0201+ patients with stage III/IV metastatic melanoma 4 A2+ healthy donors	In peripheral blood from patients vaccinated with CpG upon vaccination, differences in T effector cells specific for persistent herpesviruses (EBV and CMV)
40 patients with advanced HLA-A*0201 melanoma	Pre- and posttreatment comparison: anti–CTLA-4 Treatment induces early stage (median 2 weeks) an increase in the number of detectable melanoma-specific CD8 T cell.
144 advanced metastatic melanoma patients	NY-ESO-1–seropositive patients had a greater likelihood of experiencing clinical benefit 24 weeks after ipilimumab treatment than NY-ESO-1–seronegative patients. NY-ESO-1–seropositive patients with associated $CD8^+$ T cells experienced more frequent clinical benefit than those with undetectable $CD8^+$ T-cell response and survival advantage.
14 patients metastatic bladder	IL-18 and IFN-γ levels transiently increased and $CD8^+HLA\text{-}DR^+Ki\text{-}67^+$ cells increased
53 patients metastatic melanoma	In peripheral blood, an unusual population of blood cells expressing CD56, HLA-DR, $CD14^{mid}$ and $CD4^{mid}$ population of cells increased by 9-fold from the patients with a response to therapy.

Table 1. (continued)

Study	Year	Timing	Immunotherapy
(Dronca, Markovic et al. 2015)	2015	Baseline and at radiographic tumor evaluation	Pembrolizumab 2 mg/kg every 3 weeks
(Das, Bar et al. 2018)	2018	Baseline and after the first cycle of therapy	anti-PD-1; n=8, anti-CTLA-4; n=8 and anti-PD-1 and anti-CTLA-4 or comb therapy; n=23
(Maker, Attia et al. 2005)	2005	Baseline and 3 weeks after each tmt	every 3 weeks with an anti-CTLA-4 Ab with or without peptide immunization
(Kim, Cho et al. 2019)	2019	Baseline and Day 7 after first dose	Pembrolizumab or Nivolumab
(Tarhini, Edington et al. 2014)	2014	Baseline and 6 weeks	Neoadjuvant ipilimumab 10 mg/kg intravenously administered 3 weeks apart
(Krieg, Nowicka et al. 2018)	2018	Baseline and 12 weeks after anti-PD-1 immunotherapy	Nivolumab 3 mg/kg every 2 weeks or pembrolizumab 2 mg/kg every 3 weeks for 12 weeks
(Kitano, Postow et al. 2014)	2014	Baseline, week 6 after therapy (after 2 doses of ipilimumab)	4 doses of ipilimumab at 10 mg/kg or 3 mg/kg i.v. every 3 weeks
(Meyer, Cagnon et al. 2014)	2014	Baseline, D3/D7/D20 and after 3–30 months after treatment	Ipilimumab (15), Vemurafenib (10), Ipilimumab followed by vemurafenib (1), untreated (23)
(72)	2020	Baseline, 6 weeks after therapy	Pembrolizumab (6) 3 Nivolumab (3)
(Alvarez Secord, Bell Burdett et al. 2020)	2020	Baseline	Carboplatin and Paclitaxel with or Without Bevacizumab

Cancer type	Peripheral findings
40 (29 with baseline sample available and 14 serial) melanoma patients	In responders the levels of Bim in PD-1^{+} CD8^{+} T cells decreased after the first 3 months of treatment, and they increased/did not change in all non-responders
35 melanoma patients	CCB therapy led to decline in circulating B cells and an increase in CD21^{low} B cells (with higher PD-1 expression and higher clonality) and plasmablasts. Patients with early B cell changes experienced higher rates of grade 3 or higher IRAEs 6 months after CCB.
10 stage IV melanoma or renal cell cancer patients	No decrease in the expression of CD4+CD25+ cells in whole PBMC, nor a decrease in Foxp3 gene expression in the CD4+ or CD4+CD25+ purified cell populations posttreatment. The percentage of CD4^{+}, CD8^{+}, CD4^{+}CD25^{+} and CD4^{+}CD25^{-} T cells in PBMC expressing the activation marker HLA-DR increased following anti-CTLA-4 Ab administration
79 NSCLC	Ki-67^{+} cells among PD-1^{+}CD8^{+} T cells 7 days after the first dose significantly predicted durable clinical benefit
27 melanoma patients	Following ICB, greater decrease in circulating monocyte MDSC Lin^{-} HLA-DR^{-} CD33^{+} CD11b^{+} cells and decrease of T_{regs} CD4^{+}CD25^{hi+}Foxp3^{+} was associated with improved PFS. Baseline evidence of fully activated type I CD4^{+} and CD8^{+} antigen-specific T cell immunity against cancer-testis (NY-ESO-1) and melanocytic lineage (MART-1, gp100) antigens potentiated after ipilimumab.
Discovery cohort (20 patients) and validation cohort (31 patients) with melanoma.	Before commencing therapy, a strong predictor of progression-free and overall survival in response to anti-PD-1 immunotherapy was the frequency of CD14^{+}CD16^{-}HLA-DR^{hi} monocytes
Discovery cohort (28 patients) and validation cohort (40 patients) with melanoma.	monocytic-MDSC frequencies were inversely correlated with peripheral CD8+ T-cell expansion following ipilimumab: Having less than 14.9% m-MDSC pre-treatment was associated with improved OS among the 68 patients
49 patients	Lower percentages of Lin^{-} CD14^{+} HLA-DR^{-} MDSC in patients responding to ipilimumab treatment compared to non-responders
9 patients non-small cell lung cancer	Percentages of NK cell populations in the immune cells of PBMCs were prominently elevated in the immunotherapy responder group when compared with non-responders
751 patients: epithelial ovarian cancer	IL-6 predictive of a therapeutic advantage with bevacizumab for PFS and OS. Patients with high median IL-6 levels treated with bevacizumab had longer PFS and OS compared with placebo. IL-6 may be predictive of therapeutic benefit from bevacizumab when combined with carboplatin and paclitaxel.

Table 1. (continued)

Study	Year	Timing	Immunotherapy
(Sanmamed, Perez-Gracia et al. 2017)	2017	Baseline, 2–4 weeks after the first dose; and at response evaluation.	nivolumab or pembrolizumab or combination nivolumab (1, 2, 3 or 10 mg/kg) or pembrolizumab (2 or 10 mg/kg) intravenously every 2 or 3 weeks
(Hannani, Vétizou et al. 2015)	2015	Baseline, after 1st and 2nd tmt	ipilimumab 3 mg/kg
(Sabatino, Kim-Schulze et al. 2009)	2009	Baseline	High-dose interleukin-2 (IL-2)
(Yuan, Zhou et al. 2014)	2014	Baseline and at completion (week 12)	176 patients treated with ipilimumab at 3 (n = 98) or 10 mg/kg (n = 68).

REFERENCES

1. Clemente CG, Mihm Jr. MC, Bufalino R, Zurrida S, Collini P, Cascinelli N. Prognostic value of tumor infiltrating lymphocytes in the vertical growth phase of primary cutaneous melanoma. Cancer. 1996;77(7):1303-10.
2. Galon J, Costes A, Sanchez-Cabo F, Kirilovsky A, Mlecnik B, Lagorce-Pages C, et al. Type, density, and location of immune cells within human colorectal tumors predict clinical outcome. Science. 2006;313(5795):1960-4.
3. Fridman WH, Pagès F, Sautès-Fridman C, Galon J. The immune contexture in human tumours: impact on clinical outcome. Nature Reviews Cancer. 2012;12(4):298-306.
4. Pagès F, Mlecnik B, Marliot F, Bindea G, Ou F-S, Bifulco C, et al. International validation of the consensus Immunoscore for the classification of colon cancer: a prognostic and accuracy study. The Lancet. 2018;391(10135):2128-39.
5. Galon J, Mlecnik B, Bindea G, Angell HK, Berger A, Lagorce C, et al. Towards the introduction of the 'Immunoscore' in the classification of malignant tumours. J Pathol. 2014;232(2):199-209.
6. Kirilovsky A, Marliot F, El Sissy C, Haicheur N, Galon J, Pagès F. Rational bases for the use of the Immunoscore in routine clinical settings as a prognostic and predictive biomarker in cancer patients. International immunology. 2016;28(8):373-82.
7. Sharpe AH, Pauken KE. The diverse functions of the PD1 inhibitory pathway. Nature Reviews Immunology. 2018;18(3):153-67.
8. Alegre ML, Frauwirth KA, Thompson CB. T-cell regulation by CD28 and CTLA-4. Nat Rev Immunol. 2001;1(3):220-8.
9. Eroglu Z, Kim DW, Wang X, Camacho LH, Chmielowski B, Seja E, et al. Long term survival with cytotoxic T lymphocyte-associated antigen 4 blockade using tremelimumab. Eur J Cancer. 2015;51(17):2689-97.
10. Brahmer JR, Tykodi SS, Chow LQ, Hwu WJ, Topalian SL, Hwu P, et al. Safety and activity of anti-PD-L1 antibody in patients with advanced cancer. N Engl J Med. 2012;366(26):2455-65.

Cancer type	Peripheral findings
Discovery: 29 melanoma patients. Validation cohort: 19 NSCLC patients and 15 melanoma patients	Serum IL-8 levels decreased between baseline and best response and increased upon progression. Early changes in serum IL-8 levels (2–4 weeks after treatment initiation) were strongly associated with response.
262 MM patients	High baseline serum levels of sCD25 were associated with compromised ipilimumab effects in MM patients.
59 patients	Serum VEGF and fibronectin are easily measured pre-treatment biomarkers that could serve to exclude patients unlikely to respond to IL-2 therapy.
176 MM patients	Baseline sVEGF ≥ 43 pg/mL was associated with decreased OS no correlation between VEGF changes and clinical outcome

11. Boutros C, Tarhini A, Routier E, Lambotte O, Ladurie FL, Carbonnel F, et al. Safety profiles of anti-CTLA-4 and anti-PD-1 antibodies alone and in combination. Nature Reviews Clinical Oncology. 2016;13(8):473-86.
12. Bandura DR, Baranov VI, Ornatsky OI, Antonov A, Kinach R, Lou X, et al. Mass Cytometry: Technique for Real Time Single Cell Multitarget Immunoassay Based on Inductively Coupled Plasma Time-of-Flight Mass Spectrometry. Analytical Chemistry. 2009;81(16):6813-22.
13. Tang F, Barbacioru C, Wang Y, Nordman E, Lee C, Xu N, et al. mRNA-Seq whole-transcriptome analysis of a single cell. Nature Methods. 2009;6(5):377-82.
14. Gubin MM, Esaulova E, Ward JP, Malkova ON, Runci D, Wong P, et al. High-Dimensional Analysis Delineates Myeloid and Lymphoid Compartment Remodeling during Successful Immune-Checkpoint Cancer Therapy. Cell. 2018;175(4):1014-30.e19.
15. Chuah S, Chew V. High-dimensional immune-profiling in cancer: implications for immunotherapy. Journal for immunotherapy of cancer. 2020;8(1):e000363.
16. Delyon J, Mateus C, Lefeuvre D, Lanoy E, Zitvogel L, Chaput N, et al. Experience in daily practice with ipilimumab for the treatment of patients with metastatic melanoma: an early increase in lymphocyte and eosinophil counts is associated with improved survival. Annals of Oncology. 2013;24(6):1697-703.
17. Ku GY, Yuan J, Page DB, Schroeder SEA, Panageas KS, Carvajal RD, et al. Single-institution experience with ipilimumab in advanced melanoma patients in the compassionate use setting: lymphocyte count after 2 doses correlates with survival. Cancer. 2010;116(7):1767-75.
18. Simeone E, Gentilcore G, Giannarelli D, Grimaldi AM, Caracò C, Curvietto M, et al. Immunological and biological changes during ipilimumab treatment and their potential correlation with clinical response and survival in patients with advanced melanoma. Cancer Immunology, Immunotherapy. 2014;63(7):675-83.
19. Varricchi G, Galdiero MR, Loffredo S, Lucarini V, Marone G, Mattei F, et al. Eosinophils: The unsung heroes in cancer? Oncoimmunology. 2017;7(2):e1393134-e.

20. Martens A, Wistuba-Hamprecht K, Foppen MG, Yuan J, Postow MA, Wong P, et al. Baseline Peripheral Blood Biomarkers Associated with Clinical Outcome of Advanced Melanoma Patients Treated with Ipilimumab. Clinical Cancer Research. 2016;22(12):2908-18.

21. Ferrucci PF, Ascierto PA, Pigozzo J, Del Vecchio M, Maio M, Antonini Cappellini GC, et al. Baseline neutrophils and derived neutrophil-to-lymphocyte ratio: prognostic relevance in metastatic melanoma patients receiving ipilimumab. Annals of Oncology. 2018;29(2):524.

22. Weide B, Martens A, Hassel JC, Berking C, Postow MA, Bisschop K, et al. Baseline Biomarkers for Outcome of Melanoma Patients Treated with Pembrolizumab. Clinical Cancer Research. 2016;22(22):5487-96.

23. Rosner S, Kwong E, Shoushtari AN, Friedman CF, Betof AS, Brady MS, et al. Peripheral blood clinical laboratory variables associated with outcomes following combination nivolumab and ipilimumab immunotherapy in melanoma. Cancer Medicine. 2018;7(3):690-7.

24. Weber JS, Hamid O, Chasalow SD, Wu DY, Parker SM, Galbraith S, et al. Ipilimumab Increases Activated T Cells and Enhances Humoral Immunity in Patients With Advanced Melanoma. Journal of Immunotherapy. 2012;35(1):89-97.

25. Subrahmanyam PB, Dong Z, Gusenleitner D, Giobbie-Hurder A, Severgnini M, Zhou J, et al. Distinct predictive biomarker candidates for response to anti-CTLA-4 and anti-PD-1 immunotherapy in melanoma patients. J Immunother Cancer. 2018;6(1):18.

26. Hiniker SM, Reddy SA, Maecker HT, Subrahmanyam PB, Rosenberg-Hasson Y, Swetter SM, et al. A Prospective Clinical Trial Combining Radiation Therapy With Systemic Immunotherapy in Metastatic Melanoma. International Journal of Radiation Oncology*Biology* Physics. 2016;96(3):578-88.

27. Wistuba-Hamprecht K, Martens A, Heubach F, Romano E, Geukes Foppen M, Yuan J, et al. Peripheral CD8 effector-memory type 1 T-cells correlate with outcome in ipilimumab-treated stage IV melanoma patients. European Journal of Cancer. 2017;73:61-70.

28. Manjarrez-Orduno N, Menard LC, Kansal S, Fischer P, Kakrecha B, Jiang C, et al. Circulating T Cell Subpopulations Correlate With Immune Responses at the Tumor Site and Clinical Response to PD1 Inhibition in Non-Small Cell Lung Cancer. Front Immunol. 2018;9:1613.

29. Wei SC, Anang NAS, Sharma R, Andrews MC, Reuben A, Levine JH, et al. Combination anti-CTLA-4 plus anti-PD-1 checkpoint blockade utilizes cellular mechanisms partially distinct from monotherapies. Proc Natl Acad Sci U S A. 2019;116(45):22699-709.

30. Comin-Anduix B, Lee Y, Jalil J, Algazi A, de la Rocha P, Camacho LH, et al. Detailed analysis of immunologic effects of the cytotoxic T lymphocyte-associated antigen 4-blocking monoclonal antibody tremelimumab in peripheral blood of patients with melanoma. Journal of translational medicine. 2008;6:22-.

31. Tietze JK, Angelova D, Heppt MV, Reinholz M, Murphy WJ, Spannagl M, et al. The proportion of circulating CD45RO+CD8+ memory T cells is correlated with clinical response in melanoma patients treated with ipilimumab. European Journal of Cancer. 2017;75:268-79.

32. Kunert A, Basak EA, Hurkmans DP, Balcioglu HE, Klaver Y, van Brakel M, et al. CD45RA+CCR7– CD8 T cells lacking co-stimulatory receptors demonstrate enhanced frequency in peripheral blood of NSCLC patients responding to nivolumab. Journal for ImmunoTherapy of Cancer. 2019;7(1):149.

33. Takeuchi Y, Tanemura A, Tada Y, Katayama I, Kumanogoh A, Nishikawa H. Clinical response to PD-1 blockade correlates with

a sub-fraction of peripheral central memory CD4+ T cells in patients with malignant melanoma. Int Immunol. 2018;30(1):13-22.

34. Spitzer MH, Carmi Y, Reticker-Flynn NE, Kwek SS, Madhireddy D, Martins MM, et al. Systemic Immunity Is Required for Effective Cancer Immunotherapy. Cell. 2017;168(3):487-502 e15.

35. Borst J, Ahrends T, Bąbała N, Melief CJM, Kastenmüller W. CD4+ T cell help in cancer immunology and immunotherapy. Nature Reviews Immunology. 2018.

36. Liakou CI, Kamat A, Tang DN, Chen H, Sun J, Troncoso P, et al. CTLA-4 blockade increases IFNgamma-producing CD4+ICOShi cells to shift the ratio of effector to regulatory T cells in cancer patients. Proc Natl Acad Sci U S A. 2008;105(39):14987-92.

37. Chen H, Liakou CI, Kamat A, Pettaway C, Ward JF, Tang DN, et al. Anti-CTLA-4 therapy results in higher CD4+ICOShi T cell frequency and IFN-gamma levels in both nonmalignant and malignant prostate tissues. Proc Natl Acad Sci U S A. 2009;106(8):2729-34.

38. Carthon BC, Wolchok JD, Yuan J, Kamat A, Ng Tang DS, Sun J, et al. Preoperative CTLA-4 blockade: tolerability and immune monitoring in the setting of a presurgical clinical trial. Clin Cancer Res. 2010;16(10):2861-71.

39. Vonderheide RH, LoRusso PM, Khalil M, Gartner EM, Khaira D, Soulieres D, et al. Tremelimumab in Combination with Exemestane in Patients with Advanced Breast Cancer and Treatment-Associated Modulation of Inducible Costimulator Expression on Patient T Cells. Clinical Cancer Research. 2010;16(13):3485-94.

40. Ng Tang D, Shen Y, Sun J, Wen S, Wolchok JD, Yuan J, et al. Increased Frequency of ICOS⁺ CD4 T Cells as a Pharmacodynamic Biomarker for Anti-CTLA-4 Therapy. Cancer Immunology Research. 2013;1(4):229-34.

41. Chaput N, Lepage P, Coutzac C, Soularue E, Le Roux K, Monot C, et al. Baseline gut microbiota predicts clinical response and colitis in metastatic melanoma patients treated with ipilimumab. Ann Oncol. 2017;28(6):1368-79.

42. Wang W, Yu D, Sarnaik AA, Yu B, Hall M, Morelli D, et al. Biomarkers on melanoma patient T Cells associated with ipilimumab treatment. Journal of Translational Medicine. 2012;10(1):146.

43. Fan X, Quezada SA, Sepulveda MA, Sharma P, Allison JP. Engagement of the ICOS pathway markedly enhances efficacy of CTLA-4 blockade in cancer immunotherapy. J Exp Med. 2014;211(4):715-25.

44. Metzger TC, Long H, Potluri S, Pertel T, Bailey-Bucktrout SL, Lin JC, et al. ICOS Promotes the Function of CD4+ Effector T Cells during Anti-OX40-Mediated Tumor Rejection. Cancer Res. 2016;76(13):3684-9.

45. Wei SC, Levine JH, Cogdill AP, Zhao Y, Anang NAS, Andrews MC, et al. Distinct Cellular Mechanisms Underlie Anti-CTLA-4 and Anti-PD-1 Checkpoint Blockade. Cell. 2017.

46. Das R, Verma R, Sznol M, Boddupalli CS, Gettinger SN, Kluger H, et al. Combination therapy with anti-CTLA-4 and anti-PD-1 leads to distinct immunologic changes *in vivo*. J Immunol. 2015;194(3):950-9.

47. Yi JS, Ready N, Healy P, Dumbauld C, Osborne R, Berry M, et al. Immune Activation in Early-Stage Non–Small Cell Lung Cancer Patients Receiving Neoadjuvant Chemotherapy Plus Ipilimumab. Clinical Cancer Research. 2017;23(24):7474-82.

48. Beyrend G, van der Gracht E, Yilmaz A, van Duikeren S, Camps M, Hollt T, et al. PD-L1 blockade engages tumor-infiltrating lymphocytes to co-express targetable activating and inhibitory receptors. J Immunother Cancer. 2019;7(1):217.

49. Wei SC, Anang N-AAS, Sharma R, Andrews MC, Reuben A, Levine JH, et al. Combination anti–CTLA-4 plus

anti–PD-1 checkpoint blockade utilizes cellular mechanisms partially distinct from monotherapies. 2019:201821218.

50. Kamphorst AO, Pillai RN, Yang S, Nasti TH, Akondy RS, Wieland A, et al. Proliferation of PD-1+ CD8 T cells in peripheral blood after PD-1-targeted therapy in lung cancer patients. Proc Natl Acad Sci U S A. 2017;114(19):4993-8.

51. Huang AC, Postow MA, Orlowski RJ, Mick R, Bengsch B, Manne S, et al. T-cell invigoration to tumour burden ratio associated with anti-PD-1 response. Nature. 2017;545(7652):60-5.

52. Kim KH, Cho J, Ku BM, Koh J, Sun J-M, Lee S-H, et al. The First-week Proliferative Response of Peripheral Blood PD-1⁺CD8⁺ T Cells Predicts the Response to Anti-PD-1 Therapy in Solid Tumors. Clinical Cancer Research. 2019;25(7):2144-54.

53. Du W, Hu S, Cai S, Wang Y, Wu L, Sun D, et al. Dynamic testing of stimulative and suppressive biomarkers on peripheral blood cells at early stages of immunotherapy predicts response in advanced cancer patients. Discov Med. 2018;25(140):277-90.

54. Powles T, Eder JP, Fine GD, Braiteh FS, Loriot Y, Cruz C, et al. MPDL3280A (anti-PD-L1) treatment leads to clinical activity in metastatic bladder cancer. Nature. 2014;515(7528):558-62.

55. Herbst RS, Soria JC, Kowanetz M, Fine GD, Hamid O, Gordon MS, et al. Predictive correlates of response to the anti-PD-L1 antibody MPDL3280A in cancer patients. Nature. 2014;515(7528):563-7.

56. Jacquelot N, Roberti MP, Enot DP, Rusakiewicz S, Ternes N, Jegou S, et al. Predictors of responses to immune checkpoint blockade in advanced melanoma. Nat Commun. 2017;8(1):592.

57. Callahan MK, Horak CE, Curran MA, Hollman T, Schaer DA, Yuan J, et al. Peripheral blood and tumor biomarkers in patients with advanced melanoma treated with combination nivolumab (anti-PD-1, BMS-936558, ONO-4538) and ipilimumab. Journal for ImmunoTherapy of Cancer. 2013;1(Suppl 1):O6.

58. Rotte A. Combination of CTLA-4 and PD-1 blockers for treatment of cancer. Journal of Experimental & Clinical Cancer Research. 2019;38(1):255.

59. Larkin J, Hodi FS, Wolchok JD. Combined Nivolumab and Ipilimumab or Monotherapy in Untreated Melanoma. N Engl J Med. 2015;373(13):1270-1.

60. Maker AV, Attia P, Rosenberg SA. Analysis of the cellular mechanism of antitumor responses and autoimmunity in patients treated with CTLA-4 blockade. Journal of immunology (Baltimore, Md : 1950). 2005;175(11):7746-54.

61. Santegoets SJ, Stam AG, Lougheed SM, Gall H, Scholten PE, Reijm M, et al. T cell profiling reveals high CD4+CTLA-4 + T cell frequency as dominant predictor for survival after prostate GVAX/ ipilimumab treatment. Cancer Immunol Immunother. 2013;62(2):245-56.

62. Sharma A, Subudhi SK, Blando J, Scutti J, Vence L, Wargo J, et al. Anti-CTLA-4 Immunotherapy Does Not Deplete FOXP3⁺ Regulatory T Cells (Tregs) in Human Cancers. 2018.

63. Tarhini AA, Edington H, Butterfield LH, Lin Y, Shuai Y, Tawbi H, et al. Immune Monitoring of the Circulation and the Tumor Microenvironment in Patients with Regionally Advanced Melanoma Receiving Neoadjuvant Ipilimumab. PLOS ONE. 2014;9(2):e87705.

64. Kitano S, Postow MA, Ziegler CGK, Kuk D, Panageas KS, Cortez C, et al. Computational Algorithm-Driven Evaluation of Monocytic Myeloid-Derived Suppressor Cell Frequency for Prediction of Clinical Outcomes. Cancer Immunology Research. 2014;2(8):812-21.

65. Meyer C, Cagnon L, Costa-Nunes CM, Baumgaertner P, Montandon N, Leyvraz L, et

al. Frequencies of circulating MDSC correlate with clinical outcome of melanoma patients treated with ipilimumab. Cancer Immunology, Immunotherapy. 2014;63(3):247-57.

66. Krieg C, Nowicka M, Guglietta S, Schindler S, Hartmann FJ, Weber LM, et al. High-dimensional single-cell analysis predicts response to anti-PD-1 immunotherapy. Nat Med. 2018.

67. Pirozyan MR, McGuire HM, Emran AA, Tseng H-Y, Tiffen JC, Lee JH, et al. Pretreatment Innate Cell Populations and CD4 T Cells in Blood Are Associated With Response to Immune Checkpoint Blockade in Melanoma Patients. Frontiers in Immunology. 2020;11(372).

68. Ribas A, Shin DS, Zaretsky J, Frederiksen J, Cornish A, Avramis E, et al. PD-1 Blockade Expands Intratumoral Memory T Cells. Cancer Immunol Res. 2016;4(3):194-203.

69. Das R, Bar N, Ferreira M, Newman AM, Zhang L, Bailur JK, et al. Early B cell changes predict autoimmunity following combination immune checkpoint blockade. The Journal of Clinical Investigation. 2018;128(2):715-20.

70. Fransen MF, Schoonderwoerd M, Knopf P, Camps MG, Hawinkels LJ, Kneilling M, et al. Tumor-draining lymph nodes are pivotal in PD-1/PD-L1 checkpoint therapy. JCI Insight. 2018;3(23).

71. Soyano AE, Dholaria B, Marin-Acevedo JA, Diehl N, Hodge D, Luo Y, et al. Peripheral blood biomarkers correlate with outcomes in advanced non-small cell lung Cancer patients treated with anti-PD-1 antibodies. Journal for ImmunoTherapy of Cancer. 2018;6(1):129.

72. Cho Y-H, Choi MG, Kim DH, Choi YJ, Kim SY, Sung KJ, et al. Natural Killer Cells as a Potential Biomarker for Predicting Immunotherapy Efficacy in Patients with Non-Small Cell Lung Cancer. Targeted Oncology. 2020;15(2):241-7.

7

SUMMARIZING DISCUSSION

CANCER IMMUNOTHERAPY: WHAT IS THE RELEVANT TARGET?

The first clinical efforts to cure cancer were directed on stopping proliferation of tumor cells by blocking cell division of highly proliferating cells. The non-specificity of such approaches led to severe side effects. Alternative treatments options, such as immune checkpoint therapy, have been developed that aimed to target the immune system in order to unleash the cytotoxic power of CD4 and CD8 T cells, by blocking their inhibitory signals (immune checkpoint blockade, ICB) or by activating their stimulatory receptors.

The first ICB approved to treat metastatic melanoma was the anti-CTLA-4 inhibitor ipilimumab (1), followed by inhibitors of the PD-1/PD-L1 pathways. The clinical success of these ICBs led to their FDA approval for multiple types of cancer (2). New targets with the potential to strengthen the immune system have been discovered, leading to potential new types of cancer immunotherapy. This has conducted to a plethora of targets including CD27, CD40, CD47, CD73, 4-1BB (CD137), CSF1, GITR, ICOS, IDO, IL-2R, LAG3, OX40 (CD134), STAT3, STING, TLRs, TIGIT, TIM3. With the emerging development of new drugs targeting these molecules came the possibility of treatment tailoring to every patient. Therefore, there is an increasing need to anticipate the possible effect of immunotherapy at an early stage.

DISSECTING COMPLEX IMMUNE RESPONSES: THE INESCAPABLE SINGLE-CELL TECHNOLOGIES

We investigated the complex patterns of immunotherapeutic responses with extensive mass cytometry panels (36-marker-murine, 46-marker-human) and analyzed the data with a self-made tailored bioinformatic pipeline *Cytofast* (**Chapter 3**). We developed *Cytofast* to compare different clustering methods, and validated this novel analysis platform with two previously published datasets. *Cytofast* offered a comprehensive view of proteomic data like flow and mass cytometry with detailed explanations to guide the user (**Chapters 3 and 4**). If traditional flow cytometry was largely used to analyze the tumor microenvironment (TME), such methods are generally limited to 15 markers and are sensitive to intrinsic fluorescence background generated by tumor and other cells. Alternative methods like mass cytometry avoided the fluorescence background to replace fluorophores by metal isotopes, which can be detected according to their mass. Such methods increased the number of detectable markers up to 51 (**Chapters 5 and 6**), resulting into a deep and unbiased phenotyping of the immune system. Whereas flow cytometry is restricted by the number of available fluorochromes spectra (around 30), mass cytometry is theoretically restricted to the number of isotopes available, slightly over a hundred. A recent technique named CITE-seq (Cellular Indexing of Transcriptomes and Epitopes by Sequencing), uses nucleotide tags to identify cellular subsets. The power of this method relies on the combination of cellular and genetical information by evaluating both gene expression and protein level simultaneously on cells (3). However, thereby the limit of detection level is increased, and thus the method might not be

able to capture rare cell subsets. Another drawback of single-cell mass/flow cytometry relies on the manual dissociation of the material before being processed thereby losing the organization of these cells in the tissues. The newly imaging systems coupled to mass cytometry keep spatial conformation of the tissue, by analyzing fixed paraffin embedded tissue slices, making this information clinically relevant as the spatial organization of T cells in the tumor micro-environment is linked to clinical outcome (4). Spatially resolved single-cell analysis can characterize phenotypic heterogeneity of TILs in a disease-relevant manner. It is also now possible to anchor sc-RNA-seq experiments with chromatin difference analysis together with protein expression and keep spatial gene expression patterns (5). Even if those methods provide deep characterization of the host, these studies investigated the immune system without considering the microbiota, assumed to be responsible to modulate the efficiency of immunotherapy (6).

An efficient investigating pipeline will embrace the diverse components interacting with the immune system and modulating the host response. Constant adaptations of visualization tools like *Cytofast* are required to filter and extract biological relevant information coming from single-cell technologies.

THE PHENOTYPIC T CELL HETEROGENEITY IN THE TME REVEALS T CELL ACTIVATION

In the tumor microenvironment (TME), immunotherapy is shaping the immune system at an early stage. In a murine tumor setting, NK cells were shaped after three days of PD-L1 treatment (**Chapter 4**), which might contribute to immunotherapy efficacy. PD-L1 specifically upregulated a $CD54^{+}CD39^{+}NKG2A^{-}$ NK cell subset detected in all PD-L1 treated mice and absent in the untreated animals. The upregulation at the same time of activating markers like CD54 and inhibitory markers like CD39 triggered by PD-L1 therapy suggests that these cells might not be exhausted (7) but tumor reactive. The co-expression of activating and inhibitory molecules is not limited to NK cells.

Indeed, we further confirmed that PD-L1 treatment is upregulating a specific T cell subset co-expressing **a**ctivating and **i**nhibitory markers in the TME (**Chapter 5**). This subset, named T_{AI} cells, co-expressed NKG2A, PD-1, LAG-3, CD43 and ICOS. This duality in their phenotype might be inherent to their cytotoxicity. Inhibitory molecules could be upregulated on those cytotoxic cells to limit their toxic effects to normal cells. A panel marker gathering activating and inhibitory molecules might be sufficient to delineate tumor-reactive T cells. Defining tumor-specific CTLs requires MHC class I tetramers, which need to be designed and might not integrate all tumor-reactive-lymphocytes (8). Surrogate markers replacing MHC class I tetramers to identify tumor-specific cells are of utility to understand the diversity of CTLs. For example, it has been recently reported that co-expression of CD39 and CD103 identifies tumor-reactive CD8 T cells in human solid tumors (9). Deep phenotyping of tumor-infiltrating-lymphocytes (TILs) will allow personalized treatment by specific targeting.

THE SYSTEMIC IMMUNE RESPONSE TO CANCER: A STEP TOWARDS BLOOD SCREENING FOR CANCER PATIENT IMMUNO-MONITORING

Our above described study was based on analysis of the TME (**Chapter 5**), requiring invasive surgery to access this compartment. An alternative to TME analysis would reside in the examination of immune cells in the blood. We discovered T_{AI} subsets in the blood using scRNAseq and mass cytometry that correlated with efficient therapy in two different mouse cancer models (**Chapter 6**), suggesting the importance of an early blood-based test after administrating immunotherapy (**Chapter 2**). In both tumor models, efficient immunotherapy is accompanied by an upregulation of the same activating markers including the hyper-glycosylated form of CD43. These findings have been translated in human settings. In healthy donors, T cells appear to have a rested phenotype, limited to CD27 expression. In the responder group, and especially after therapy, patient CTLs in blood specifically show an upregulation of CD56 or CD161, demonstrating the systemic immunity response of immunotherapy. If CD161 is specific to responders only, not every single responding patient present a high level of CD161, making this molecule a reliable indicator of responsiveness of $CD8^+$ T cells in blood of cancer patients (**Figure 1**).

After profiling the immune response in blood with a 46-surface antibody panel we validate the results with a minimal set of markers identified by *Hypergate* (10). It will give

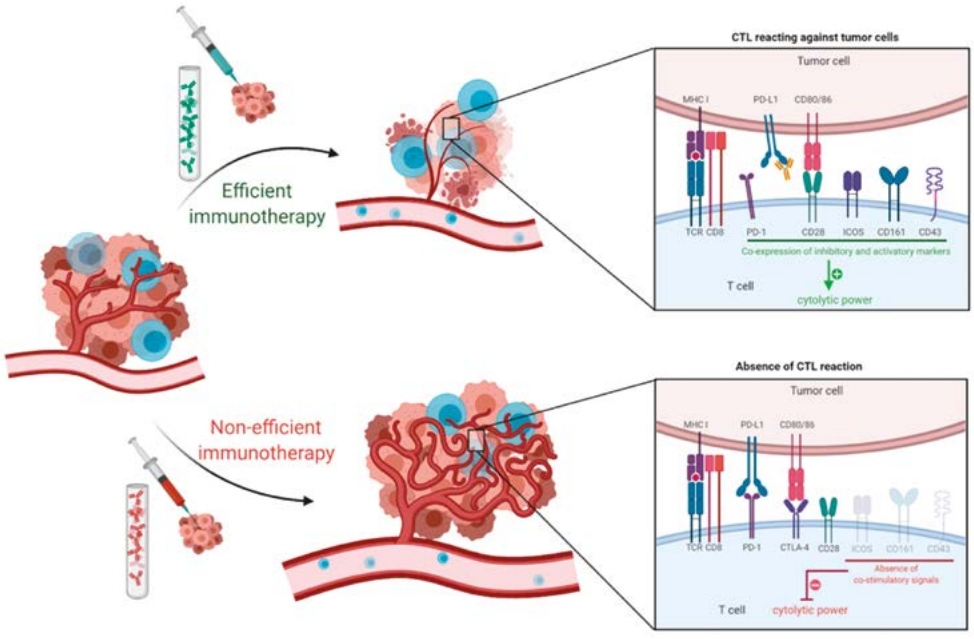

Figure 1. Summary of the differences found on T cells between different immunotherapy efficiency levels.

a faster way to discriminate healthy donor from responder and non-responder patients by flow cytometry, which is of faster use compared to mass cytometry and routinely used it in the clinic.

In the murine model we also showed the impact of our therapy in lymphoid organs like the bone marrow, spleen and lymph nodes. Our study suggests that T cells are systemically shaped by PD-L1 blockade in the bone marrow and the spleen, meaning that the T cell reservoir in the lymphoid organs plays a role in tumor immunity. A systemic impact of tumor cells and immunotherapy has also been observed by others (11, 12), suggesting the potential benefit of blood screening to follow tumor evolution. The underlined connections between the lymphoid organs demonstrated here reinforced the highlighted role of the draining lymph nodes and its potency to present tumor neoantigens through a cross-talk with the tumors already shown by others (13-15)

COMBINATORIAL IMMUNOTHERAPY

The ultimate goal of single-cell analysis is to tailor cancer treatments on a patient-basis to reach a maximal effect. As illustrated in **Chapter 5**, identifying T_{AI} cells by single-cell analysis could be a first step towards a tailored-treatment to reach tumor clearance. Indeed, we observe an concomitant increase in T_{AI} cells in more effective combination ICB therapies in our mouse models. However, the timing component needs also to be taken in consideration. If the combination of successive OX40 and PD-L1 seems to be efficient in mice (**Chapter 6**) and in aggressive tumor models like pancreatic cancer (16), the simple concurrent addition of PD-1 to OX40 induces the opposite effect (17, 18) due to a significant induction of apoptosis on $CD8^+$ T cells. Such a pattern should be evaluated before engaging combinatorial treatment. Several clinical trials are ongoing with results being expected (NCT02221960, NCT02410512).

Combination therapy with CTLA-4 with PD-1 is clinically approved, and other combination approaches are under investigation regarding their efficacy in the clinic. As an example, LAG-3 and ICOS targeting, also studied in **Chapter 5**, is currently being tested in combination with PD-1 blockade (NCT02460224 and NCT03829501, respectively) after successful preclinical results being reported (19). A better use of such combinations might rely on the systematic deep phenotyping of patient material and avoid side effects, which can vary from colitis to diabetes (20, 21).

Combinatorial immunotherapy should not be limited in targeting extracellular markers expressed by T lymphocytes using antibodies but could also, for example, consist of enhancing antigen presenting cells by adjuvants such as CpG (**Chapter 6**, (22)) or create a pro-inflammatory environment in the tumor by injecting particular cytokines (23, 24) or oncolytic viruses (25).

CONCLUDING REMARKS

The results presented here challenge the idea that inhibitory markers on T lymphocytes are delineating only exhausted T cells. The classical vision to restrict expression of markers like PD-1 or LAG-3 to an exhausted state can be questioned by high-dimensional phenotyping. These "exhausted" cells still present a cytotoxic power through the presence of activating markers, unleashed by blocking their inhibitory receptors (Figure 1).

Finally, transposing these findings in the clinic would suggest to investigate the presence of T cells co-expressing inhibitory and stimulatory molecules, being relevant immunotherapy targets. Current improvements in single-cell technologies like mass cytometry, single-RNA-sequencing or the combination of both together with better analyzing tools development will allow a more systematic phenotyping approach before treating patients with immunotherapeutic agents. The research presented in this thesis aimed for a closer connection between immunotherapy of cancer and bioinformatics (Figure 2) and integrate it as a whole, which may improve strategies for personalized therapy.

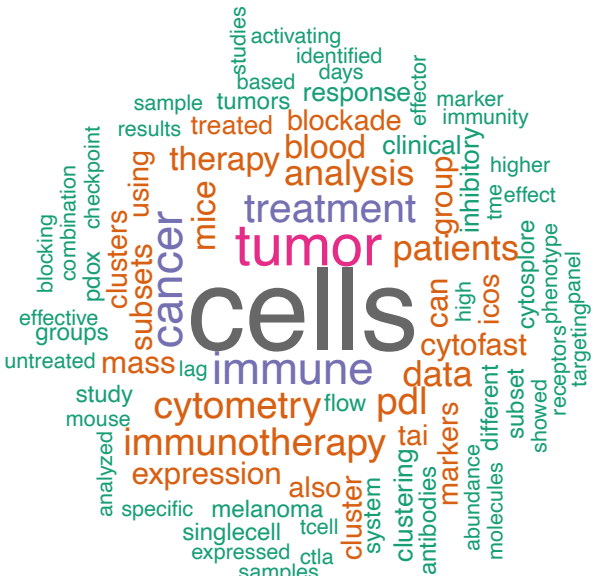

Figure 2. Word mapping of the presented thesis: an overview of the theme.

REFERENCES

1. Hodi FS, O'Day SJ, McDermott DF, Weber RW, Sosman JA, Haanen JB, et al. Improved survival with ipilimumab in patients with metastatic melanoma. N Engl J Med. 2010;363(8):711-23.
2. Gong J, Chehrazi-Raffle A, Reddi S, Salgia R. Development of PD-1 and PD-L1 inhibitors as a form of cancer immunotherapy: a comprehensive review of registration trials and future considerations. Journal for ImmunoTherapy of Cancer. 2018;6(1):8.
3. Stoeckius M, Hafemeister C, Stephenson W, Houck-Loomis B, Chattopadhyay PK, Swerdlow H, et al. Simultaneous epitope and transcriptome measurement in single cells. Nature Methods. 2017;14(9):865-8.
4. Jackson HW, Fischer JR, Zanotelli VRT, Ali HR, Mechera R, Soysal SD, et al. The single-cell pathology landscape of breast cancer. Nature. 2020;578(7796):615-20.
5. Stuart T, Butler A, Hoffman P, Hafemeister C, Papalexi E, Mauck WM, 3rd, et al. Comprehensive Integration of Single-Cell Data. Cell. 2019;177(7):1888-902 e21.
6. Roy S, Trinchieri G. Microbiota: a key orchestrator of cancer therapy. Nat Rev Cancer. 2017;17(5):271-85.
7. Canale FP, Ramello MC, Nunez N, Furlan CLA, Bossio SN, Serran MG, et al. CD39 Expression Defines Cell Exhaustion in Tumor-Infiltrating CD8(+) T Cells. Cancer Res. 2018;78(1):115-28.
8. Simoni Y, Becht E, Fehlings M, Loh CY, Koo SL, Teng KWW, et al. Bystander CD8(+) T cells are abundant and phenotypically distinct in human tumour infiltrates. Nature. 2018.
9. Duhen T, Duhen R, Montler R, Moses J, Moudgil T, de Miranda NF, et al. Co-expression of CD39 and CD103 identifies tumor-reactive CD8 T cells in human solid tumors. Nature Communications. 2018;9(1):2724.
10. Becht E, Simoni Y, Coustan-Smith E, Evrard M, Cheng Y, Ng LG, et al. Reverse-engineering flow-cytometry gating strategies for phenotypic labelling and high-performance cell sorting. Bioinformatics. 2018;35(2):301-8.
11. Spitzer MH, Gherardini PF, Fragiadakis GK, Bhattacharya N, Yuan RT, Hotson AN, et al. IMMUNOLOGY. An interactive reference framework for modeling a dynamic immune system. Science. 2015;349(6244):1259425.
12. Allen BM, Hiam KJ, Burnett CE, Venida A, DeBarge R, Tenvooren I, et al. Systemic dysfunction and plasticity of the immune macroenvironment in cancer models. Nature Medicine. 2020.
13. Fransen MF, Schoonderwoerd M, Knopf P, Camps MG, Hawinkels LJ, Kneilling M, et al. Tumor-draining lymph nodes are pivotal in PD-1/PD-L1 checkpoint therapy. JCI Insight. 2018;3(23).
14. Wu TD, Madireddi S, de Almeida PE, Banchereau R, Chen YJ, Chitre AS, et al. Peripheral T cell expansion predicts tumour infiltration and clinical response. Nature. 2020;579(7798):274-8.
15. Mayoux M, Roller A, Pulko V, Sammicheli S, Chen S, Sum E, et al. Dendritic cells dictate responses to PD-L1 blockade cancer immunotherapy. Sci Transl Med. 2020;12(534).
16. Ma Y, Li J, Wang H, Chiu Y, Kingsley CV, Fry D, et al. Combination of PD1 Inhibitor and OX40 Agonist Induces Tumor Rejection and Immune Memory in Mouse Models of Pancreatic Cancer. Gastroenterology. 2020.
17. Shrimali RK, Ahmad S, Verma V, Zeng P, Ananth S, Gaur P, et al. Concurrent PD-1 Blockade Negates the Effects of OX40 Agonist Antibody in Combination Immunotherapy through Inducing T-cell Apoptosis. Cancer Immunol Res. 2017.
18. Messenheimer DJ, Jensen SM, Afentoulis ME, Wegmann KW, Feng Z, Friedman DJ, et al. Timing of PD-1 Blockade Is Critical to Effective Combination Immunotherapy with Anti-OX40. Clin Cancer Res. 2017.

19. Woo SR, Turnis ME, Goldberg MV, Bankoti J, Selby M, Nirschl CJ, et al. Immune inhibitory molecules LAG-3 and PD-1 synergistically regulate T-cell function to promote tumoral immune escape. Cancer Res. 2012;72(4):917-27.

20. Kracht MJL, Zaldumbide A, Roep BO. Neoantigens and Microenvironment in Type 1 Diabetes: Lessons from Antitumor Immunity. Trends Endocrinol Metab. 2016;27(6):353-62.

21. Bajwa R, Cheema A, Khan T, Amirpour A, Paul A, Chaughtai S, et al. Adverse Effects of Immune Checkpoint Inhibitors (Programmed Death-1 Inhibitors and Cytotoxic T-Lymphocyte-Associated Protein-4 Inhibitors): Results of a Retrospective Study. J Clin Med Res. 2019;11(4):225-36.

22. Cerundolo V, Hermans IF, Salio M. Dendritic cells: a journey from laboratory to clinic. Nature Immunology. 2004;5(1):7-10.

23. Forni G, Fujiwara H, Martino F, Hamaoka T, Jemma C, Caretto P, et al. Helper strategy in tumor immunology: Expansion of helper lymphocytes and utilization of helper lymphokines for experimental and clinical immunotherapy. Cancer and Metastasis Reviews. 1988;7(4):289-309.

24. Berraondo P, Sanmamed MF, Ochoa MC, Etxeberria I, Aznar MA, Pérez-Gracia JL, et al. Cytokines in clinical cancer immunotherapy. British Journal of Cancer. 2019;120(1):6-15.

25. Ribas A, Puzanov I, Gajewski T, Long GV, Dummer R, Kirkwood JM, et al. A multicenter, open-label trial of talimogene laherparepvec (T-VEC) plus pembrolizumab vs pembrolizumab monotherapy in previously untreated, unresected, stage IIIB-IV melanoma. Journal of Clinical Oncology. 2015;33(15_suppl):TPS9081-TPS.

NEDERLANDSE SAMENVATTING

ACKNOWLEDGMENT

LIST OF PUBLICATIONS

CURRICULUM VITAE

NEDERLANDSE SAMENVATTING

In ons lichaam deelt er dagelijks ongeveer 2 biljoen keer een cel. Tijdens deze delingen kunnen er fouten ontstaan in de DNA replicatie. Hierdoor kunnen gemuteerde cellen ontstaan die ongeremd verder blijven delen en uiteindelijk tumoren kunnen vormen. Er is ontdekt dat sommige stoffen, chemotherapeutica genaamd, de deling van kankercellen kunnen stoppen maar dit gaat ook gepaard met toxiciteit.

Als een alternatief op chemotherapie zijn immuuntherapieën ontwikkeld die aangrijpen op het immuunsysteem in plaats van de tumorcellen. De ontwikkeling van immuuntherapie heeft de behandeling van kanker sterk verbeterd, hoewel maar een deel van de patiënten helemaal geneest. Afgelopen jaren zijn verschillende immuuntherapieën ontwikkeld zoals anti-PD-1/anti-PD-L1 en anti-CTLA-4, waarvoor de ontdekkers in 2018 de Nobelprijs hebben gekregen.

Hoewel er verschillende immuun-gerelateerde geneesmiddelen ontdekt zijn, zijn we nog steeds op zoek naar de beste therapeutische strategie met de minste bijwerkingen. Het immuunsysteem wordt versterkt door immuuntherapie, wat leidt tot relevante systemische veranderingen in de compositie en activatiestatus van immuun cellen. Om deze mechanismen en hun invloed op tumor immuniteit verder te onderzoeken, zijn analyses gedaan op individuele cellen, op zowel RNA (single cell RNA-sequencing) als op eiwit niveau (massa cytometrie). Er is eerst een nieuw bio-informatica programma ontwikkeld die eerst gevalideerd is met data uit de literatuur (**Hoofdstuk 2**) en vervolgens is gebruikt om de rol van NK cellen te bestuderen (**Hoofdstuk 3**). Deze immuun cellen worden al 3 dagen na het starten van de anti-PD-L1 therapie gevormd. De nieuwe analyse methode is ook gebruikt om het effect van anti-PD-L1 op de tumoromgeving te laten zien in een muismodel voor colorectale kanker (**Hoofdstuk 4**). Hierdoor kon immuuntherapie verbeterd worden door specifieke biomarkers op T-cellen te gebruiken die geïdentificeerd waren door middel van massa cytometrie. Het onderzoek is voortgezet door ook bloedcellen van kankerpatiënten te analyseren, waarbij de resultaten in muizen ook in de mens bevestigd werden. Met name NK-cel receptoren op T-cellen werden geïdentificeerd en gebruikt als therapeutische doelen om de cytotoxische kracht van die cellen te versterken. Het idee achter deze therapeutische strategie is de kracht van deze T-cellen nieuw leven in te blazen door remmende receptoren te blokkeren en systemische immuniteit tegen kanker mogelijk te maken, voornamelijk door stimulatie via NK-cel familie receptoren en chemokinen.

Vervolgens is de systemische response op immuuntherapie onderzocht. Nadat de focus eerst lag op de tumor, zijn hier individuele cellen van het bloed, de lymfeklieren, milt en beenmerg onderzocht. Dit onderzoek laat zien dat de efficiëntie van immuuntherapie weerspiegeld wordt in het bloed, door het screenen van enkele biomarkers zoals CD43 (**Hoofdstuk 5**). Ook enkele andere markers geïdentificeerd door RNA analyse van individuele cellen bleken belangrijk, zoals CXCR3 en NKG2D. Deze data zijn bevestigd in de humane setting door het screenen van bloed van kankerpatiënten. Markers als CD56

en CD161 zijn geassocieerd met klinisch voordeel, wat de hypothese van systemische immuniteit die meetbaar is in het bloed, ondersteunt. In Hoofdstuk 6 bespreken we de rol van bloedanalyse als immunologisch compartiment tijdens immunotherapie, welke een belangrijke rol speelt voor monitoring van de immuuntherapie zoals waargenomen in dit proefschrift. Tot slot zijn de bevindingen en de interpretatie van de resultaten voor immuuntherapie van kanker bediscussieerd in Hoofdstuk 7.

ACKNOWLEDGMENT

This journey has been made possible thanks to **Ramon** and **Ferry**, who hired me. I am grateful for the opportunity they offered me to work with them. In 4 years, you helped me developing my skills in tumor immunology and bioinformatics. I have been well surrounded during my PhD. **Marcel**, my beloved crazy neighbor with exceptional talks that I could only have with him, always available to help me. **Jan Willem**, my English and French teacher, always coming up with relevant remarks and specific jokes. **Esmé**, I was glad I could work with you and we could support each other during our long CyTOF trips. It was a relief knowing I could always count on you and sharing our fears, struggles, laughs and tea breaks has always been resourceful during those years. **Iris**, thanks for the "traditie", our laughs and jokes. **Anke**, your support and kindness have been inspiring. **Ayse**, you made the two first years lighter as being the perfect mix between a colleague ready to help from 6 a.m. and an amazing friend. **Suzanne** and **Tom**, I am thankful for the physical help and psychological support you gave me. I am pleased I could also count on other lab members: **Brett**, **Elena**, for their advices and feedback; **Jeroen**, for the nice talks and sharing gym sessions. **Floor**, our talks made me more comfortable and brought me joy along laughs in unexpected circumstances. I am glad you were here to help me out during the last years of my PhD. **Jana**, I will definitely miss our nice conversations and laughs, your help inside and outside work had a great added value. **Tetje**, your scientific advice and support helped me during the end of my PhD.

Elham, your help and kindness made my experiments each time easier, together with **Camilla**. I am glad you two always volunteered to help me. I will definitely remember our laughs. **Marit**, I am so grateful we attended the NVVI together, it was definitely THE meeting of the year. **Noel**, I am grateful for the scientific advice you gave me through my PhD journey, as well as your relevant analysis, not limited to science. Your insight and advice were more than helpful.

Yoanne, your wise vision of life has been an eye-opener to me, your contagious laugh a symbol of peace and joy. **Koen**, I am happy we could develop *Cytofast* together. **Gonca**, you have always impressed me by your charism and your very correct and sharp words, inspiring me in many ways. I will definitely continue to take my vital dose of humor around you. **Natasja**, I am glad we could meet during our PhD. Working and travelling around the world to conferences together have been a great experience, from Stockholm to Breckenridge. **Thomas**, I will definitely miss our sport session on Fridays, a great way to talk about science while spending calories. **Tamim**, thank you for your support regarding the sc-RNA-seq analysis and your flexibility. **Arnaud**, **Françoise**, merci pour votre attention, vos conseils pertinents, votre intérêt et bienveillance. Vous m'avez permis de m'apaiser à travers votre hospitalité et votre humour ; vos encouragements ont été essentiels à ma progression.

Jessica, our tea breaks were my fuel and your kindness and lightness hiding a profound intelligence have been an example for me. **Monique**, dear buurvrouw, you impressed me by your work, your kindness and your patience. I thank you for your help and the good moments spent together. My days have also been delighted by heartwarming words coming from **Tessa**, **Laura**, **Jim**, **Marjolijn (**Hameetman**)** and **René** (thanks both for helping me at the CyTOF), **Lianne** (I will miss the orchestra), **Vincent** (for your sharp humor) and **Anita** (for your energy). L'animalerie regorge de rencontres incroyables mais réjouissantes, qui peuvent mener à une belle amitié : **Eliott**, **Flo,** nos parenthèses françaises à Leiden ont été rafraichissantes.

Sarah, ta vision et ta franchise ont enchanté mes journées de thèse par de nombreux rires avec à la clé un séjour mémorable corse aux côtés de **Diane**, dont le calme impérieux force l'admiration. Je suis reconnaissant pour ton aide, ton soutien et ta générosité. **Sam** et **Justine**, infatigables compagnons de route depuis la Suisse, je suis reconnaissant d'avoir pu

vous rencontrer et de voir que notre amitié continue d'apporter son lot de joies. **Aymeric**, merci pour ton aide et ton hospitalité en Suisse, ton intérêt et ta curiosité. Ces amis que j'ai rencontrés en Suisse, avec **Pève**, **Erwan**, ont toujours été source de joie et d'apaisement et je suis ravi d'avoir fait ce chemin avec vous.

Ma famille de cœur a énormément compté pour moi, j'ai pu me ressourcer et entrecouper ma thèse de séjours en Suisse : **Caro**, tu m'as toujours inspiré par ta bienveillance, entourée d'**Inès** et **Hélène**, irradiant par votre énergie positive. **Jean-Richard**, par ta générosité, ta douceur, ton intérêt, tu as toujours sur me réconforter. Avec vous, j'ai toujours pu me sentir entier et apaisé. Venir me ressourcer auprès de vous m'a apporté le calme, la sérénité et la joie de vivre qui a été un moteur et un soulagement incontestable durant ces heureuses années. **Schatzie**, **Emmanuelle**, merci pour ton accueil, tes mots justes, nos fous rires et notre complicité. Notre lien qui nous unit me nourrit encore aujourd'hui du même indispensable réconfort qui m'a sauvé quelques années plus tôt.

Enfin mes amis, **Célia**, **Quentin**, **Félix** et **Julien**. Je suis reconnaissant de voir notre amitié perdurer, en ville comme forêt, ou à la plage, toujours proches les uns des autres. Passer mes vacances avec vous et vous revoir régulièrement m'apporte toujours une harmonie apaisante. **Laura**, j'espère pouvoir continuer nos interludes musicaux et lorrains encore longtemps.

Ma famille a su être là pour me soutenir, ma tante **Anick**, ma cousine **Héloïse**, toujours disponibles et prêtes à m'aider : merci pour nos fous rires et nos bons moments de complicité. Mes grands-parents, **Papy** et **Mamie**, pour qui j'ai toujours reçu leur affection, m'ont soutenu pendant mon chemin avec bienveillance et fierté, mais ont dû me quitter avant de pouvoir me voir terminer cette étape, que je rêvais de pouvoir partager avec eux. Ma **Mamie**, partie trop tôt pour pouvoir me voir commencer mon travail de thèse mais son affection passée m'a donné l'élan nécessaire pour franchir cet obstacle. **Pascal**, **Dominique, Fanny,** votre altruisme, votre écoute et votre intérêt m'ont toujours inspiré. **Georgette**, tu me donneras ton secret pour garder ta vivacité d'esprit. **Nicole** et **René**, en aidant mes parents et en étant présents pour eux, je vous remercie indirectement pour votre support, sans doute trop sous-estimé. Merci aux autres membres de ma famille, **Pierre-André**, **Anna**, **Chantal**, **Louis**, **Philip**, **Camille**, **Julien**.

I will finish by the start of all my journey as a PhD candidate in Leiden. I came in Leiden for you **Perrine**. En étant mon plancher à travers cette épreuve, tu m'as permis de me dépasser, et je suis heureux de pouvoir franchir cette ligne d'arrivée avec toi ; ce qui me rend fier de nous. En m'ayant intégré dans ta famille, **François**, **Françoise**, et **Marion** m'ont apporté le réconfort nécessaire pour commencer cette nouvelle aventure et je garde en mémoire le sourire et l'accueil de ta **Maminou**. I am happy that my days in Leiden were enlightened by **Auke** through your smile, your humor and kindness. I am relieved that our ways crossed each other and it is a great joy to know that both of you are still my part of my life. I am thankful to your parents, **Marga** and **Theo**, for the resourcing week-ends in Meddo. **Maurits**, by joining the last finish step of this race, I am grateful for your positive thoughts, your support, your patience and our complicity during the last months of my PhD. I thank your **family** for their warmth and welcome.

C'est sans nul doute que je dois cet accomplissement à mes parents **Madeleine** et **Denis**. "En proie à tous les problèmes que je leur posais, mes pleurs, mes colères, ils m'ont aimé sans conditions, se sacrifiant pour m'aider - petit à petit, jour après jour. Ils sont mes héros." Daniel Tamett – *Je suis né un jour bleu*. Je leur dois leur patience, leur indispensable réconfort résistant à toute épreuve et leur infatigable écoute. Ils ont nourri des forces en moi sans lesquelles cette thèse n'aurait jamais pu commencer, me tirant sans cesse vers le haut. Ce livre est moins le résultat de mon travail acharné que celui de leur ténacité et de leur incommensurable soutien. Ce livre leur est dédié.

LIST OF PUBLICATIONS

PD-L1 blockade engages tumor-infiltrating lymphocytes to co-express targetable activating and inhibitory receptors.
Beyrend G, van der Gracht E, Yilmaz A, van Duikeren S, Camps M, Höllt T, Vilanova A, van Unen V, Koning F, de Miranda NFCC, Arens R, Ossendorp F.
J Immunother Cancer. 2019 Aug, 7(1):217

Cytomegalovirus infection and progressive differentiation of effector-memory T cells.
Pardieck IN, **Beyrend G**, Redeker A, Arens R.
F1000Res. 2018 Sep, 7

Visualizing Dynamic Changes at the Maternal-Fetal Interface Throughout Human Pregnancy by Mass Cytometry.
van der Zwan A, van Unen V, **Beyrend G**, Laban S, van der Keur C, Kapsenberg HJM, Höllt T, Chuva de Sousa Lopes SM, van der Hoorn MP, Koning F, Claas FHJ, Eikmans M, Heidt S.
Front Immunol. 2020 Oct, 11(2430), 435

Visualization and Quantification of High-Dimensional Cytometry Data using Cytofast and the Upstream Clustering Methods FlowSOM and Cytosplore.
Beyrend G, Stam K, Ossendorp F, Arens R.
J Vis Exp. 2019 Dec, (154)

Host genetics and tumor environment determine the functional impact of neutrophils in mouse tumor models.
van Elsas M, Kleinovink JW, Moerland M, Feiss G, **Beyrend G**, Arens R, Mei H, Nibbering PH, Jirka SM, van Hall T, van der Burg SH.
J Immunother Cancer. 2020 Sep, 2(8) 877

Memory CD8+ T cell heterogeneity is primarily driven by pathogen-specific cues and additionally shaped by the tissue environment.
van der Gracht ETI, **Beyrend G**, Abdelaal T, Pardieck IN, Wesselink TH, van Haften FJ, van Duikeren S, Koning F, Arens R.
iScience. 2020 Dec, 24(1), 101954

Cytofast: A workflow for visual and quantitative analysis of flow and mass cytometry data to discover immune signatures and correlations.
Beyrend G, Stam K, Höllt T, Ossendorp F, Arens R.
Comput Struct Biotechnol J. 2018 Oct, 24 (16), 435

CURRICULUM VITAE

Guillaume started his studies at the High Preparatory School in Biology in France, from which he holds a MSc in Biotechnology in 2012. After working four years for Novartis and UCB at the Center of Expertise for Biologics in Switzerland, he was enrolled as a Marie Curie Early stage researcher at the LUMC, to study the cellular mechanisms of effective immunotherapy in solid tumors. He focused on bridging innovative single-cell technologies with tumor immunology to unravel the complex cellular immunity during immunotherapy and to bring precision medicine to the clinic. He applied single-cell RNA-sequencing and mass cytometry in the context of human and mouse tumor immunology. He developed and is the co-author of new algorithms such as Cytofast, which enables a rapid identification of immunological profiles in experimental models and patients. At the end of 2020, he founded VisuaLyte, a web-based training in R applied in cytometry analysis. The same year, he completed his scientific profile by being successfully admitted to the fast-track of medicine cursus (Passerelle) at the University of Lille, France, with the ultimate goal to combine science and medicine.